2018

SURFACE ENGINEERING AND MONOMER DESIGN FOR LIGHT-MEDIATED RING OPENING METATHESIS POLYMERIZATION

Ishan A. Fursule
University of Kentucky, ishan.fursule@uky.edu
Digital Object Identifier: https://doi.org/10.13023/ETD.2018.028

STUDENT AGREEMENT:

I represent that my thesis or dissertation and abstract are my original work. Proper attribution has been given to all outside sources. I understand that I am solely responsible for obtaining any needed copyright permissions. I have obtained needed written permission statement(s) from the owner(s) of each third-party copyrighted matter to be included in my work, allowing electronic distribution (if such use is not permitted by the fair use doctrine) which will be submitted to UKnowledge as Additional File.

I hereby grant to The University of Kentucky and its agents the irrevocable, non-exclusive, and royalty-free license to archive and make accessible my work in whole or in part in all forms of media, now or hereafter known. I agree that the document mentioned above may be made available immediately for worldwide access unless an embargo applies.

I retain all other ownership rights to the copyright of my work. I also retain the right to use in future works (such as articles or books) all or part of my work. I understand that I am free to register the copyright to my work.

REVIEW, APPROVAL AND ACCEPTANCE

The document mentioned above has been reviewed and accepted by the student's advisor, on behalf of the advisory committee, and by the Director of Graduate Studies (DGS), on behalf of the program; we verify that this is the final, approved version of the student's thesis including all changes required by the advisory committee. The undersigned agree to abide by the statements above.

Ishan A. Fursule, Student

Dr. Bradley Berron, Major Professor

Dr. Thomas Dziubla, Director of Graduate Studies

SURFACE ENGINEERING AND MONOMER DESIGN FOR LIGHT-MEDIATED RING OPENING METATHESIS POLYMERIZATION

DISSERTATION

Dissertation submitted to the faculty of the graduate school

in partial fulfillment of the requirements for the degree of Doctor of Philosophy

in the College of Engineering at the University of Kentucky

By

Ishan A. Fursule

Director: Dr. Bradley Berron, Associate Professor of Chemical and Materials Engineering, University of Kentucky, Lexington, Kentucky

2017

ABSTRACT OF DISSERTATION

SURFACE ENGINEERING AND MONOMER DESIGN FOR LIGHT-MEDIATED RING OPENING METATHESIS POLYMERIZATION

Stimuli-responsive materials are changing the landscape of actuated materials, optoelectronics, molecular machines, solar cells, temporary memory storage, and biomedical materials. Specifically, photo-responsive polymers have gained acceleration in research and application since the last two decades in the form of a surface coating and micro-patterns. Light as a stimulus can be coherent, mono or polychromatic, tunable for power (intensity) and energy (wavelength), and has precise spatiotemporal control. Conventional surface coating techniques such as spin coating are unable to impart properties to the coatings in terms of sturdiness, homogeneity, uniformity over the complex surface, post deposition modification, and process efficiency. Also, in the field of photoreponsive polymers, there is no simple technique for surface-patterning of photo-responsive polymers, which is an important missing link between current research and future potential applications.

This dissertation designs new strategies for light-mediated ring opening metathesis polymerization (ROMP) to synthesize a diverse class of stable photo-responsive polymers and coatings.

Firstly, we propose a new synthetic route to functionalize surface-initiated ring opening metathesis polymerization (SI ROMP) coatings. The backbone of ROMP polymers has internal carbon-carbon double bonds which are potential sites to introduce additional functionalities like stimuli-responsive functional groups. We leverage these unsaturated bonds to incorporate functionalized side chains using thiol-ene click chemistry. Thiol-ene chemistry is a versatile approach to attach diverse functional groups at the site of a carbon-carbon double bond. This approach was tested by grafting 3 types of thiols with different functional tail groups and can be readily used for any polyolefin coatings.

Secondly, oxidative degradation of SI ROMP coatings in the organic solvent is a common problem resulting in a decrease in the film thickness due to polymer chain cleavage. We incorporated a custom designed crosslinker to the polynorbornene (pNB) coatings to prepare *in situ* crosslinked pNB coatings. This approach provides a crosslinked coating of

pNB with significantly increased stability against organic solvents by decreasing the film loss from 73 % to 28 %.

Lastly, a novel approach of making photo-responsive polymer by light mediated ROMP is demonstrated. Light mediated control over rate of polymerization is the key feature required for patterning surface with photoresponsive polymers. We achieved this goal by designing and synthesizing a monomer that effectively controls the activity of the catalyst by temporarily deactivating it on irradiation with UV 365 nm light and reactivating it back by irradiation with blue 455 nm light to resume the ROMP.

Keywords: *Azobenzene, polynorbornene, photoresponsive ROMP, SI ROMP, crosslinker, coating*.

Ishan A. Fursule

12/01/2017

SURFACE ENGINEERING AND MONOMER DESIGN FOR LIGHT-MEDIATED RING OPENING METATHESIS POLYMERIZATION

By

Ishan A. Fursule

Dr. Bradley Berron
Director of Dissertation

Dr. Thomas Dziubla
Director of Graduate Studies

Date
12/01/2017

To my Mother, Father, and Brother.

ACKNOWLEDGEMENTS

The very first person to whom I would like to express my deepest gratitude is Dr. Bradley Berron. He has not only guided me throughout my doctoral research work by his profound knowledge, creative ideas, and welcoming new projects proposed by me but also has been a 'Mentor' to me. During my research, I did take time to learn new laboratory practices, using instruments, and getting results through the highs and lows, but he has always been encouraging, positive and very patient. Being ahead of time, the importance of hard work and having a big vision towards your work are the three things that I learned from him and will be the pillars for my future career. To summarize, without his support, insight, and vision, my journey through Ph.D. would have been much difficult. I am really honored to work with him and thankful for being my research advisor. I am also extremely thankful to all my committee members Dr. Matthew Beck, Dr. Stephen Rankin, and Dr. Mark Watson for their guidance, valuable suggestions, and oversee completion of my dissertation thesis. Many thanks to Dr. Marcelo I. Guzman for agreeing to serve as my external examiner.

Secondly, I would like to thank my parents, late mother Mrs. Manda Fursule, and father Mr. Anupkumar Fursule for shaping me into a person who I am with their love, encouragement, and belief in me. Also, I would like to thank my elder brother, Dr. Anurag Fursule who is the biggest inspiration for me for his hardworking and helping nature.

Special thanks to all my friends 'Virginia Mandal' especially Shreya, Abhishek, Prachi, Raghava, Priyesh, and everyone who made my life in Lexington very exciting and unforgettable. I am also grateful to my fellow lab members, Dr. Aman Preet Kaur, Dr. Leila Safazadeh, Dr. Jacob Lilly, Charles Watkins Jr., Calvin Cahall, Dr. Anuhya Gottipati, Pei-Jung Wu, Cong Li and Landon Mills. They have made my time in laboratory fun and enjoyable.

Finally, I would like to acknowledge CeNSE, ERTL, NMR facility at UKy, and other academic laboratories for allowing me to use their analytical instruments and professors who spent their precious time in discussing and providing their valuable suggestion on my research ideas. Finally, this work was supported by National Science

Foundation under Award CMMI-1334403. Acknowledgment is also made to the Donors of the American Chemical Society Petroleum Research Fund (52743-DNI5 and 57619-DNI10) for partial support of this research.

Table of contents

List of tables

List of figures

List of Abbreviations

LB	Langmuir Blodgett
SIP	Surface initiated polymerization
SAM	Self-assembled monolayer
ROP	Ring opening polymerization
SI ROMP	Surface initiated ring opening metathesis polymerization
ROMP	Ring opening metathesis polymerization
SI ATRP	Surface initiated atom transfer radical polymerization
SI RAFT	reversible addition-fragmentation chain transfer Polymerization
DMF	Dimethyl formamide
pNB	Polynorbornene
RCM	Ring closing metathesis
CM	Cross metathesis
ROM	Ring opening metathesis
C=C	Carbon=carbon
N=N	Nitrogen=nitrogen
UV	Ultraviolet
Ru	Ruthenium
$NBCl_2$	Trans-3,6-endomethylene-1,2,3,6-tetrahydropthaloyl chloride
UHP	Ultra-high purity
DiNB	Dinorbornene
DCM	Dichloromethane
NB	Norbornene
RAIRS	Reflection absorption infrared spectroscopy
IR	Infra-red
FTIR	Fourier transform infrared spectroscopy
EIS	Electrochemical impedance spectroscopy
KCl	Potassium chloride
UV-Vis	Ultraviolet-visible
NMR	Nuclear Magnetic Resonance
GPC	Gel permeation technology
PDI	Polydispersity index
Mn	Number average molecular weight
Mw	Weight average molecular weight
XPS	X-ray photoelectron spectroscopy
AFM	Atomic force microscopy
EtOH	Ethyl alcohol
I-184	Irgacure-184
DiNB-pNB	Crosslinked polynorbornene

PEG	Polyethylene glycol
NBAC	5-norbornene-2-carboxylic acid
DCC	N,N'-dicyclohexylcarbodiimide
DMAP	4-(dimethylamino) pyridine
$CDCl_3$	Chloroform
^{1}H-NMR	Proton NMR
AB	Azobenzene
ABn	4,4'-Diaminoazobenzene
L(m,n)	Linker
AB(m,n)	Azobenzene with linker
RSE	Ring strain energy
ADMET	Acyclic diene metathesis polymerization
CDP	Cyclodepolymerization
RBF	Round bottom flask
TEA	Triethylamine
ESI-MS	Electron spray ionization mass spectroscopy
DEDAM	Diethyl diallyl malonate
G2	Grubbs catalyst 2nd generation
NMA	Norbornene monoazobenzene
NCA	Norbornenecarboxylic acid
ABOH	4-phenylazophenol
EVE	Ethyl vinyl ether
HPLC	High pressure liquid chromatography
THF	Tetrahydrofuran
G3	Grubbs catalyst 3rd generation
TMS	Trimethylsilane
TLC	Thin layer chromatography
MS	Mass spectroscopy
DCM-d_2	Deuterated methylene chloride

1 Introduction

Stimuli-responsive molecules are the building blocks for the functional materials whose response is controlled by the external environmental stimulus. The response is accompanied by variation in physical and chemical properties of the material. The stimulus can be of any form such as temperature, light, electric current, pH[1]. In the last decade, light-responsive polymer coatings have gained huge attention in scientific research. Because light represents an ideal stimulus due to its precise spatiotemporal resolution (coherence, pulsed signal), it can be mono/polychromatic, and the ability of selective excitation of target chromophore in a non-invasive manner. The light intensity and wavelength can be easily modulated to comply with the system competently. These properties are of utmost importance to design exciting applications of light/photo-responsive polymers. Photo-responsive polymers are typically alkane chains with azobenzene as a pendant to main chain[2, 3] or in the main chain of the polymer[4]. Azobenzene is the most commonly used photo-responsive moiety to impart photo-responsive nature to polymers or macromolecules. Photo-responsive coatings are the surface coatings of these polymers which change their physical or chemical surface properties when irradiated with a particular wavelength of radiation. They have numerous applications due to a unique property of reversible photoisomerization of azobenzene, in the form of planar and patterned surface coatings both. For instance, A. Riul Jr. and co-workers have prepared artificial taste sensors using Langmuir-Blodgett (LB) film of azobenzene containing polymers which can differentiate between four different types of tastes (salty, sour, sweet, and bitter)[5]. Ho Sun Lim and co-workers have made a photo-switchable superhydrophobic surface from azobenzene containing material with an erasable and rewritable pattern that can switch between superhydrophobic and superhydrophilic on exposure to UV/Visible radiations[6]. Moreover, similarly, Mamiko Narita and co-workers have demonstrated photoinduced immobilization of antibody (immunoglobulin G) on a surface spin-coated with the azopolymer[7]. These are some very innovative applications that form the basis for further research in diverse fields. Similar existing opportunities for photoresponsive polymer coatings also exist in optoelectronic

devices[8, 9], solar cells[10, 11], micro-fluidics[12], diffraction gratings[13, 14] and nano/micro-devices[15, 16].

Typically, these surface coatings are made by spin coating, LB method, and layer by layer deposition[17-19]. However, these deposition methods are not compatible with forming precise coatings on the complex surface geometries used in the most exciting applications[4, 19]. Spin coating or similar techniques produce physically adsorbed surface coatings. Hence, they are very susceptible to wear off due to small mechanical shear forces. In addition, if the viscosity, temperature, angular velocity and solvent utilized in the spin coating are not right then it is very common to get defects such as chuck marks, striation patterns, and bubbles[20, 21]. Spin coating cannot be used to pattern surface and generate complex architectures. A layer by layer spin coating method is performed to make multilayer architectures[22, 23] but this approach also has limitations to be extended to more complex micro/nanostructures. Another less explored technique for preparing photoresponsive coating is LB process[24, 25]. LB process is one of the efficient methods to make monolayers of organic molecules on a planar surface by immersing substrate into a solution of surface associating molecules[26]. However, it can be used only for preparing monolayers and cannot make surface-bound polymers. Other drawbacks include instability, inhomogeneous, and poorly structured monolayers[27].

Currently, the most common method of creating surface patterns of photoresponsive polymers of azobenzene is irradiating the photoresponsive coating with the interference pattern of polarized light. On exposure, the azobenzene tends to align itself perpendicular to the plane of polarization and move in the darker region of the interference pattern. This creates surface relief gratings or linear surface patterns of photoresponsive polymers. When circularly polarized light is used, a circular pattern is observed on the coating[14]. However, this method is too complicated and needs a surface pre-coated with the photoresponsive polymer.

In brief, we need a better method to prepare photoresponsive polymer coating with higher mechanical stability, that can be employed over any complex surface geometries, and that can be used for surface patterning of the photoresponsive polymers to create surface geometries.

Surface-initiated polymerization (SIP) represents a versatile approach to form functional surface coatings[28]. This “grafting from” method grows the polymer brushes from initiator groups that are chemically bound to the self-assembled monolayer (SAM) on the substrate[29]. Hence, they are chemically coupled to surface providing higher strength against desorption. A SAM is a highly ordered, single molecule thin layer formed by spontaneous adsorption of molecular constituents from its anchor group on the suitable substrate[29, 30]. As compared to spin coating and dip coating, SIP provides robust coatings due to the covalent bond between coating and substrate, better control over coating thickness even on the non-planar surface, and the density of polymer brushes on the surface can be controlled by tuning the density of SAM [28, 31-33].

There are various types of SIP techniques like surface initiated ring opening metathesis polymerization (SI ROMP), surface initiated atom transfer radical polymerization (SI ATRP), and reversible addition-fragmentation chain transfer polymerization (SI RAFT). SI ATRP is one of the conventional methods of preparing surface coupled polymer brushes primarily due to the commercial availability of monomers and highly controllable polymerization nature[34, 35]. However, SI ATRP is extremely slow; typically, coating growth is limited to a few nanometers per hour. Additionally, ATRP is typically restricted to inert atmospheres. Similarly, SI RAFT is also commonly used surface polymerization method with the excellent ability to polymerize wide range of vinyl monomers, high tolerance towards functional groups, and chain end functionalization[36-39]. Additionally, SI RAFT can be executed on several substrates using many different kinds of monomers[40, 41]. However, RAFT is highly sensitive to the polymerization temperature, which typically limits the film growth rate to the slow rates seen in SI ATRP.

When compared to SI ATRP and SI RAFT, SI ROMP provides advantages including polymerization in ambient temperature, tolerance to oxygen and other functional groups, higher rate of polymerization, formation of high molecular weight polymer brushes, and preservation of the olefin functionality in the resulting polymer brushes[42-45]. SI ROMP can also be performed on several different substrates including gold, and silicon/silicon dioxide[46, 47]. Several types of monomers are available for ROMP, including cyclic alkenes, and cyclic dienes, and bicyclic alkenes [43, 48]. We modified the most commonly

used ROMP monomer, norbornene with azobenzene as a branch on its cyclic structure, enabling the photo-switching of ROMP in solution.

Polymer surface coatings engineered with desired properties are necessary for numerous research areas such as microelectronics[49], membranes[50, 51], solar cells[52, 53] and biomedical applications[54]. Modification of substrates serves the purpose of making them available for specific applications. For example, functionalizing surface to get an ultralow surface energy alters its wettability and makes it resistant to corrosion[55]. Another example is a modification of coating to get antibacterial surface has a vast number of applications in the medical field, consumer market and research laboratories[56-58]. Hence the flexibility of surface coating towards functionalization is of immense importance. The spin-coated photo-responsive polymer films cannot be modified further to alter or add the new chemical functionality to the polymer chains.

SI ROMP polymer coatings with desired surface functionality can be prepared by using cyclic monomer modified with the same functional group. However, with this approach, synthesis of the new monomer is the essential requirement, and the introduction of new functional groups affects the rate of SI ROMP and hence the thickness of the coating[59]. Hence, to prepare SI ROMP coatings with target functionality, a new approach is required which will expand the spectrum of applications for SI ROMP coatings.

The coatings prepared by SI ROMP contain alternate unsaturated functionality, i.e., carbon-carbon double bonds, a potential site for adding new molecules. We used a photochemistry approach to graft thiol molecules with modified tail functional groups across these carbon-carbon double bonds in polymer brushes. Thiol-ene reactions are a hydrothiolation reaction where thiols are added to inactivated carbon-carbon double bonds to yield an internal thioether [60]. Typically, they are incredibly versatile and rapid in ambient atmospheric conditions of temperature, and pressure. Moreover, most importantly, a wide variety of activated or non-activated thiols can be used on even multiply substituted olefinic bonds.

The research work presented here addresses the issue about the current techniques of making photo-responsive coatings (planar and patterned), and lack of a versatile method for their modification thereby dividing complete work into three primary objectives.

Firstly, we propose a new way of adding functionalized thiol molecules to SI ROMP coatings of norbornene. Here we leverage unsaturated functionalities of SI ROMP polymer brushes and thiol-ene click chemistry to modify the surface functionality of coatings.

Secondly, we incorporate a crosslinker to the SI ROMP coatings to get in-situ crosslinked surface coatings. This objective is derived from the observations of the first objective, where although the polynorbornene coating was modified three different functional group derivatized thiol molecules but significant polymer chain cleavage was recorded during surface engineering.

Lastly, a novel class of ROMP monomer is introduced with the property of light-mediated process of ROMP. We propose two different designs with a fundamental difference in their structure and its changes on photoisomerization leading to light-mediated ROMP. and exploit their synthesis independently. With this method, the polymerization can be switched ON and OFF in a non-invasive manner, i.e., without adding any external reagent. The typical approach to terminating metathesis reaction is the addition of excess ethyl vinyl, which completely shuts down the reaction by deactivating the catalyst in the solution. Our work creates a reversible approach towards photocontrol of polymerization, where metathesis activity it can be temporarily switched on and switched off as desired.

2 Background

2.1 Surface initiated polymerization (SIP)

Most conventional and established film deposition methods are dip coating, and spin coating to create polymer coatings that exhibit weak adhesive forces. They are a non-covalent interaction (Van der Waals forces or hydrogen bonding) with the surface[28, 61] that weakens the performance of coatings rendering them unstable against external factors like solvents, high temperature, and mechanical forces[62]. To overcome these drawbacks, it is crucial to establish the chemical bonds between polymer chains and the surface[63]. Surface initiated polymerization (SIP) is the versatile route of creating polymer coatings chemically bound to a surface, i.e., it grows polymer brushes directly from initiator groups that are chemically coupled to the self-assembled monolayer (SAM). SAM is a well-ordered film of single molecule thick layer that is created by spontaneous adsorption of small molecules from the solution to the appropriate substrate[64]. In contrast to traditional methods, SIP offers the capability of tailoring the surface properties of solid substrate while exhibiting various advantages, including chemical coupling between the surface and polymer chains, conformal and uniform coating on surfaces exhibiting planar and nonplanar architectures, and efficient control over composition, film thickness, and grafting density[28]. These practical benefits have allowed SIP to functionalize fine particles[44, 61], porous substrates[65, 66], and a wide variety of substrates including organic polymers, silicon dioxide, alumina, and gold[66]. To be functional, SIP requires the immobilization of initiating species onto the surface before polymerization which is achieved by self-assembly techniques[61, 67]. Subsequent exposure to the activated substrate to an appropriate monomer solution promotes polymerization directly from the surface[31]. There are many types of SIP, differentiating from each other by reaction mechanism for propagation[28], surface initiated ring opening metathesis polymerization (SI ROMP)[68], surface initiated atom transfer radical polymerization (SI ATRP)[67], and surface initiated radical addition fragmentation chain transfer (SI RAFT)[36].

2.2 Metathesis reactions

The transformation, comprising the cleavage and formation of double bonds is also referred as alkene metathesis. Carbon-carbon bond forming reactions are amongst the most

powerful family of reactions in organic synthesis, and over the past decade, metathesis reaction which is a metal-catalyzed exchange of alkylidene moieties between alkenes has emerged as a powerful method of formation of carbon-carbon double bonds[69]. High reactivity with olefinic substrates and tolerance to even more strong functional groups has led the extensive use of ruthenium-based catalysts in organic synthesis and polymer synthesis[70, 71].

The generally accepted mechanism of metathesis reaction, i.e., Chauvin mechanism is primarily a sequence of formal [2+2] cycloadditions/cycloreversions involving alkenes, metal carbenes, and metallacyclobutane intermediates[72]. However, the discovery of alkylidene complexes followed by the insight that some species of this type constitute well behaved single component catalysts for olefin metathesis gave an essential clue for settling the long-lasting debate on the actual mechanism of metathesis[72, 73]. The tungsten and molybdenum catalysts developed by Schrock and co-workers and ruthenium carbine complex introduced by Grubbs and co-workers are undoubtedly the most versatile and popular catalysts for metathesis[74, 75]. As metathesis necessarily converts one alkene to a new one, this reaction is predisposed to subsequent transformations. Domino processes incorporating different metathesis events, i.e., ring closing olefin metathesis (RCM)/ring opening metathesis (ROM)/cross metathesis (CM) or RCM/ROM/RCM introduces a tremendous amount of molecular complexity in a single catalytic and atom-economical step. Since all the steps of catalytic cycles are reversible and an equilibrium mixture of olefins is obtained.

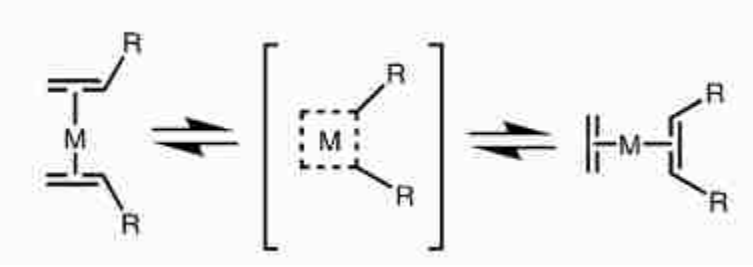

Figure 2.1: Schematic representation of olefin metathesis reaction mechanism[76]

Historically, olefin metathesis has been studied both from a mechanistic standpoint and in the context of polymer synthesis (i.e., ring opening metathesis polymerization or

ROMP)[69, 77]. Recently, however, RCM of acyclic dienes has received considerable attention as a highly efficient methodology for functionally diverse carbocycles and heterocycles[78].

2.3 Surface initiated ring opening metathesis polymerization (SI ROMP)

ROMP was patented by DuPont[79], and polymerization of norbornene was reported by Truett and co-workers[80] in 1960. Discovery of more robust (tolerance to oxygen, moisture and a significant number of functional groups) catalysts by Grubbs[81] and Schrock[82] fueled the research area for ROMP. ROMP exhibits properties in terms of rapid kinetics under mild conditions, producing the thickest surface initiated films[83, 84]. Norbornene, cyclobutenes, cis-cyclooctanes, and cyclopentenes are the variety of strained ring monomers can be used for ROMP[42]. SI ROMP can be performed on some different substrates such as SI-SiO^2[85], polymeric supports[83], silicon wafers[86], Wang resins[87], carbon nanotubes[88], and gold[59]. Surface initiated ROMP on gold occurs by anchoring an olefinic initiator group to the surface via thiolate/Au linkage, i.e., self-assembled monolayer. The olefin functionality in the covalently bound monolayer is exposed to a metathesis catalyst (Grubbs Catalyst) to generate active sites bound to the surface. The non-bound catalyst is rinsed away, and the surface is exposed to a ROMP active monomer. The predominate ROMP monomer studied in surface-initiated cases has been norbornene and its functional derivatives. ROMP has a unique feature that it allows synthesis of conjugated, unsaturated macro-molecules with carbon-carbon double bonds being conserved in the final polymer (Figure 2.2). Polymerization of unfunctionalized norbornene yields primarily hydrophobic films with low dielectric constants, and they can further be modified to prepare polymeric supports[89], bioactive surfaces[47, 90], and biopolymer[47]. Functional derivatives of norbornene can polymerize to produce films with wide-ranging properties and applications, including functionalization of chromatographic supports[91, 92] to improve selectivity, and modification of carbon nanotubes to improve dispersibility in common solvents[28]. Some techniques also boost the thickness to more than a micrometer[93]. The reactivity of a ROMP monomer is typically related to the ring strain of the monomer. The high ring strain of the norbornene family tends to result in highly reactive monomers. Typical surface initiated ROMP experiments are run for short time periods (5 - 60 min). Since the most preferred thermodynamic conditions for ROMP are at low temperatures[69], most experiments

are run at room temperature[83, 94]. Chain terminating reactions include the reaction of the active site with olefin functionality in the pNB backbone (inter- or intra-molecular) and vinyl terminated initiators, the ring closing reaction with neighboring uncatalyzed vinyl groups. This is also called as backbiting.

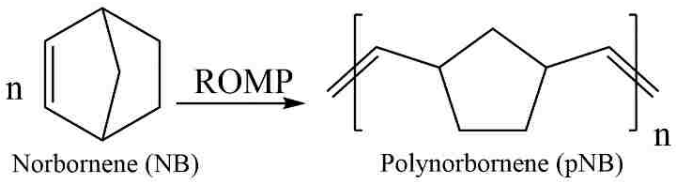

Figure 2.2: ROMP of norbornene to polynorbornene

2.4 Ring closing metathesis (RCM)

First employed by Villemin and by Tsuji nearly four decades ago, now RCM of dienes is one of the most important methodologies to synthesize cyclic organic compounds[95, 96]. Owing in large part to the easily handled catalysts enabling better control over reaction, this reaction has risen to impressive prominence in organic synthesis over the past two decades, [81, 82]. The common rings of 5-7 members have historically been dominant. Owing to the part to their greater ease of access, significant advances have been made in the synthesis of medium[97, 98] and macrocyclic rings[98, 99]. The synthetic efficiency of RCM is limited by the competition between intramolecular ring closing and intermolecular oligomerization reactions. It has also been used in inter alia, construction of synthetically valuable building blocks such as heterocyclic ring containing different elements[100, 101], aromatic heterocycles[102], spyrocycles[103, 104], and so on. It is the thermodynamic distribution of living metathesis products[69, 72]. Ring chain equilibrium can be established involving cyclodepolymerization of oligomers or polymers, or oligomerization of the intended RCM product. Thermodynamic control is particularly relevant in the RCM synthesis of many medium-sized or macrocyclic products[105]. The nature of the substrate, extruded olefin, the competence of the catalyst, and the experimental conditions decide the extent of the reversibility of reactions. In many cases these reactions are reversible. Also, the solvent used for RCM also plays very crucial role in influencing the rate and *cis*/*trans* stereoselectivity of the product[106, 107]. For e.g. Figure 2.3 shows RCM of diethyl diallylmalonate using Grubbs catalyst 2nd generation.

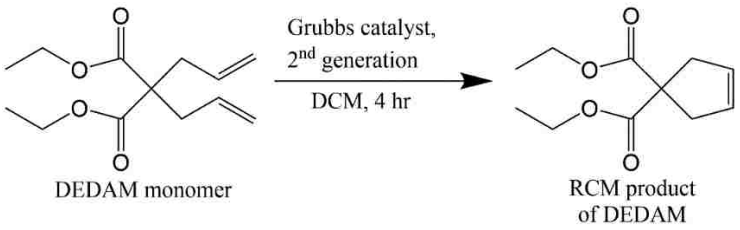

Figure 2.3: RCM of diethyl diallyl malonate (DEDAM)

2.5 Click chemistry

Introduced by K. Barry Sharpless in 2001, click chemistry is a set of reactions with properties such as high yield for product and inoffensive by-product, regiospecificity, versatile, easy to purify without chromatographic methods and can be conducted in easy to remove benign solvents[108, 109]. The click chemistry has a diverse range of applications in the fields of drug delivery, nanoparticle surface modification, bioconjugation, pharmaceutical related polymer chemistry and material science[108].

Click reaction is mainly classified into four types (Figure 2.4): cycloaddition reactions like diels-alder and 1,3-dipolar cycloaddition reaction; nucleophilic ring opening reactions like aziridines, epoxides, aziridinium ions, episulphonium ions, etc.; non-aldol type carbonyl chemistry like formation of urea, thio-ureas, amides, heterocyclic aromatics, etc.; and the last addition to carbon-carbon multiple bonds as in epoxidation, michael addition, sulfenyl halide addition, etc[110, 111]. Among all, cycloaddition, particularly Cu^{I}-catalyzed Huisgen 1,3-cycloaddition, i.e., cycloaddition of alkynes and azides to yield 1,2,3-triazoles is most widely researched, used due to its general ease of execution, facile reaction conditions, nature of orthogonality and almost 100% of published literature on click chemistry is based on this type of reaction[112].

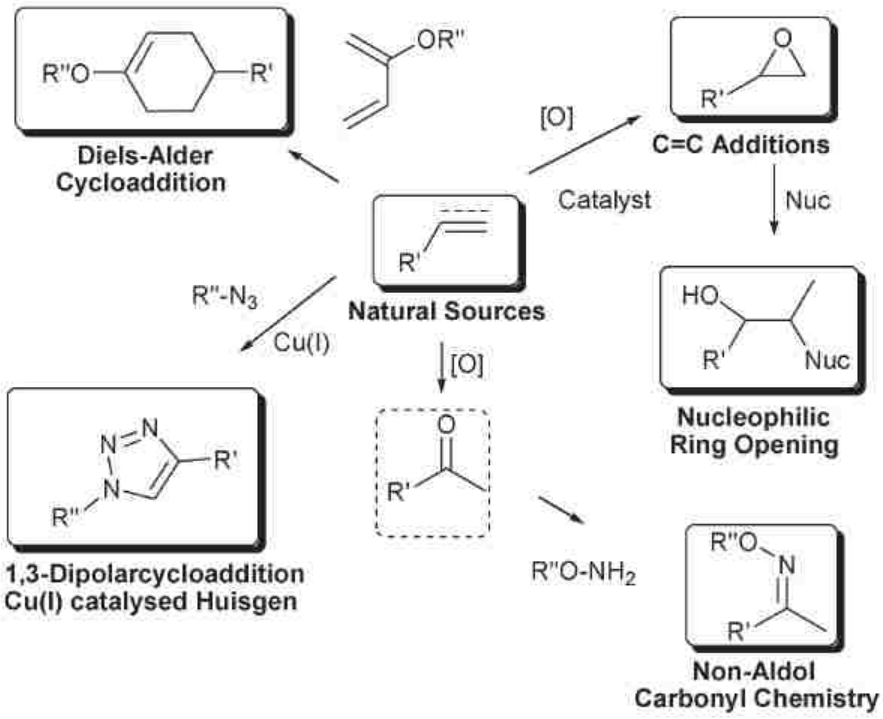

Figure 2.4: Types of click reaction[113]

2.6 Thiol-ene chemistry

Thiols are very prone to react with a multitude of substrates under varied conditions due to its high reactivity in the form of thiyl radical or catalyzed process under very mild reaction conditions[113, 114]. Although one major advantage of reaction orthogonality gets compromised when thiols are part of reactants in click chemistry, the thiol click chemistry is still widely used for the synthesis of small molecules and polymers. Figure 2.5 depicts the various thiol-based reactions with many aspects of click chemistry, which allows us to create or modify the range of molecules and materials using a family of thiols into new materials with altered physical, chemical and mechanical properties to meet the target requirements[114].

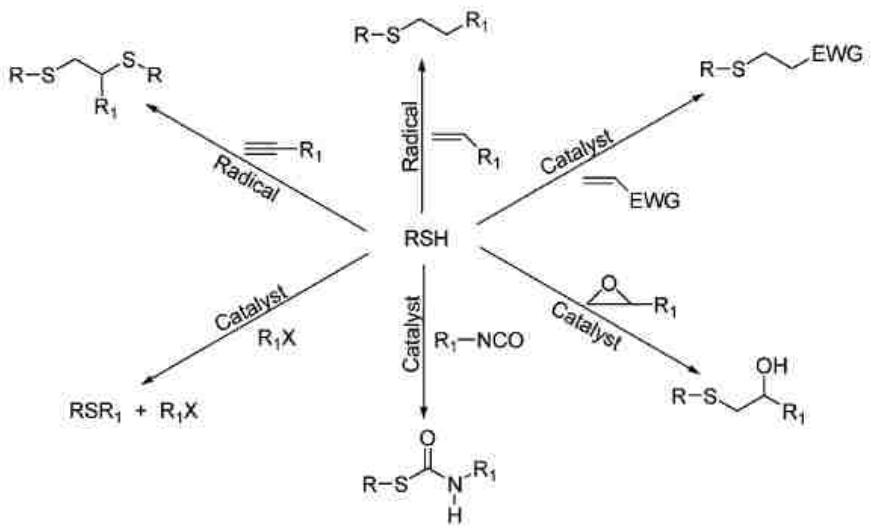

Figure 2.5: Types of reactions by thiol[114]

During mid-19th century, the Goodyear vulcanization process was the birth of classical commercial application of thiol-ene chemistry[115]. Thiol-ene click chemistry also referred as hydrothiolation process by many researchers, is the reaction that can proceed under different conditions including thiyl radical formation by catalytic processes mediated by nucleophiles, acids, bases in the absence of catalyst in highly polar solvents[116] or via catalytic pathway using b-cyclodextrin[117]. Reactivity can vary considerably depending on the type of thiols, i.e., S-H bond strength and cleavage mechanism, and type of C=C bond, i.e., activated, non-activated or multiply substituted olefinic bond. However, typically, they are rapid in ambient temperature, pressure, air/oxygen, moisture, and does not need to be carried out in the inert gas atmosphere[118].

Practically, the thiol-ene reaction is mostly studied in the form of photochemically or thermally triggered to generate radicals and mediate the process[119, 120]. The process typically is initiated by photo-induced formation of thiyl radicals by hydrogen extraction from thiol functional group and its addition to C=C bond resulting in the formation of an intermediate radical of carbon followed by chain transfer to next thiol. At the completion of each addition, an activated thiyl radical is generated which propagates the reaction by anti-Markonikov orientation. The process is terminated by radical-radical coupling

reaction[114, 120]. Figure 2.6 shows the schematic representation of initiation and propagation of thiol-ene click reaction.

Figure 2.6: Thiol-ene click reaction mechanism

2.7 Photoisomerization

Azobenzene undergoes clean and reversible conformal changes upon photon absorption called as photoisomerization (Figure 2.7). It leads to the significant changes in the physical and chemical properties of the molecules. Basically, for an azobenzene molecule with no substituent, the distance between the para positions decrease by 44%[121] and the dipole moment increases from 0 D to 3.0 D upon *trans* to *cis* isomerization[122].

Upon illumination, a steady state is reached between the photoinduced and thermally driven reactions by an azobenzene containing a sample, and along with the nature of chromophore, the stability of this state depends on many factors. The energy of the absorbed photon can drive the reaction towards either *trans* to *cis* or *cis* to *trans* isomerization. Since the *trans* isomer is more stable [123], the *cis* to *trans* reaction can also occur thermally. There is an order of magnitude difference in the timescale of photoinduced and thermally driven isomerization. The former takes place in picoseconds[124] and the later on the order of hours to seconds. Energy (wavelength) of an absorbed photon is the primary factor governing the photoisomerization. The energy barrier or the excitation energy required to raise the molecules to the photoexcited state is about 200 kJ/mol. π to

π* and n to π* are the two kinds of transitions mainly resulting from the excitation of delocalized π electron of the N-N double bond and the excitation of an electron localized on one of the nitrogen atoms respectively. Typically, two distinct peaks are visible for these excitations in the ultraviolet-visible spectrum. For the *trans* isomer, the n to π* transition is forbidden due to symmetry reasons, so in the ambient conditions, the *trans* π to π* transition band dominates the UV visible absorption spectrum of azobenzene molecules.

The wavelength of the UV-Visible absorption maximum (λmax) can be tuned by substituting the azobenzene using functional units with different electron donating or accepting properties. As a result, azobenzene absorbing anywhere from UV to green can be prepared.

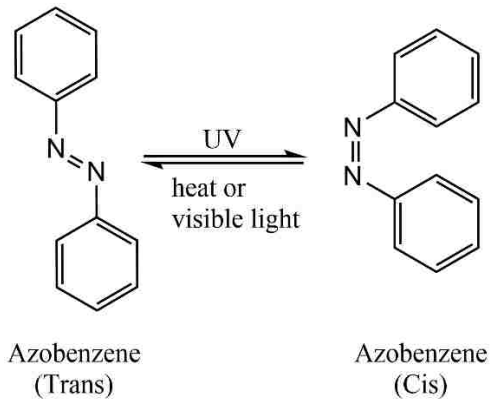

Figure 2.7: Photochemical and thermal isomerization of azobenzene

For azobenzene, two energetically allowed isomerization mechanisms exist: out of the plane rotation and in-plane inversion around the N-N double bond. Although the exact mechanism depends on the material and environment, the inversion requires much less sweeping volume and hence it is preferred[125]. The thermal isomerization determines the stability of the *cis* isomer and the applicability of the derivatives. The spectrum of the molecule and thermal *cis* lifetime provide useful insight into the molecules applicability, stability in *trans* or *cis* required in many photoswitching applications is best achieved by azobenzene type molecules with clearly separated *trans* and *cis* absorption bands and long *cis* lifetime. Solution and the bulk state both have a significant difference in the time scale of photo and thermal isomerization reactions[126].

3 Experimental procedures and characterization methods

3.1 Polymerization

3.1.1 Solution phase polymerization

We performed ring opening metathesis polymerization (ROMP) by adding an aliquot of catalyst solution to the appropriate monomer solution. Monomer solutions were prepared in dichloromethane (DCM) in most of the cases keeping volume between 1 ml to 2 ml. Immediately prior to use, a ruthenium (Ru) catalyst solution was prepared using Grubbs catalyst 2nd generation or 3rd generation. A fresh catalyst solution was used in all the cases due to its relatively low stability in the solubilized state as compared to solid state. The catalyst solution was added to monomer solution immediately and allowed to polymerize at room temperature and pressure. To deactivate the catalyst and terminate ROMP, 2-3 drops of ethyl vinyl ether was added to each sample, creating an inactive Ru-Fisher type carbene complex $(PCy_3)_2Cl_2Ru{=}C(H)OEt$ [127].

3.1.2 Thin film deposition and surface polymerization

3.1.2.1 Physical vapor deposition

Goal coated substrates were prepared by sputter coating gold on a silicon wafer. Chromium was used as intermediate layer (100 Å) between gold (1000 Å) and silicon wafer to provide adhesion between two layers. Hummer 8.1 DC sputtering machine was used to deposit chromium and gold in the silicon wafer. After sputter coating, the wafer was annealed at 220º C for 3 hours to obtain a very uniform layer of gold. The gold samples were cut out of wafer to the size of 1 x 3 cm, rinsed with ethanol and dried under UHP nitrogen jet before use.

3.1.2.2 Surface initiated ring opening metathesis polymerization (SI ROMP)

Gold coated substrates were placed in 1 mM solution of 11-mercapto-1-undecanol in ethanol for at least 60 minutes to form a crude, hydroxyl-terminated, self-assembled monolayer. Samples were rinsed with ethanol and dried under a stream of ultra-high purity (UHP) nitrogen. Monolayer coated substrates were exposed to a 5 mM solution of trans-3,6-endomethylene-1,2,3,6-tetrahydropthaloyl chloride ($NBCl_2$) in DCM for 30 minutes, yielding a norbornene functionalized surface [128]. Samples were rinsed with ethanol and

dried under a stream of nitrogen. Grubbs catalyst was immobilized on these substrates by immersing them in 5 mM solution of Grubbs 1st generation catalyst in DCM for 15 minutes. After 15 minutes, they were washed with DCM to remove unbound catalyst from the surface. Catalyst coated substrates were immediately put in a norbornene-based monomer solution for SI ROMP. Control surfaces of SI ROMP polynorbornene were prepared with a 0.5 M solution of norbornene (NB) in DCM. Crosslinked SI ROMP surfaces were prepared through the incorporation of up to 0.25 mol% of the DiNB crosslinker. Reaction time was adjusted to control coating thickness. Reaction times ranged from a few seconds to 2 hours.

3.2 Surface Characterization techniques

3.2.1 Contact angle goniometer

A Rame-Hart contact angle goniometer (Model 100) was used to measure the advancing and receding contact angle on polymer coated surfaces at room temperature and ambient relative humidity using deionized water as the solvent. The data was collected on the one side of the droplet and is reported as the mean ± standard deviation of at least eight samples.

Contact angle goniometer is one of the quickest, simplest and most convenient method for analyzing surface properties of thin films with respect to wettability and surface free energy[129, 130]. We used sessile drop method to measure the surface properties where a drop of about 5 μL was placed on the surface and measurements were performed by increasing or decreasing drop volume to record advancing or receding contact angle (Figure 3.1). The interfacial tension between solid-vapor (γ_{SV}), solid-liquid (γ_{SL}) and liquid-vapor (γ_{LV}) determine the shape of the droplet. Contact angle (Θ) is defined as the angle between liquid-solid interface and tangent to the liquid-vapor interface. A force balance between the interfacial tensions can be used to define contact angle mathematically. This is called as Young's equation, and hence the angle is also known as Young contact angle (Θ_Y)

$$\gamma_{SV} = \gamma_{SL} + \gamma_{LV} \mathrm{Cos}(\Theta_Y)$$

Typically, water or hexadecane are used to determine the surface properties such as surface's relative hydrophobicity/hydrophilicity and oleophobicity/oleophilicity

respectively. Contact angles can be divided into static and dynamic contact angle out of which static contact angle measurement is the most common method for characterization. Dynamic contact angle measurements are common among self-cleaning[131], responsive surfaces[132] and where surface properties change with time[133]. The contact angle recorded during expanding and contracting of a solvent droplet on the surface is called advancing (Θ_a) and receding (Θ_r) contact angle respectively. Surface composition is a major factor in altering the interaction of solvent and surface producing different contact angles for different surfaces. The contact angle hysteresis (Θ_a - Θ_r) is the measure of surface roughness and surface chemical heterogeneity[134].

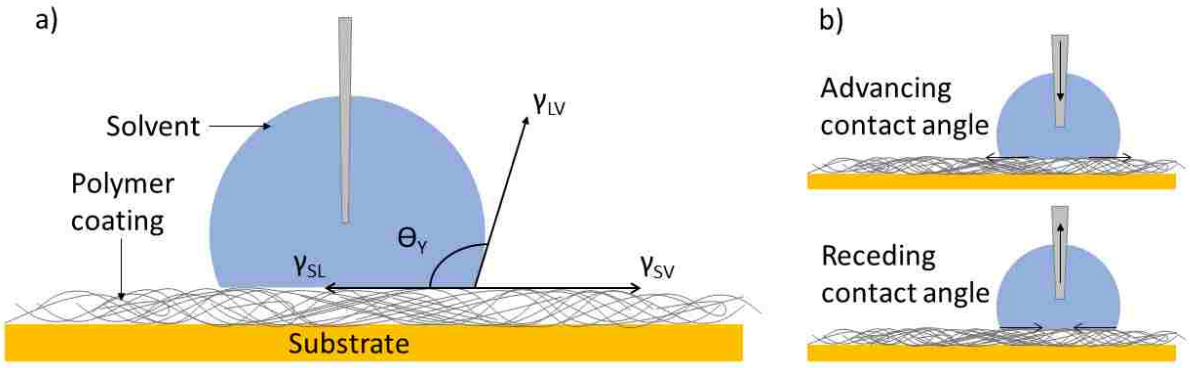

Figure 3.1: Schematic illustration of contact angle measurement in two different ways

3.2.2 Reflection absorption infrared spectroscopy

We used reflection absorption infrared spectroscopy (RAIRS) method to characterize and determine the surface compositional information of thin organic coating on reflective surfaces. Infra-red spectra are often specific to sample's composition, with absorption peaks which correspond to the frequencies of vibrations (bending, stretching, scissoring.) between the bonds of the atoms present in the organic coating. We used Agilent 680 Fourier transform infrared spectroscopy with an MCT external detector for compositional analysis of polymer coatings (Figure 3.2). The instrument was equipped with a Universal Sampling Accessory for grazing angle analysis of thin polymer coatings on metal surfaces. The p-polarized IR beam was reflected off the surface at an angle 80 degrees from the surface normal. 100 scans of background and each sample were performed at a resolution of 4 cm^{-1} from 800 cm^{-1} to 4000 cm^{-1}.

Sample analysis by RAIRS starts with the infra-red beam passing through the interferometer which has beam splitter and moving mirrors using which the beam energy on the organic coatings is controlled. This IR beam then enters the sample compartment and gets reflected off the sample, i.e., metal substrate with an organic coating on it. Here the light of a specific frequency characteristic to the coating composition are absorbed, and beam travels to the external detector to detect and record energy versus time data. This information is interpreted by a computer and is converted to energy versus frequency data using a fourier transformation, and final spectrum with absorption/transmission peaks associated with the molecular bonds and functional groups is presented.

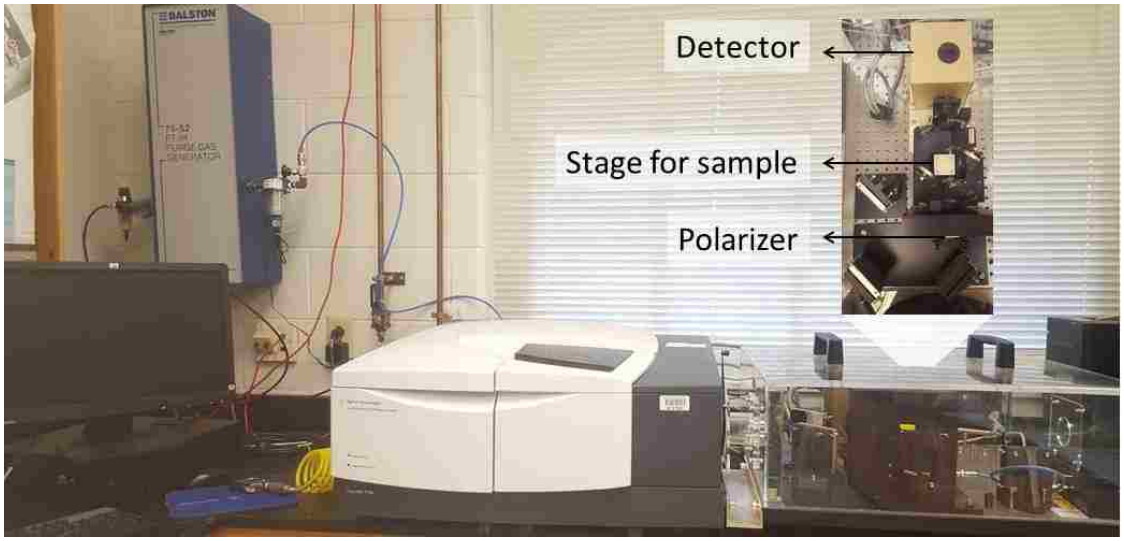

Figure 3.2: Photograph of FTIR spectroscopy instrument used with RAIRS setup in inset

The peak intensity for a given mode from RAIRS is proportional to the square of a component of its dynamic dipole moment normal to the surface represented by the following equation[135].

$$I \alpha \cos^2\Theta_{mz}$$

Where I represents the spectral intensity, Θ_{mz} represents the average angle made by transition dipole moment for the particular band and a surface normal (z). This directional dependence is due to the polarization of incoming beam parallel to the substrate, generating an electric field normal to the substrate[136]. Hence, functional groups present in the

coating with dipole moment normal to the substrate ($Cos^2\Theta_{mz}\rightarrow 1$) will have a higher spectral intensity than group dipoles parallel to the substrate.

3.2.3 Raman spectroscopy

Raman spectroscopy is one of the useful analysis tools for specific identification of molecules. The protocol requires merely shinning a laser source on an unknown chemical sample where some of this light is absorbed by the target substance, and most of it is scattered elastically in the direction of the laser source or different directions. A tiny percentage of light is inelastically scattered in series of different wavelengths that indicate the vibrational transitions in the molecule, which is analogous to the molecular fingerprint. This inelastic scattering of photons by molecules excited to higher vibrational or rotational levels is known as Raman scattering or the Raman effect[137]. The Raman effect was first reported by C. V. Raman and K.S. Krishnan[138], and independently by Grigory Landsberg and Leonid Mandelstam[139], on 21 February 1928. C. V. Raman received a noble prize for this discovery in 1930[140].

Scattered wavelengths are categorized into three types (Figure 3.3): Rayleigh scattering (no energy exchange), Stokes Raman scattering (scattered photons of less energy than incident photons), and anti-Stokes Raman scattering (scattered photons have more energy than incident photons). Surface enhanced Raman spectroscopy is a surface specific technique that enhances the Raman scattering by surface molecules on the reflective metal substrate, and the scattering is amplified by over 10^{10} to 10^{11} times. These substrates must have high uniformity and high field enhancement[141].

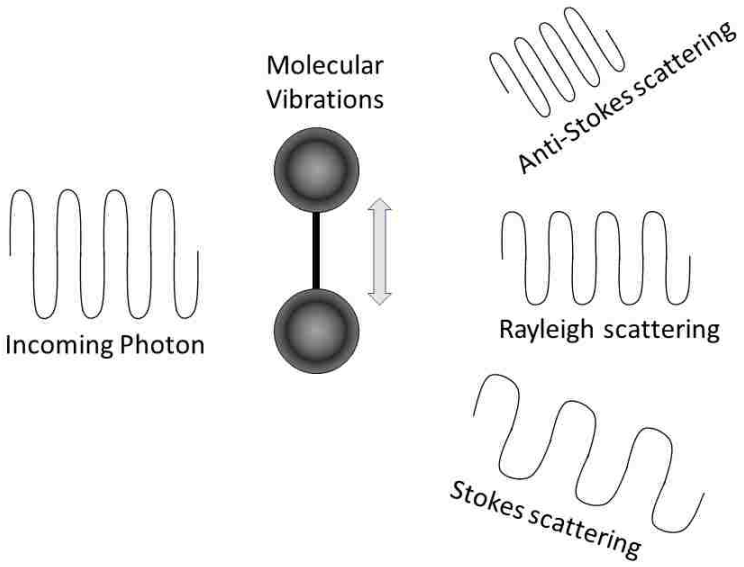

Figure 3.3: Schematic illustration of different form of scattering of incoming photo/wave through molecule

We used Raman spectroscopy to confirm the presence of low concentration of crosslinker in the thin coating. A Thermo Scientific DXR Raman microscope and Smart Raman spectrometer (532 nm laser) were used to analyze specific locations on the coated sample.

3.2.4 Electrochemical Impedance Spectroscopy

Electrochemical impedance spectroscopy (EIS) is a very powerful technique to measure barrier properties and understand the chemical structure of polymer coatings. EIS is very useful for sensor development, coating characterization, and corrosion analysis. We used a three-electrode electrochemical cell configuration consisting of a working electrode, a counter electrode, and a reference electrode. The polymer coated metal substrate is working electrode in contact with a liquid electrolyte solution containing other electrodes to close the circuit and define relative cell potential, all connected to alternating current source. Measurements are performed to determine the effect of the solution resistance to the ion transport through the thin coating, the charge of the double layer, and related current diffusion at altering the frequency of the AC source[142].

Equivalent circuits with resistors and capacitors for coating, interface, and solution, are used to model charge transfer through the coating. * Total impedance Z for the system can be represented using real (Z_{real}) and imaginary (Z_{imag}) components as follows.

$$Z = \sqrt{{Z_{real}}^2 + {Z_{imag}}^2}$$

$Z_{real} = R$

$Z_{imag} = \frac{1}{j\omega C}$

Where Z is the magnitude of total impedance Z, and R is the real resistance and C is capacitance. From the equation, we can confirm that higher film resistance and lower capacitance will result in higher total impedance, i.e., higher inhibition to ion transport [143].

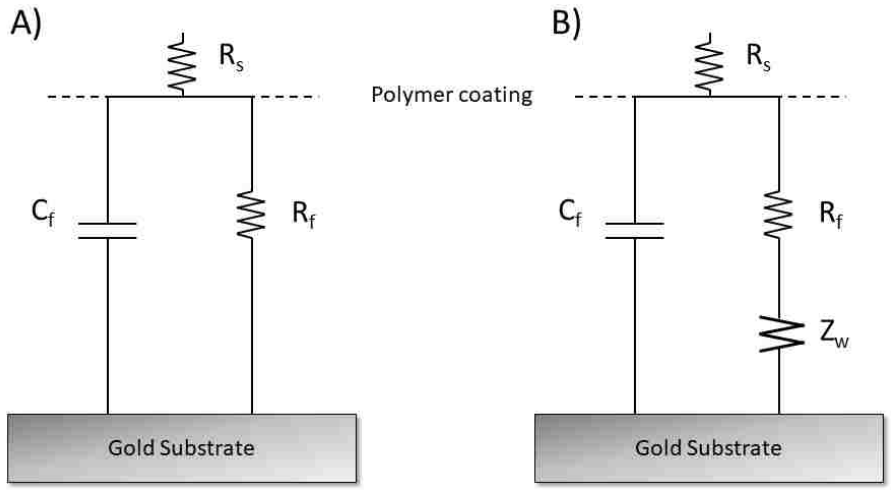

Figure 3.4: Equivalent circuit used to model impedance spectra for polymer coatings on gold;(A) Randles circuit model; (B) Randles circuit model with Warberg impedance

For our EIS we used flat cell (Princeton Applied Research, model K0235) and a Gamry Reference 600 potentiostat (Figure 3.5). The substrates were mounted on the flat cell with a fixed working electrode area of 1 cm^2. The polymer coated sample was used as a working electrode in combination with an Ag/AgCl/saturated KCl (aq.) reference electrode and a bare gold coated silicon substrate counter electrode in an electrolyte solution of 1 mM $K_3[Fe(CN)_6]$, 1 mM $K_4[Fe(CN)_6]$ and 0.1 M Na_2SO_4. Spectra were collected between 10^{-1}

and 10^4 Hz. A Randles equivalent circuit modified with Warburg Impedance was fit to the collected data to determine the film resistance and capacitance (Figure 3.4). All experiments were performed at room temperature. All reported data are the mean ± standard deviation of the measurement from at least eight samples.

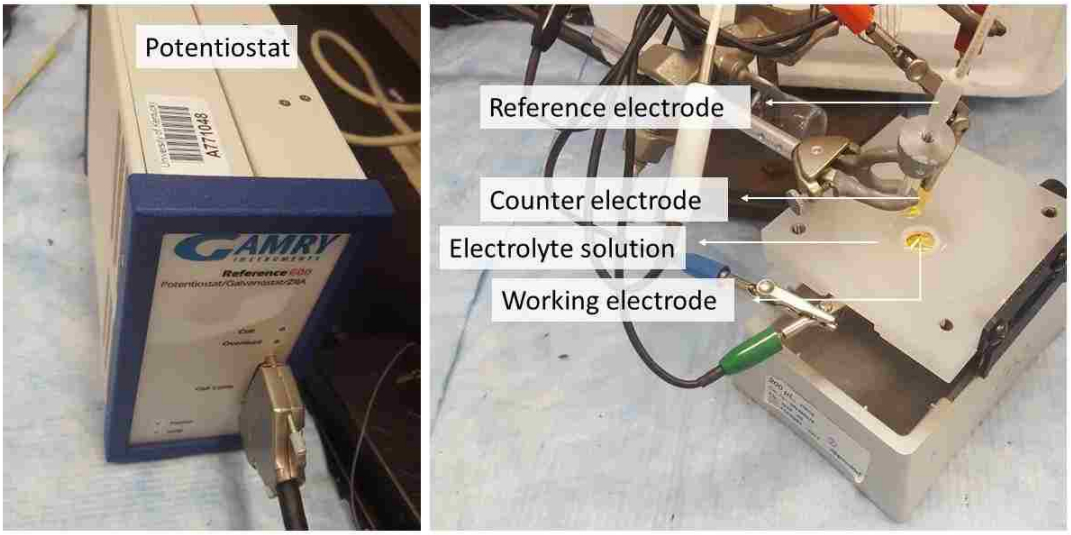

Figure 3.5: Potentiostat (left) and setup (right) used for electrochemical impedance spectroscopy

3.2.5 Ultraviolet-visible spectroscopy

Ultraviolet-visible spectroscopy is a type of absorption spectroscopy which provides the light absorption information by molecules due to their electronic excitation in ultraviolet and visible spectral region. The compound absorbances are mainly due to the excitation of either π electrons or non-bonding n electrons (Figure 3.6). These electrons absorb energy which corresponds to the lowest energy gap between highest occupied molecular orbital and lowest unoccupied molecular orbital[144].

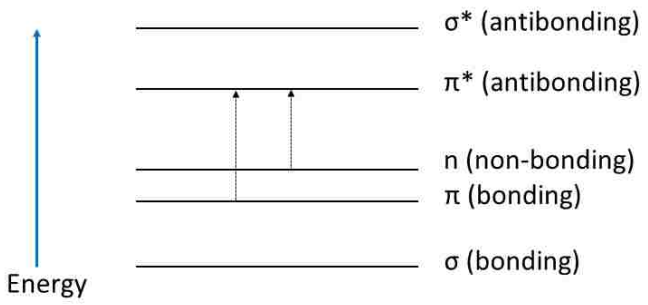

Figure 3.6: Schematic illustration of electronic excitation in molecular orbitals

We used UV-Vis spectroscopy in two different modes (single scan and kinetics) to collect the absorption properties of light responsive molecules. A single scan was gathered to identify the maximum absorption wavelength of light responsive compounds in *trans* conformation. Then these compounds were irradiated with LED UV (365 nm), green (530) and royal blue (455 nm) lamp, and UV-Vis spectrum was collected immediately to obtain absorption spectrum when the majority of molecules are in the *cis* conformation. Another software was used to collect the kinetics of relaxation of molecules from *trans* to *cis* while having external irradiation ON, and back from *cis* to thermodynamically stable *trans* conformation in dark or again under external irradiation, with respect to time. All the experiments of collecting thermal relaxation were conducted in the dark to avoid interference by stray light.

Orthogonal irradiation was used in experiments where external irradiation was required during spectral data collection (Figure 3.7). The external radiations were incident on the solution in a manner so as not to interfere with the radiations by the internal light source.

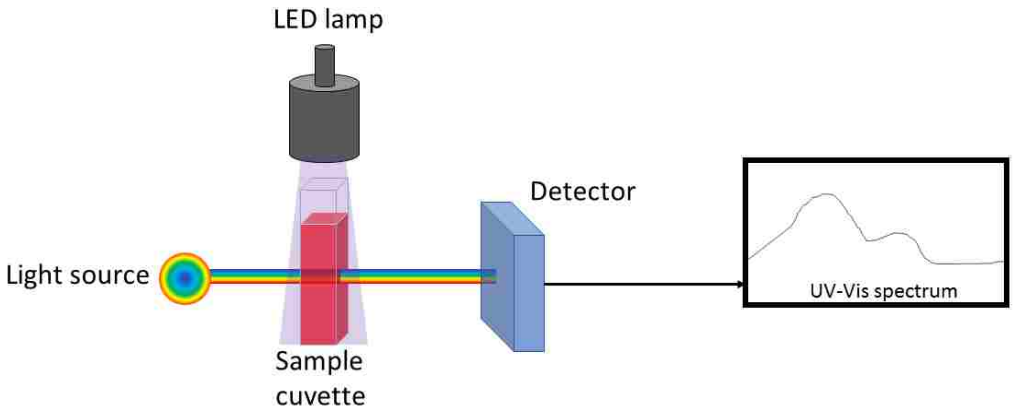

Figure 3.7: Schematic representation of UV-Vis setup used to determine absorption properties

We used Varian Cary 50 Bio UV-Visible spectrophotometer equipment to collect absorption spectra of all the light responsive monomers.

3.2.6 Nuclear Magnetic Resonance spectroscopy

Since the discovery of Nuclear Magnetic Resonance spectroscopy by Felix Bloch and Edward Mills Purcell in 1952, it has grown to a standard technique in the determination of the structure and dynamics of molecules at atomic resolution. NMR provides qualitative and quantitative information about the chemical species present in the sample. The fundamental principle behind NMR spectroscopy is absorption and re-emission of electromagnetic radiation by nuclei when placed in the external magnetic field. When placed in the external magnetic field, NMR active nuclei like ^{1}H and ^{13}C absorb electromagnetic radiation at a frequency characteristic to each isotope [145]. Nuclei have their unique spin, but only those who have a spin of ½ are NMR active and can be observed by NMR. Different NMR techniques depending on the isotope of the element (^{31}P, ^{19}F, ^{1}H, ^{13}C) to be monitored used in the analysis. We used proton NMR to obtain all the qualitative and quantitative information like type of hydrogen (α or β to functional group present) and a number of hydrogen present. This technique utilizes deuterated solvents to minimize the interference of absorption of electromagnetic radiations by protons in the solvent.

NMR spectroscopy was used for the chemical characterization of the crosslinker, photo-responsive monomers, intermediate compounds and to confirm conversion of solution

phase polymerization. Varian 400 MHz NMR spectroscopy equipment was used for proton NMR spectroscopy with the minimum number of 32 scans for quantitative determination of peak position and integration.

3.2.7 Spectroscopic Ellipsometry

Ellipsometry is a non-invasive, non-contact, and non-destructive optical technique used to measure the thickness and refractive index of monolayers, polymer coatings, or multilayer films[146]. Depending on the homogeneity of the coating, thickness as low as 0.1 nm and as high as 100 μm can be measured with this tool[147]. A beam of linearly polarized light of specific wavelength is shone on the coating on a reflective metal substrate (Figure 3.8). The optical interaction of the light with the coated surface causes the reflected light to be elliptically polarized, and the detector collects the phase (Δ) and amplitude (Ψ) of the light polarization. This information is utilized to fit into theoretical model layers representing the coating on the surface. The generic two-term Cauchy layer model is common to analyze polymer coatings [148].

$$n = A_n + \frac{B_n}{\lambda^2}$$

Where *n* is the refractive index of the coating, A_n and B_n are the model fit parameters, and λ is the wavelength of incident linearly polarized light. As both parameters, coating refractive index and coating thickness are to be determined, the Cauchy layer model allows them to be calculated by fitting model to experimental data and minimizing the mean square error between them[149]. Data were collected from three different angles of 55º, 65º, and 75º and over an extensive wavelength range from 400 nm – 700 nm. In this work, all the data was best fit for A= 1.45 and B = 0.01[150].

All measurements were collected with a J.A. Woollam Ellipsometer M-2000 (Figure 3.9). Optical modeling and data analysis were performed using the WVASE 32 software package. Theoretical structures were created in the form of the optical model in the software, and the physical and optical properties of each layer were extracted accordingly. We created a four-layer model to account for the silicon dioxide, chromium, gold, polymer layers in our system.

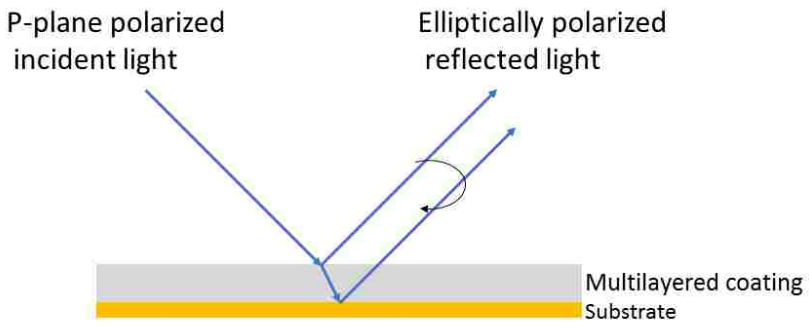

Figure 3.8: Schematic representation of path of radiation through polymer coating in ellipsometry

Figure 3.9: Photograph of J.A.Woollam Ellipsometer M-2000

3.2.8 Profilometer

A contact stylus type profilometer was used to determine film thickness of the polymer coatings. The polymer coating was scratched with a wooden pick to remove the polymer coating along a narrow region while the underlying gold coated silicon substrate was unaffected. As the tip follows the contour of the surface, the vertical displacement of the stylus attached to the cantilever is proportionally translated into voltage change as output which is then converted to the thickness using appropriate calibration[151]. The difference in height between the coated and uncoated region is interpreted as the polymer coating thickness.

A Dektak6m programmable surface profiler measuring system was used to measure the scratch depth at an applied force of 3 mg and a 1.000 mm scan length, and employing the

hills and valleys detection mode (Figure 3.10). The scan results were presented in the form of vertical displacement (change in height) from mean height versus horizontal displacement from starting position using the same software of the instrument. The data represented here is average value and error of at least 8 independently prepared samples.

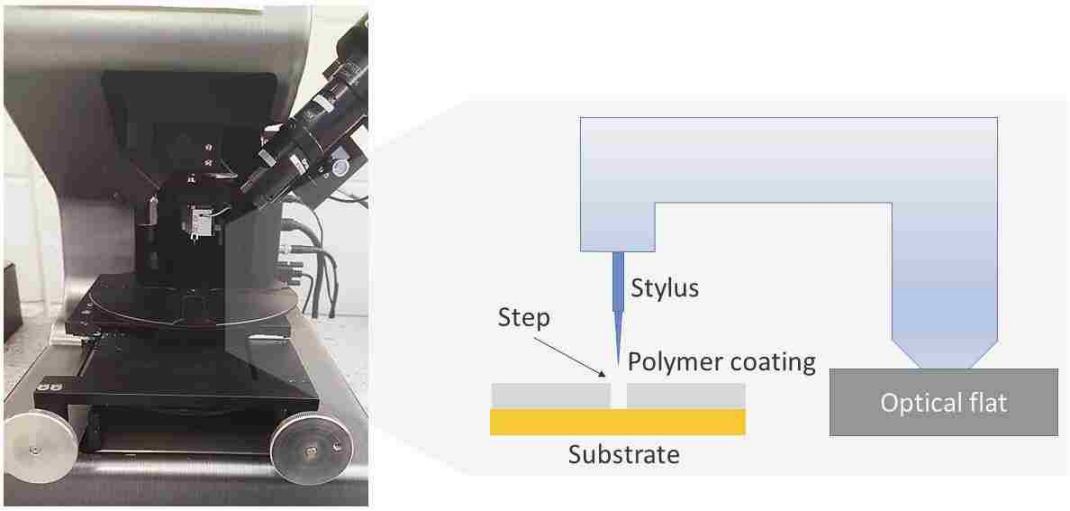

Figure 3.10: Photograph of profilometer instrument and schematic representation of stylus and coating

3.2.9 Gel permeation chromatography

Gel permeation technology (GPC) is a standard analytical technique to determine molecular weight distribution of soluble macromolecular species. GPC is a type of size exclusion chromatography where analytes are separated based on hydrodynamic size and pore size of packing material used in the column. Packing material can be either beads of rigid porous gel, highly crosslinked porous polystyrene, or porous glass packing.

A sample of the dilute polymer solution is injected into the mobile phase, and as the polymer chains flow through the column, they get separated based on their size. Smaller molecules diffuse into pores while macromolecules cannot enter the pores. As a result, small molecules have more accessible volume in the column and are retained in the column longer than larger molecules. The elution time of each species is compared to the elution time of polymer standards of known molecular weight to determine estimate molecular weight distribution and polydispersity index (PDI). Molecular weight according to the

different definition of number average molecular weight (Mn), and weight average molecular weight (Mw) can be obtained.

In our experiments, we used pure tetrahydrofuran (THF) as mobile phase (1 mL/minute) with polystyrene standards. The column was purchased from Shimadzu, and refractive index detector.

3.2.10 X-ray photoelectron spectroscopy

X-ray photoelectron spectroscopy also known as electron spectroscopy for chemical analysis, is a sensitive technique for determination of qualitative and quantitative elemental composition in top 10 nm of material. XPS spectra are obtained by irradiating the material with a high intensity focused beam of x-ray which triggers the emission of electrons from top 0-10 nm of materials. The kinetic energy of these emitted electrons is measured to analyze the surface chemistry. XPS is routinely used to find contamination in bulk or surface of the sample, empirical formula of material, chemical state of elements present, or binding energy. It is used in all diverse fields of photovoltaics[152], corrosion[153], nanomaterials[154], and thin coatings[155]. Typically, XPS spectrum of the material is obtained before and after treatment to compare the change in elemental composition. XPS system mainly consists of sample introduction chamber, a sample stage, ultra-high vacuum stainless-steel chamber with a vacuum pump, an electron collection lens, and electron detector system. X-ray can be made incident at different angles to vary the surface penetration.

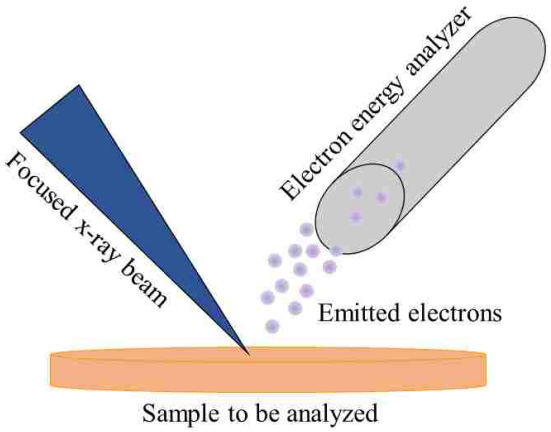

Figure 3.11: Schematic representation of XPS setup

XPS spectra were collected using X-rays generated by a Mg-K-α source (1253.6 eV, PHI 04-548 dual anode X-ray source), an 11" diameter hemispherical electron energy analyzer with the multichannel detector, with pass energies of 23.5 eV and 0.025 eV step size (PHI 5600). All the samples were measured with 45º take-off angle.

3.2.11 Atomic force microscopy

Atomic force microscopy (AFM) or scanning force microscopy is a form of scanning probe microscopy, designed to measure surface topography, friction, magnetism, etc. AFM is used in wide range of disciplines, and has found particular utility in semiconductor technology, natural sciences, polymer chemistry, and cell biology [156-158]. This information is collected by either continuously contacting the surface with a probe or tapping the surface continuously using a fine tip [159, 160]. AFM has a cantilever with a sharp tip of diameter on the order of nanometers which undergoes deflection in the proximity of the surface due to the forces between them (van der Waals forces, dipole-dipole moment, electrostatic forces, etc.) according to the Hooke's law. These deviations are recorded using change in the position of the laser on position sensitive detector and converted to the required readable format, i.e., image or text format.

In our studies, we exploit tapping mode (dynamic) AFM techniques. Tapping mode has an advantage over contact mode AFM preventing the tip from sticking the surface due to short-range forces. In tapping mode, the cantilever is oscillating up and down near its resonance frequency using small piezo element, and the oscillation frequency, phase, and amplitude are altered over surface irregularities.

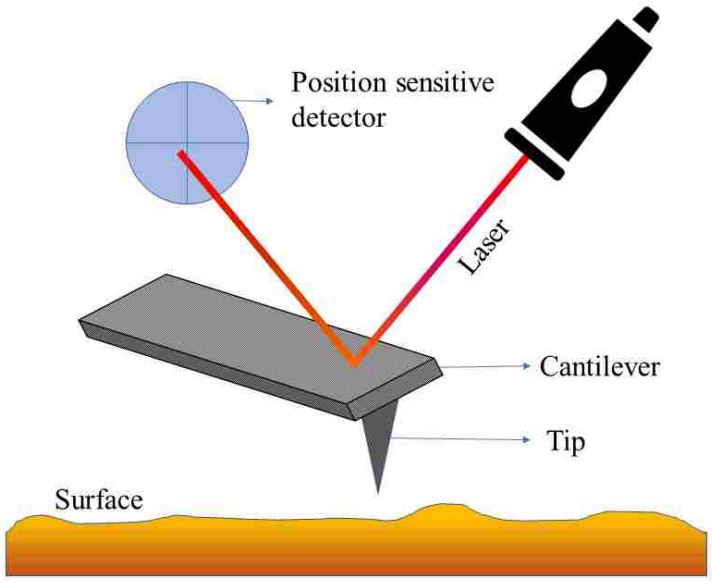

Figure 3.12: Schematics of AFM setup

We used Agilent Technologies 5500 scanning probe molecular imaging AFM instrument. Images of 10 μm x 10 μm are collected in tapping mode with silicon tip of average frequency 300 kHz.

4 Modification of SI ROMP polynorbornene brushes by thiol-ene click chemistry

4.1 Introduction

The surface coating is an integral part of any instrument used in the industrial environment, research, medical applications, and household applications to protect it from overtime damage due to the environment. However, along with the ability to protect, additional surface properties enable profound impacts on the target application. Hence, polymer coatings are usually modified with different functional groups to tune the surface with properties such as hydrophobicity or hydrophilicity[24], adhesiveness[161], and surface charge[162] as desired in the final application. Polymer coatings prepared by 'grafting from' technique like surface initiated polymerization techniques (SIP) are replacing conventional coating methods in many applications, due to their superior control over thickness, greater coating uniformity for thin coatings, and greater resistance to delamination from shear forces [163]. Moreover, the most important advantage is its ability to grow a film on any complex surface. There are various types of SIP methods like surface initiated atom transfer radical polymerization (SI ATRP)[31], surface initiated reversible addition-fragmentation chain transfer polymerization (SI RAFT)[36], surface initiated ring opening metathesis polymerization (SI ROMP)[68] and many others.

Here, we focus on functionalized polynorbornene (pNB) coatings grown using SI ROMP. Ring opening metathesis polymerization (ROMP) is well studied and established method for controlled polymerization of strained cyclic olefin monomers such as norbornene, cyclopentane, and cyclobutene [164]. ROMP has several advantages over other methods of polymerization in terms of control over the rate of polymerization, molecular weight distribution, tolerance towards functional groups, high molecular weight polymer under mild conditions, living type of polymerization, and short reaction times[46, 85, 163, 165, 166]. Norbornene and its derivatives are the most commonly used monomers for ROMP studies[167]. See Figure 4.1. While SI ROMP is a relatively new coating chemistry, it has been used in diverse applications, including upgrading surfaces with better adhesive properties[90], the functionalization of carbon nanotubes and graphene oxide [168-170],

the formation of photo-responsive surface[171], and tailoring fuel cell electrode interfaces[172]. Norbornene is an attractive ROMP monomer owing to high internal ring strain, chemical inertness, and excellent solubility in different solvents [46, 84, 85, 165, 166, 173-175]. It has ring strain of 21.6 kcal/mol which is significantly higher than the minimum ring strain (13.3 kcal/mol) required for propagation of ring opening polymerization[48, 176]. However, as we add a functional group or alkane chain to the cyclic ring of norbornene, the ring strain energy slightly expected to change[176]. The rate of ROMP is directly proportional to the ring strain energy of cyclic ring monomer [94, 177, 178]. Hence if we want to generate polynorbornene chains with a functional group as a branch on the backbone, then we have to compromise the rate of chain growth due to lower ring strain of monomer and also achieve lower final thickness as compared to film thickness obtained by pNB[128]. Also, the synthesis of derivatives of norbornene by diels alder reaction yields endo isomer product predominantly[175]. Whereas exo isomer of norbornene derivative is more active towards ROMP[179]. Hence synthesis of customized monomer for functionalized SI ROMP coatings is more tedious approach.

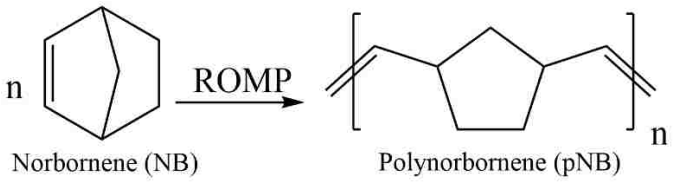

Figure 4.1: Ring opening metathesis polymerization of norbornene

As an alternative, here we have explored the new approach of functionalizing the pNB coatings. Here we adopted the technique of 'grafting-onto' and click chemistry to modify pNB polymer brushes. There are carbon-carbon double bonds in the backbone of pNB (Figure 4.2). We used these unsaturated functionalities to add desired functionality as a branch without compromising the high rate of polymerization and coating thickness of pNB. We use simple molecules with the head group as desired functionality in modified coating and tail group as a functional group like thiols or primary amines that can be added across carbon-carbon double bond easily. As we use simple NB monomer with very high ring strain energy, it enables us to reach thickness from nanometers to micrometers. We

used thiol-ene click reaction to add functionalized thiol molecules using free radical addition across carbon-carbon double bonds of pNB polymer brushes.

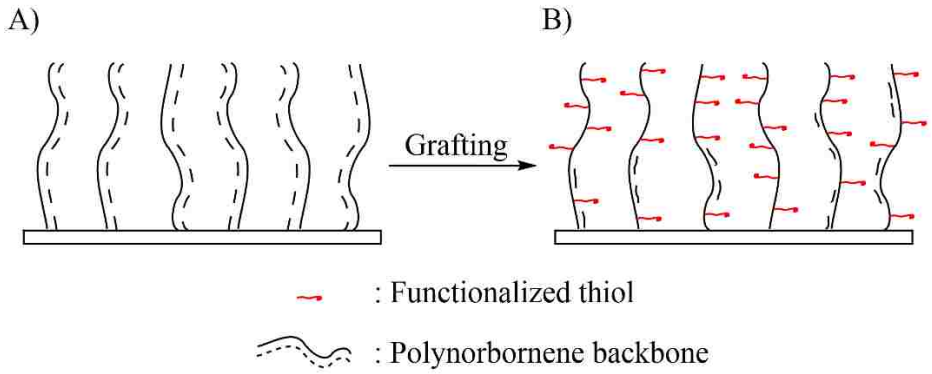

Figure 4.2: Schematic representation of polymer brushes before after grafting; A) pNB polymer brushes before grafting, B) pNB polymer brushes after grafting with thiol molecules

Click chemistry is a set of reactions with properties like high yield for product and inoffensive by-product, regiospecificity, versatile, rapid, easy to purify without chromatographic methods and can be conducted in easy to remove benign solvents[108, 109]. Thiols are very prone to react with a multitude of substrates under varied conditions due to its high reactivity in the form of thiyl radical or catalyzed process under very mild reaction conditions[113, 114, 180]. Although one major advantage of reaction orthogonality gets compromised when thiols are part of reactants in click chemistry. However, the thiol click chemistry is still widely used for the synthesis of small molecules and polymers.

Thiol-ene click chemistry is the reaction that can proceed under different conditions including thiyl radical formation by catalytic processes. Reactivity can vary considerably depending on the type of thiols, i.e., S-H bond strength, cleavage mechanism, and type of C=C bond, i.e., activated, non-activated or multiply substituted olefinic bond. However, they are typically rapid at ambient temperature, pressure, air/oxygen, moisture, and does not need to be carried out in the inert gas atmosphere[60, 114, 118].

Practically, the thiol-ene reaction is mostly studied in the form of photochemically or thermally triggered to generate radicals and mediate the process[119, 120, 181]. The process typically is initiated by photo-induced formation of thiyl radicals by hydrogen

extraction from thiol functional group and its addition to C=C bond resulting in the formation of an intermediate radical of carbon followed by chain transfer to next thiol. At the completion of each addition, an activated thiyl radical is generated which propagates the reaction by anti-Markonikov orientation. The process is generally terminated by radical-radical coupling reaction[114, 120].

4.2 Materials

11-Mercapto-1-undecanol (97%), *trans*-3,6-endomethylene-1,2,3,6-tetrahydonedropthaloyl chloride (97%), Grubbs catalyst - first generation (benzylidene-bis(tricyclohexylphosphine) dichlororuthenium) (97%), Bicyclo [2.2.1]hept-2-ene (99%), Irgacure-184 (I-184), 1-dodecanethiol (98%), 1H,1H,2H,2H-Perfluorodecanethiol (97%), 1,6-Hexanedithiol (96%). Dichloromethane (DCM) (99.9%), Ethyl alcohol (EtOH) (99.8%).

4.3 Result and discussion

Polynorbornene coatings were made prior to functionalization by surface initiated ring opening metathesis polymerization. The detailed procedure for making SI ROMP coatings of norbornene is in section 3.1.2.2. The polymer coatings were then characterized using surface characterization methods to determine its surface properties in terms of composition and thickness. Contact angle goniometer was used immediately (within 3-4 minutes) after making SI ROMP coatings to determine surface hydrophilicity or hydrophobicity, reflection absorption infrared spectroscopy (RAIRS) was used to find molecular composition of SI ROMP coatings giving detail information about types of covalent bonds present in the polymer chain, and ellipsometer was used to determine thickness of the surface polymer coatings. SI ROMP coatings were characterized using all three methods before and after their modification with pendant functional groups. We used thiol-ene click chemistry to graft functionalized alkane chains in the backbone of surface PNB brushes. Irgacure-184 photoinitiator was used to generate free radicals for initiation of photochemical reaction/grafting. The polymer chains in the SI ROMP coatings were immersed in DCM solutions of I-184 photoinitiator and thiol. After 1 minute, the sample was irradiated with UV 365 led lamp by Thorlabs (700MA and 190mW minimum) at maximum intensity (~15 mW/cm^2) to generate free radicals of photo-initiator. These active

thiyl radicals then undergo thiol-ene addition across the carbon-carbon unsaturated functionalities present in the backbone of polynorbornene chains. We optimized the concentration of I-184 and thiol to be grafted and the time required to get the optimum amount of grafting. Different functionalized thiols were used to investigate the flexibility of the process. The resulting coatings were then washed with dichloromethane, ethanol, and water, and dried with UHP nitrogen jet to get dry coatings for further characterization. Our system was designed to minimize the distance between light source and target surface to have the least absorption by the solution as shown in Figure 4.3.

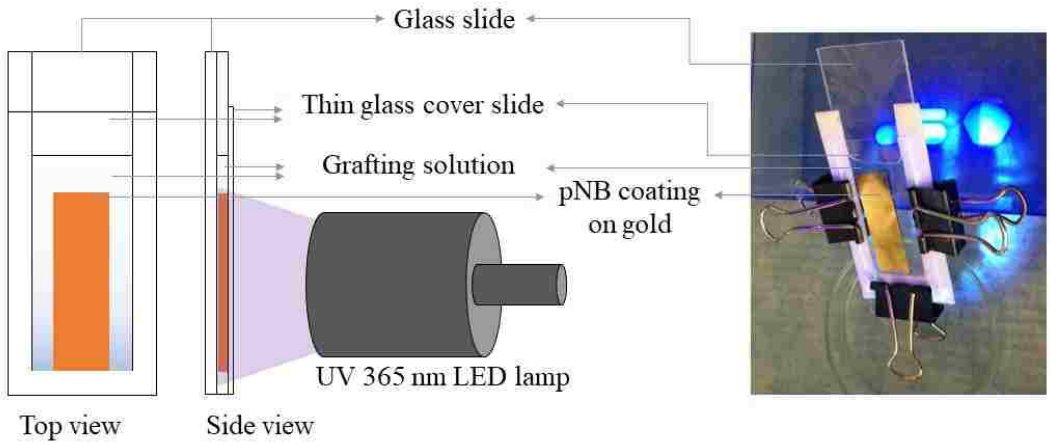

Figure 4.3: Schematic representation of experimental setup

4.3.1 Grafting across pNB brushes

Three distinct types of thiol molecules (Figure 4.4); 1-Dodecanethiol, 1H,1H,2H,2H-Perfluorodecanethiol and 1,6-Hexanedithiol were used for free radical grafting across pNB SI ROMP coatings. 1-Dodecanethiol was used to confirm the surface chemistry by observing the changes in the methylene vibration peaks in RAIRS. 1H,1H,2H,2H-Perfluorodecanethiol is also a linear molecule but has fluorine atoms at the terminal carbons atoms in the chains. We expect to change the surface hydrophobicity drastically due to the presence of fluorine atoms on the surface. Lastly, 1,6-Hexanedithiol is also a linear molecule but has twice the number of thiol groups in same structure than previous two types of molecules. These three thiol molecules with different structures were selected to investigate the grafting-onto technique with various aspects.

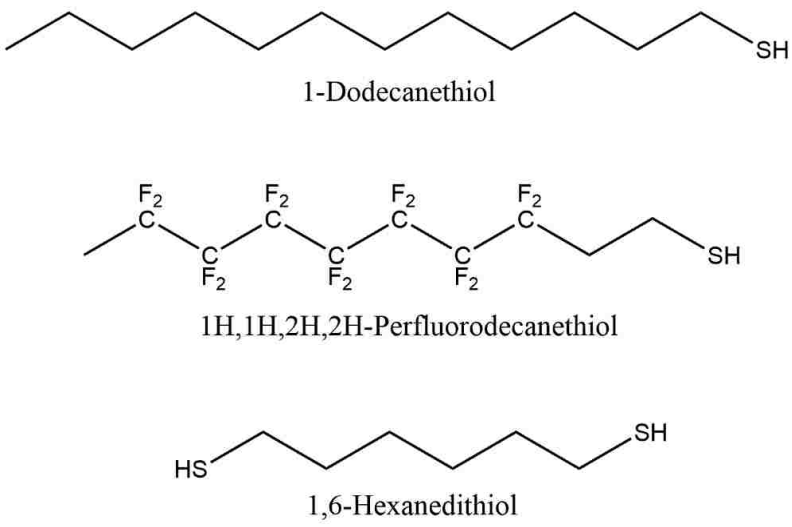

Figure 4.4: Three types of functionalized thiol molecules used for grafting-onto pNB polymer brushes

4.3.1.1 1-Dodecanethiol

1-Dodecanethiol was used as the first grafting thiol-molecule because it has no other functional group except thiol in its molecular structure. Our first goal is to confirm the surface chemistry, and this would provide information only about the chemical reaction between thiol functional group and polymer brushes. Polynorbornene coatings were grafted with 1-dodecanethiol at the unsaturated functionality in the polymer backbone using thiol-ene chemistry. A solution containing 100 mM of 1-dodecanethiol and 1 wt% of I-184 was prepared in DCM. The solution vials were wrapped with aluminum foil to avoid the formation of disulfides on exposure to UV radiations in sunlight. The thiol and photoinitiator concentration used for the experiments fall in the typical concentrations range used in thiol-ene polymerizations or similar reactions[182-184].

On complete grafting of pNB brushes by thiol molecule, we expect an increase in the film thickness and change in the film composition. We investigated the process of thiol grafting from 1 minutes to 20 minutes. However, having a higher time of surface reaction/UV exposure resulted in side reactions causing surface polymer brushes to cleave resulting in a decrease in the film thickness of forming a non-uniform coating with ‘island’ type residues of coating on a substrate with rough surface topography. This was confirmed by an ellipsometer, as it was calculating measurable thickness values at some spot and resulted in zero thickness at different region on the same sample after thiol-grafting. Whereas very

short reaction times did not result in any measurable conversion of unsaturated functionality to saturated carbon-carbon bond with pendant thiol molecule, confirmed by RAIRS. However, the reaction time of 3 minutes resulted in detectable grafting confirmed by RAIRS and ellipsometer with minimal film loss.

To measure surface composition, the modified coatings were immediately characterized by contact angle goniometry before the polymer brushes dry out and form a well-packed coating on the surface. The pure PNB coatings are hydrophobic in nature which can be confirmed from its relatively high advancing contact angle. The average advancing contact angle for pure PNB coatings was found to be 95º. Moreover, the receding contact angle was 64º. For PNB coatings grafted with 1-dodecanethiol, the average advancing contact angle was 95º, and the average receding contact angle was 76º. The contact angle did not change much as there was no compositional difference before and after addition of simple alkane molecule. Structure of polymer brushes before and after the addition is shown in the figure. When there were pure polynorbornene chains, the main structure had on cyclic CH_2 and unsaturated CH between cyclopentane rings. Both impart hydrophobic nature to the surface. After adding alkanethiol to the chain, the addition was mainly of saturated CH_2 introducing no major difference in the composition and hence we did not expect and observed any change in advancing contact angle. The receding contact angle, a measure of hydrophilicity of coating had difference after the modification which can be attributed to the minute difference in the polarity of unsaturated CH and saturated CH_2. In pure PNB coatings we had 2 out of 7 carbons as unsaturated CH_2, but after modification, they were replaced by saturated alkane chains and more saturated CH_2 were added which resulted in the decrease in the hydrophilicity of chains and hence increase in the receding contact angle.

IR spectrum was used to confirm the grafting of alkane chains across polymer backbone. In the spectra for the pNB coatings (Figure 4.5), distinct methylene peaks were observed for symmetric stretching, asymmetric stretching, and scissoring modes. The C-H stretching region for pNB coating IR spectra has strong cyclic methylene peaks at 2946 cm^{-1} (asymmetric) and at 2863 cm^{-1} (symmetric) with an additional stretching peak at 2908 cm^{-1} [185]. Methylene scissoring peak for methylene in cyclic structure is seen at 1455 cm^{-1}

indicating a relatively homogenous and well-ordered chain structure [186]. The out of plane bending peaks for C=CH olefin functionality [185, 187] are seen at 968 cm^{-1} and a shoulder-like C=CH stretching peak at 3030 cm^{-1} [185, 187]. We did not observe any peak for C-S absorption as it generates very weak peak as compared to other IR peaks. Also, we did not see any S-H peak from residual thiols if there was any after washing coatings, which indicated the surface had only modified pNB coatings.

After free radical grafting, the addition of alkanethiol increased the alkyl functionality on the spectrum with almost undetectable alkene functionality. The complete removal of 968 cm^{-1} and 3030 cm^{-1} peaks are indicative of successful addition of 1-dodecane thiol to the surface coating. Addition of acyclic methylene and decrease in C=CH out of plane bending at 968 cm^{-1} was seen in the opposite pattern. C=CH stretching peak at 3030 cm^{-1} also got diminished after surface grafting experiment. The contribution by cyclic methylene peak position is altered indicating the changes in the packing structure after modification. The stretching peak for acyclic methylene is seen distinctly at 2923 cm^{-1} (asymmetric) and at 2852 cm^{-1} (symmetric) while contribution by cyclic methylene stretching decreases reversely at 2953 cm^{-1} (asymmetric) and a small shoulder on the left part of the peak at 2851 cm^{-1} (symmetric). Methylene scissoring peak remains almost same at 1455 cm^{-1} indicating no change in the cyclic structure of cyclopentane ring. A tiny shift in the peak of cyclic scissoring is indicative of changes in the crystallinity of coating after modification. IR spectrum of modified pNB coatings had similar IR spectrum but with significant difference providing the solid proof of grafting across carbon-carbon unsaturated bond.

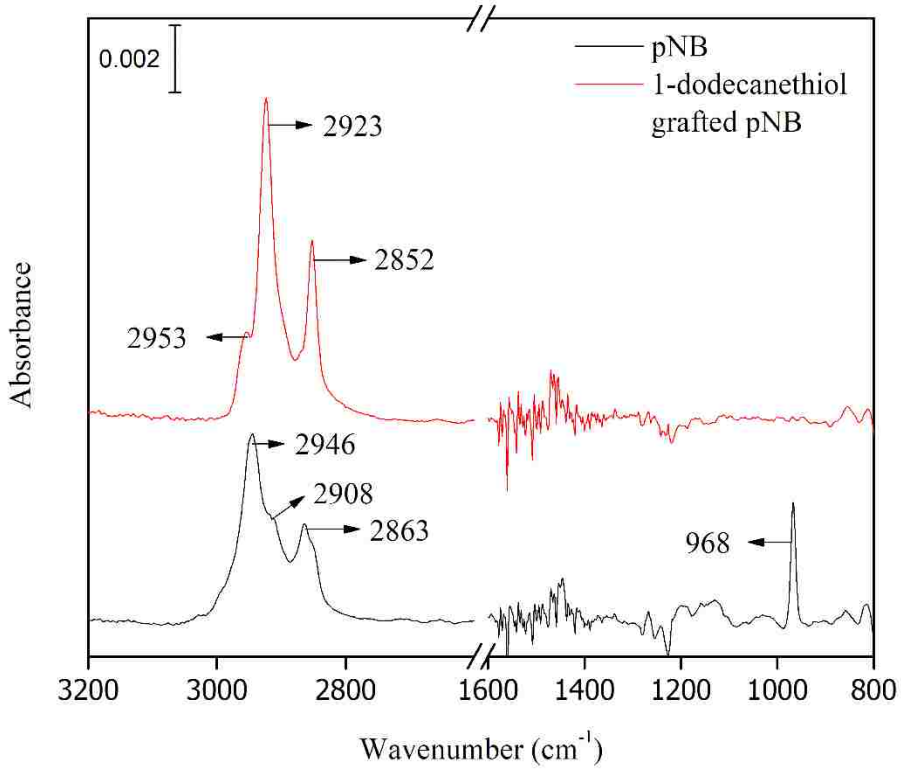

Figure 4.5: RAIRS spectrum of pNB grafted by 1-dodecanethiol

4.3.1.2 1H,1H,2H,2H-Perfluorodecanethiol

After confirming this process of surface engineering by click chemistry, we extended it to another functionalized thiol; fluorine functionalized thiol. Here we used fluorinated thiol; 1H,1H,2H,2H-perfluorodecanethiol and generated its thiyl radicals in the same fashion as before. Fluorinated polymer coatings exhibit excellent barrier properties[188], very low critical surface tension[189] and low adhesion property[190]. However, it is difficult to make a film of the fluorinated polymer due to its relatively low solubility in common organic solvents[190, 191].

Similar concentrations for thiol and I-184, i.e., 100mM and 1weight% were used for this experiment of photochemistry. The optimized time for photochemistry was about 4 minutes, yielding modified coatings with least film loss and most grafting. We analyzed the surface immediately after drying the modified coating with contact angle goniometry. The average advancing contact angle we obtained was 130º, whereas the average

advancing contact angle for pNB coating we obtained is 95º. The significant change in contact angle is the indicative of a change in surface composition from mildly hydrophobic to the highly hydrophobic surface, which is indicative of addition of successful grafting of fluorinated molecules in the polymer chains.

We interrogated the 1H,1H,2H,2H-perfluorodecanethiol coatings with RAIRS to confirm the modification of pNB with fluorinated thiols. Carbon-fluorine bonds are well known for producing strong and sharp absorption peaks in IR spectroscopy suppressing other absorption peaks on the surface[192, 193]. In Figure 4.6, the strong C-F absorption peaks are observed between 900 cm^{-1} and 1400 cm^{-1} for the modified coating. The symmetric and asymmetric stretching peak were the most affected peaks as there is a substantial decrease in absorbances between 2800 cm^{-1} and 3100 cm^{-1}. For this experiment, the presence of strong absorption peaks by C-F stretching is confirmation of grafting across the pNB surface polymer brushes.

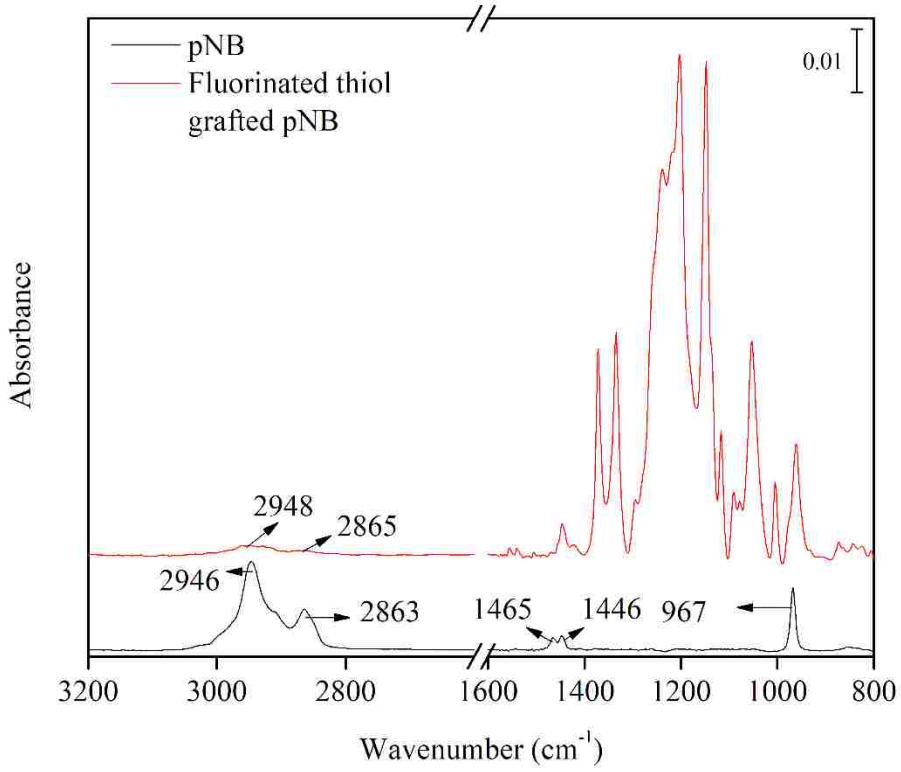

Figure 4.6: RAIRS spectrum of pNB grafted by fluorinated thiol

4.3.1.3 1,6-Hexanedithiol

Several groups have observed the surface degradation of polyolefin coatings when exposed to organic solvents in the ambient atmosphere[194]. We hypothesize that the dithiol grafting stabilizes coatings by eliminating the cleavage-susceptible double bonds and also crosslinking polymer chains in the coating. We used 1,6-hexanedithiol to graft across pNB chains, and we hypothesized that two terminals of dithiol would graft to two adjacent pNB chains thereby bridging them together.

The expected change in the contact angle was to be same as in case of grafting by 1-dodecanethiol. However, surprisingly the average advancing contact angle was much lower than that of pure pNB coating, and it was found to be 56º, and the average receding contact angle was 12º.

Using RAIRS, we analyzed the surface composition which confirmed the changes in film composition. We observed minute changes in all the peaks of the polymer backbone and detected additional signature peak for acyclic methylene groups by 1,6-hexanedithiol. The symmetric and asymmetric peak for cyclic methylene stretching were still detectable at 2944 cm^{-1} and 2851 cm^{-1}, but new strong stretching peak for methylene of 1,6-hexanedithiol was also seen at 2925 cm^{-1}. The methylene scissoring for cyclic CH_2 was as it was at 1450 cm^{-1} along with its typical Davydov splitting. The out of plane bending peak at 967 cm^{-1} had decreased absorption intensity but was in the same ration with CH_2 stretching peaks. This can be due to grafting at smaller extent as compared to the grafting of alkanethiol or fluorinated thiol.

The coating thickness for this grafting experiment was determined using spectroscopic ellipsometry. The thickness observed was variable in all the samples and at the different region of the same specimen. The low advancing/receding contact angle, variable thickness, and less grafting observed in RAIRS can be attributed to the phenomenon that where grafting chemistry gets dominated by film degradation.

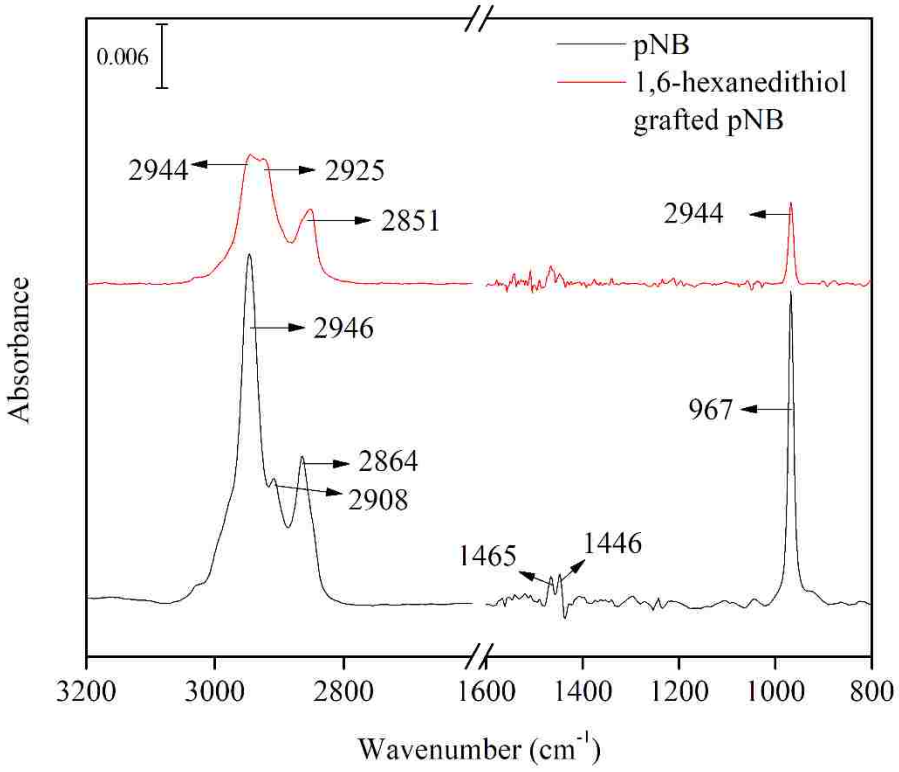

Figure 4.7: RAIRS spectrum of pNB before and after grafting by 1,6-hexanedithiol

4.3.2 Film loss

As mentioned earlier, we observed film loss during grafting process for most of the samples during the experiments. Hence, we decided to find out the reason for the film loss or polymer brushes degradation. Following the results by Lerum and Chen group, we continued to explore the effect of oxygen in the deterioration of polynorbornene[194].

There are different possible phenomenon due to which polymers get degraded when exposed to the atmosphere resulting in poor mechanical properties, altered chemical structure, and reduces life[195]. It depends on the type of polymer structure and composition, the environment the polymer is repeatedly exposed and the chemical composition of the environment. It can undergo solvolysis in presence water if the polymer has carbonyl functional groups, oxidative degradation or ozonolysis if the atmosphere has oxygen or ozone, a galvanic action which is similar to corrosion of metals, chlorine-induced cracking of polymers, etc.[196]. Polydienes, in general, are susceptible to

oxidative degradation but since we observe chain cleavage, under UV and in the presence of oxygen, we hypothesized it to be the contribution of different photo-driven chemical reactions of oxygen and its radicals.

There are many possible photocatalyzed reactions that result in the change in molecular structure of polymer chains[197]. Ozonolysis is also one of photo-triggered reaction contributing polymer chain cleavage at alkene functionality[198].

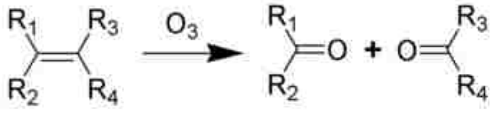

Figure 4.8: Oxidative cleavage of alkene bond

Polynorbornene polymer brushes contain unsaturated carbon-carbon double bonds which are susceptible to photo-oxidative degradation, singlet oxidative oxidation, and photodegradation[199]. Under UV exposure polynorbornene undergoes various types of photo-driven oxidation reactions forming different functional groups like epoxides, carbonyl functional groups and oligomers depending on the type of free radical formation[199].

To investigate the film degradation observed during the photochemical surface reactions of thiol-grafting, further experiments were designed where we used three solvents, UV irradiation, and photoinitiator. We hypothesize that photoinitiator accelerates the formation of oxygen radicals in solution thereby resulting in rapid oxidative reactions. Polynorbornene coatings with thickness around 50 nm were used for experiments.

Here we experimented with 3 different solvents with different polarity. We used pNB coating with similar initial thickness and irradiated them with UV light (15 mW/cm^2) in presence and absence of photoinitiator in each solvent for 5 minutes. These are same experimental conditions as in thiol-ene grafting experiments except the thiols are not present in the solution. UV irradiation helps the formation of free photoinitiator radicals which further triggers generation of oxygen radicals, and other photochemical reactions of oxygen.

Table 4.1 shows the data about mean coating thickness before and after irradiation in different conditions. The coating thickness is almost negligible after irradiation in cases when the solvent was polar, and photoinitiator was present. Moreover, when photoinitiator was absent, there is no significant decrease in the film thickness. Hence, these results support our hypothesis that UV radiation exposure, soluble oxygen in solvent and photoinitiator resulted in degradation of polymer brushes by different photochemical reactions. These observations motivated us to propose a new project where we strengthen the coatings using a crosslinker without sacrificing the unsaturated functionality. Details of the project are in chapter 5

Table 4.1: Thickness (ellipsometric) of coatings in different solvents in various conditions

Number	**Solvent**	**Photoinitiator**	**Initial thickness (nm)**	**Final thickness (nm)**
1	Cyclohexane	No	47.1	37.1
2	Cyclohexane	Yes	49.2	39.2
3	Toluene	No	48.3	47.1
4	Toluene	Yes	46.6	5.1
5	Dichloromethane	No	42.7	42.2
6	Dichloromethane	Yes	52.2	0.8

4.4 Conclusions

In conclusion, SI ROMP coatings of polynorbornene were modified by adding three types of thiol molecules using thiol-ene click reaction. The grafting of molecules was confirmed by contact angle measurement and RAIRS. Along with the loss of the peak for out of plane bending and stretching of C=CH, the signature peaks for added thiol molecules are seen in IR spectrum. Despite successful surface engineering, deterioration of polymer brushes was observed during this process. This deterioration resulted in decrease in the film thickness

and substrate with non-uniform polymer coating. The reason for the reduction in film thickness is attributed to the photochemical oxidative cleavage of polymer chains triggered by UV irradiation and a photoinitiator in the grafting setup. We confirmed that UV irradiation and photoinitiator helps the production of oxygen radicals thereby accelerating the process of oxidative degradation. Although this approach has encountered a practical limitation, the protocol can be optimized in future by modifying the experimental setup, such as using a degassed solvent during complete process of grafting which may reduce the degradation significantly. But it will compromise the attractiveness of this approach. Another solution is to introduce a crosslinker in the polymer coating which would prevent the film loss due to film degradation. Hence, a crosslinker is designed and incorporated into these coating whose details are presented in the next chapter.

5 In situ Crosslinking of Surface-Initiated Ring Opening Metathesis Polymerization of Polynorbornene for Improved Stability

The work presented in this chapter has been published in the following peer-reviewed journal paper: Fursule, I., Abtahi, A.,Watkins, C., Graham, K., Berron, B., "In-situ crosslinking of Surface-Initiated Ring Opening Metathesis Polymerization of Polynorbornene for improved stability," Journal of Colloid and Interface Science, 2017, 510, 86-94

5.1 Introduction

Functionalized polymer coatings are pervasive throughout the scientific literature, including applications as self-healing materials [200, 201], dielectric layers [46, 202, 203], responsive materials [204, 205], membrane modifiers [65], insulating barriers[172] and conductive surfaces [206]. In particular, surface-initiated polymerization (SIP) techniques [46, 163, 165, 166] are attractive owing to fine control over growth rate [46, 85] and a capacity to create a conformal coating over complex morphologies [28, 165, 207]. While many surface properties are accessible through SIP of appropriate monomers, the post-polymerization functionalization of a coating provides an opportunity for more diverse surface chemistries than are presently attainable. For example, many ionomer systems are based on polymers which are both fluorinated and sulfonated [208]. A surface-initiated strategy to combine these functional groups requires polymerization followed by sulfonation to avoid the low polymerization rates of sulfonated monomers [128, 209, 210].

Of the SIP approaches, surface-initiated ring opening metathesis polymerization (SI ROMP) offers the simplest approach for post-polymerization modification through the unsaturated bonds in polymer backbone [43, 85, 173]. While most polymerization routes consume the alkene group, SI ROMP opens strained ring monomers by a metathesis catalyst which rearranges and preserves the alkene [85, 164, 173]. When using ruthenium-based metathesis catalysts, SI ROMP can be performed in ambient environmental conditions with a high rate of polymerization and precise control over surface coating thickness [163, 211]. In addition, ROMP is relative faster than other SIP methods. ROMP

can produce micron thick coatings in minutes whereas other SIP methods typically require hours.

The instability of the SI ROMP coatings represents a critical obstacle in post-modification reactions. Lerum and Chen first observed the decrease in the thickness of these SI ROMP coatings during exposure to the organic solvents (Figure 5.1A, B) [212]. They observed a 93% loss in film thickness following exposure of polybutadiene (PBd) to dichloromethane in an ambient atmosphere [212]. The stability of the silane linkage to the SiO_2 substrates indicated damage to the polymer coating layer. By contrasting the film loss upon solvent rinsing in ambient conditions to loss in a nitrogen environment, they proposed that the damage is the result of oxidative cleavage of the internal alkene in the ROMP backbone. As this oxidation is not commonly observed in solution phase ROMP chains, they proposed an entropic driving force to promote the cleavage of a surface-tethered chain. Other groups have also observed a decrease in SI ROMP coating thickness following exposure to organic solvents [48, 128, 213, 214]. For any solution phase processing of these coatings, film loss during solvation is a critical concern. This challenge is highlighted a previous study of the sulfonation of SI ROMP coatings. The instability of the coating resulted in significant film loss during the solution phase reaction, ultimately requiring thicker initial films to achieve the target thickness of the sulfonated film [128].

In the present study, we hypothesize that a crosslinking additive will improve the stability of SI ROMP coatings during solvent exposure and chemical functionalization of the deposited grown coatings. We designed a simple crosslinking molecule for ROMP polymerization consisting of a dinorbornene polyethylene glycol (PEG), and we studied changes to an SI ROMP polynorbornene (pNB) coating with and without incorporation of this crosslinker. The solvent stabilities of pNB and crosslinked polynorbornene (DiNB-pNB) coatings were contrasted via repetitive exposure to dichloromethane, where minimal film loss was observed for crosslinked coating as compared to the non-crosslinked coating.

Our general approach illustrates a straightforward strategy for stabilizing SI ROMP coatings against solvation-induced degradation to facilitate complex coating chemistries. SI ROMP is a highly utilized coating technique for rapid, conformal coatings on complex surfaces. To date, nitrogen purging has been the only published approach to stabilize SI

ROMP coatings to solvent accelerated degradation [212]. We anticipate these crosslinked, solvent stable SI ROMP coatings to be ideal for modification of the olefin backbone in thiol-ene click reactions [114, 215, 216]. This pairing of a highly specific, orthogonal click-type reaction and rapid growth of a stable film is expected to enable a diverse class of thick, conformal coatings containing with difficult to polymerize functional groups.

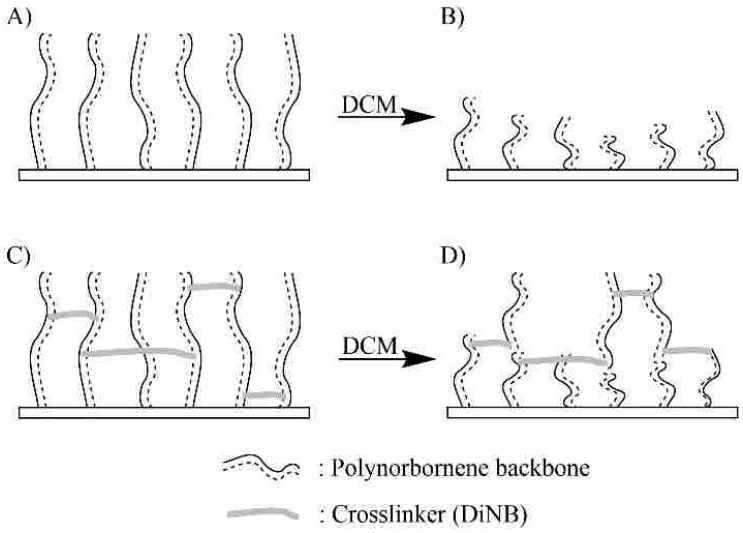

Figure 5.1: The role of crosslinking in stabilizing an SI ROMP coating. A) Non-crosslinked polynorbornene film structure. B) Non-crosslinked polynorbornene backbone after washing with dichloromethane (DCM). C) Crosslinked polynorbornene film structure. D) Crosslinked polynorbornene backbone after washing with dichloromethane.

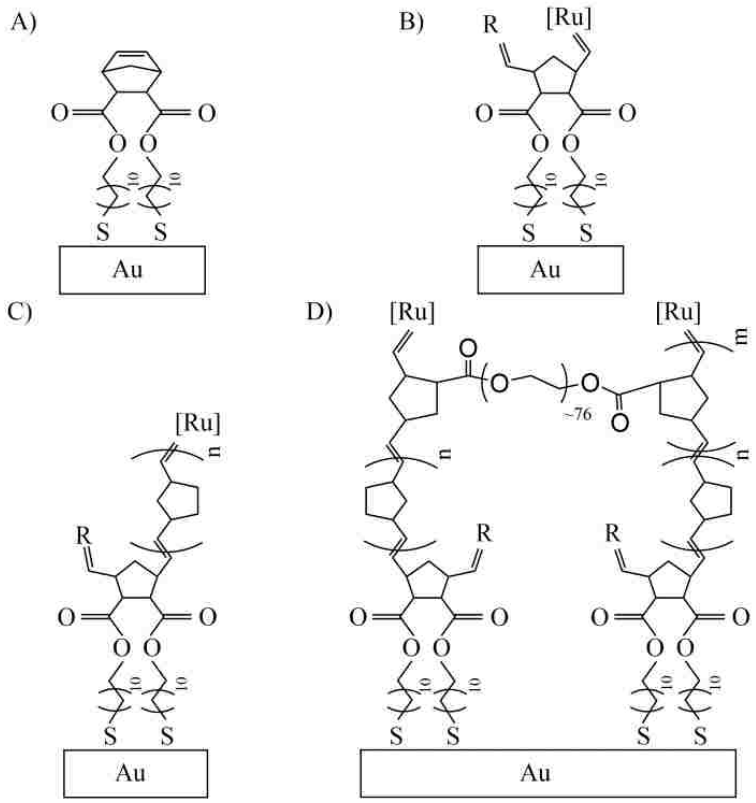

Figure 5.2: Schematic representation of crosslinked SI ROMP coating preparation. A) Norbornenyl (NBCl2) decorated SAM, B) Grubbs catalyst attached to norbornenyl surface, C) SI ROMP of polynorbornene, D) SI ROMP of crosslinked polynorbornene through random co-polymerization

5.2 Materials

Polyethylene glycol 3350 (PEG 3350), 5-norbornene-2-carboxylic acid (NBAC), N,N'-dicyclohexylcarbodiimide (DCC), 4-(dimethylamino) pyridine (DMAP), pyridine, sodium chloride, sodium hydroxide, glycine, 11-mercapto-1-undecanol, *trans*-3,6-endomethylene-1,2,3,6-tetrahydropthaloyl chloride 97% ($NBCl_2$), Grubbs 1st generation catalyst and bicyclo[2.2.1]hept-2ene (norbornene) were ordered from Sigma Aldrich. All solvents were ordered from Acros (Fisher) and were used as received.

5.3 Synthesis of dinorbornene-crosslinker (DiNB)

Dinorbornene-crosslinker was synthesized by referring the protocol by Rehmann et al. [217] (Figure 5.3B). Two different solutions were made using degassed dichloromethane (DCM). First, 0.574 mg of DCC and 0.681 mL of NBAC was mixed in 50 mL of DCM under nitrogen environment. Second, a solution consisting of 0.017 g PEG3350 and 0.933

g DMAP was mixed in 50 mL of DCM in a nitrogen environment. After 20 minutes, 0.225 mL pyridine was added to the PEG solution, and then the PEG solution was added to the NBAC solution in a nitrogen environment and stirred overnight. The product solution was then filtered under vacuum to separate insoluble dicyclohexylurea from the soluble dinorbornene-crosslinker product. The soluble product was recrystallized by concentrating the solution under vacuum and then adding 10 times volume excess of cold diethyl ether. The supernatant ether was discarded, and the precipitate was dissolved in chloroform. This solution was then washed twice with aqueous solutions of 0.05 M glycine, 0.05 M sodium hydroxide, and 0.05 M sodium chloride. Finally, the organic solution was washed with 5.1 M solution of sodium chloride. The product was recrystallized again and washed with 10 times volume excess of cold ether and centrifuged to separate the final product. A 400 MHz Varian Nuclear magnetic resonance (NMR) spectroscopy was used confirm the composition of the PEG dinorbornene crosslinker. A minimum of 32 scans was used for quantitative determination of peak position and integration. HNMR ($CDCl_3$): δ = 2.9, 3.04, 3.22 (4H, m, >C*H*-CH=), δ = 1.3-1.47(4H, m, >CH-CH_2-CH<), δ = 5.94, 6.1, 6.14, 6.19(4H, m, -C*H*=), δ = 2.26, 2.97(2H, m, >C*H*-CO-), δ = 1.27, 1.53, 1.85 to 1.97(4H, m, -CH_2-CH-CO), δ = 3.46, 3.63, 3.81, 4.17, 4.25(4H, m, O-CH_2-CH_2-).

5.4 Surface-initiated ring opening metathesis polymerization

The detailed protocol to fabricate SI ROMP coating is given in section 3.1.2.2. In brief, SI ROMP coatings were made by creating a self-assembled monolayer of alkanethiol molecules which is used to bind norbornenyl dichloride. This surface was decorated with metathesis catalyst to initiate polymerization as soon as it is exposed to the monomer solution. Control surfaces of SI ROMP pNB were prepared with a 0.5 M solution of norbornene (NB) in DCM. Crosslinked SI ROMP surfaces were prepared through the incorporation of up to 1 mol% of the DiNB crosslinker. Reaction time was adjusted to control coating thickness. Reaction times ranged from a few seconds to 2 hours.

5.5 Results and discussion

The crosslinking monomer design is based on the expected distance between polymer chains in an actively polymerizing SI ROMP surface. In SI ROMP, neighboring chains are anchored to the substrate at locations which are primed by catalyst attachment. The catalyst

surface density is dictated by grafting density of $NBCl_2$ and the subsequent grafting of the Grubbs catalyst. Based on estimates of ~ 10^{12} molecules per cm^2 of Grubbs catalyst in a prior study using a similar catalyst attachment scheme [93], the expected distance between pNB backbone chains to be approximately 4 nm (Figure 5.3A). The crosslinker is designed to be of comparable length (or distance between 2 ends of crosslinker) as the distance between chains to encourage intermolecular crosslinking. PEG 3350 is used as a linker for two 5-norbornene-2-carboxylic acid molecules to yield a molecule with an all *trans* end to end distance of ~ 28 nm. While 28 nm is excessive for crosslinking across chains separated by 4 nm, the solvated structure of the crosslinking chain is significantly smaller than the all *trans* length of the molecule. The radius of gyration of PEG in dichloromethane is not readily available. We approximate the radius of gyration of PEG 3350 in dichloromethane to be similar to the radius of gyration of PEG 3350 in water (~2.3 nm) [218]. This estimate of solvated chain length is comparable to that of the distance between initiation sites and is expected to be appropriate for crosslinking this surface-initiated system. Longer crosslinking chains are also expected to crosslink a surface initiated system, but these longer chains are expected to decrease the film growth rate through dilution of the norbornene reactive groups.

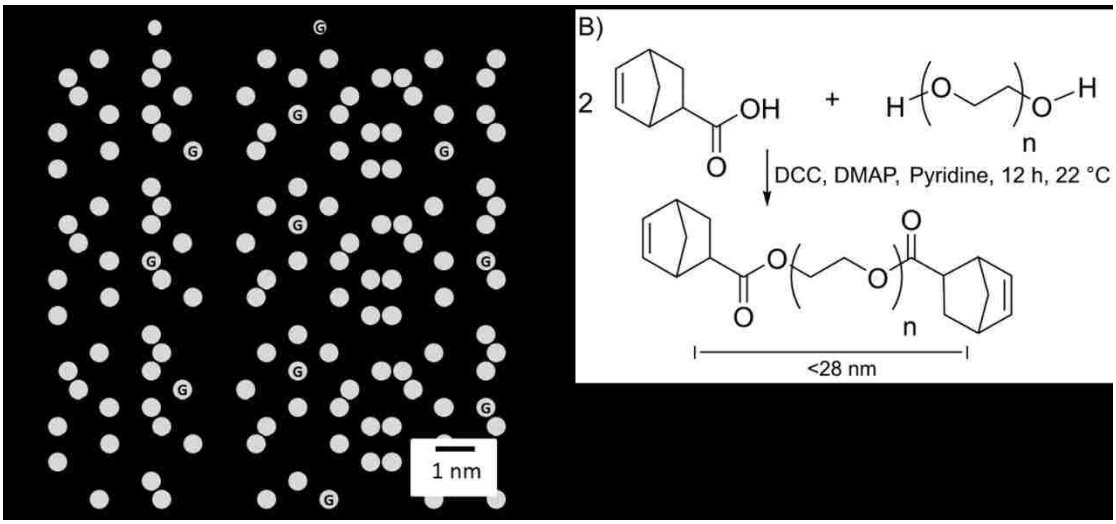

Figure 5.3: Relationship between polymer backbone density and dinorbornene linker length. A) Schematic representing the density of catalyst-related molecules in SI ROMP from a hydroxyl terminated SAM. B) Synthesis and all-trans length scale for the dinorbornene crosslinker.

5.5.1 Influence of Dinorbornene-crosslinker on SI ROMP coating composition and structure

The incorporation of the crosslinking molecule was confirmed via FTIR. In the spectra for the pNB coatings, distinct methylene peaks were observed for symmetric stretching, asymmetric stretching, and scissoring modes. The C-H stretching region for pNB coating IR spectra has strong cyclic methylene peaks at 2945 cm^{-1} (asymmetric) and at 2862 cm^{-1} (symmetric) with an additional stretching peak at 2907 cm^{-1} [185]. A cyclic methylene scissoring peak is seen at 1455 cm^{-1} with signature Davydov splitting into 1465 cm^{-1} and 1448 cm^{-1} indicating a relatively homogenous and well-ordered chain structure [186]. The out of plane bending peaks for C=CH olefin functionality [185, 187] are seen at 968 cm^{-1} and a shoulder-like C=CH stretching peak at 3030 cm^{-1} [185, 187].

For pNB coatings grown with the addition of 0.25, 0.5, or 1 mol % DiNB crosslinker, all characteristic peaks for pNB are conserved, and additional peaks consistent with the IR absorbance of PEG are introduced (Figure 5.4 A and B). The fingerprint region for PEG C-O-C absorption by PEG around 1029 cm^{-1} [219-221] was observed at crosslinker concentrations as low as 0.25 mol %. At this minimum concentration, the C=CH out of plane bending peak is in the same position as in non-crosslinked pNB coating suggesting no major changes in the environment of the olefin functionality after crosslinking. The position of the methylene scissoring peaks is similarly conserved at 1465 cm^{-1} and 1446 cm^{-1}. The asymmetric and symmetric methylene C-H stretching peaks (2950 cm^{-1} and 2865 cm^{-1}) are typically sensitive to alterations in polymer crystallinity [222], where these peaks shift by over 10 cm^{-1} with a change in chain-chain interactions [32, 223]. The crosslinked pNB is red shifted by 3-5 cm^{-1} when compared to these absorbances in the pure pNB coating. This red shift is supportive of a change in the chain packing with the addition of the DiNB crosslinking monomer. Since our goal is to stabilize SI ROMP films while leaving their functionality intact, we focused the remaining studies on 0.25 mol% DiNB.

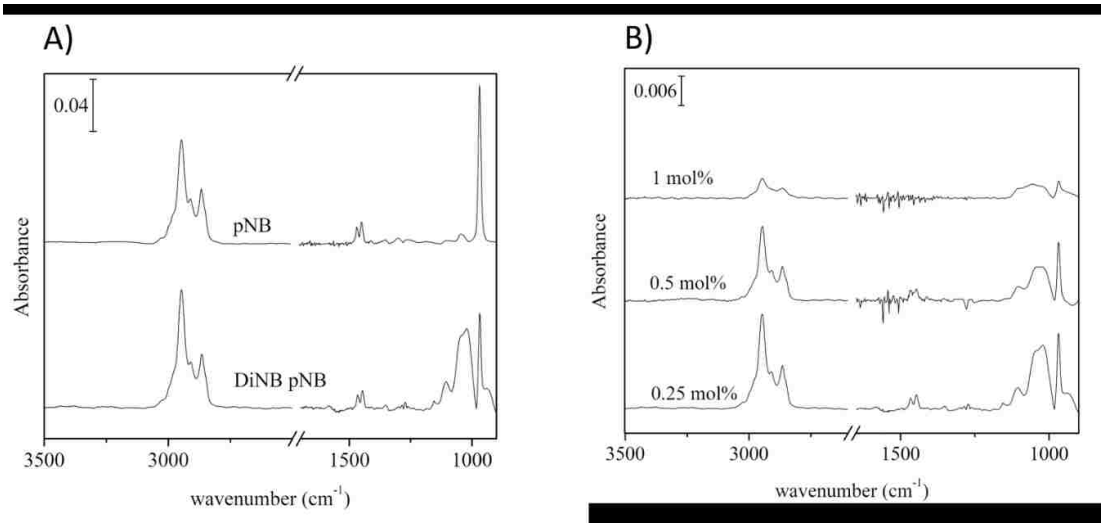

Figure 5.4: Reflection absorption infrared spectroscopy of SI ROMP of A) polynorbornene (pNB) and crosslinked polynorbornene with 0.25 mol % crosslinker (DiNB-pNB), B) crosslinked polynorbornene with 0.25 mol %, 0.5 mol% and 1 mol% crosslinker (DiNB-pNB).

The presence of the crosslinker in the film is further supported by the O1s peak in the XPS spectra. The incorporation of the DiNB crosslinker in the pNB coatings is further supported by analysis of the XPS spectra of the films (Figure 5.5). When compared to the spectra of the pNB coatings, the spectra of the DiNB-pNB coatings include a shoulder centered at 534.5 eV, consistent with the ethereal oxygen in the PEG functionality of the DiNB crosslinker[224, 225]. The XPS spectra for both films include peaks at ~533 eV consistent with carbonyl oxygen. Critically, the DiNB-pNB coatings are expected to include <0.1 atom % carbonyl oxygen from the ester bound norbornene, and the pNB coatings are not expected to contain any oxygen in the bulk polymer layer. The high carbonyl oxygen content of the coatings is consistent with previously observed degradation products of polymers[226]. While Lerum and Chen postulated the entropy accelerated oxidation of SI ROMP pNB coatings, the spectral observation of these degradation products has not been reported to date [212]. The presence of carbonyl oxygen peaks in the XPS spectra strongly supports the oxidative degradation of these coatings in ambient environments.

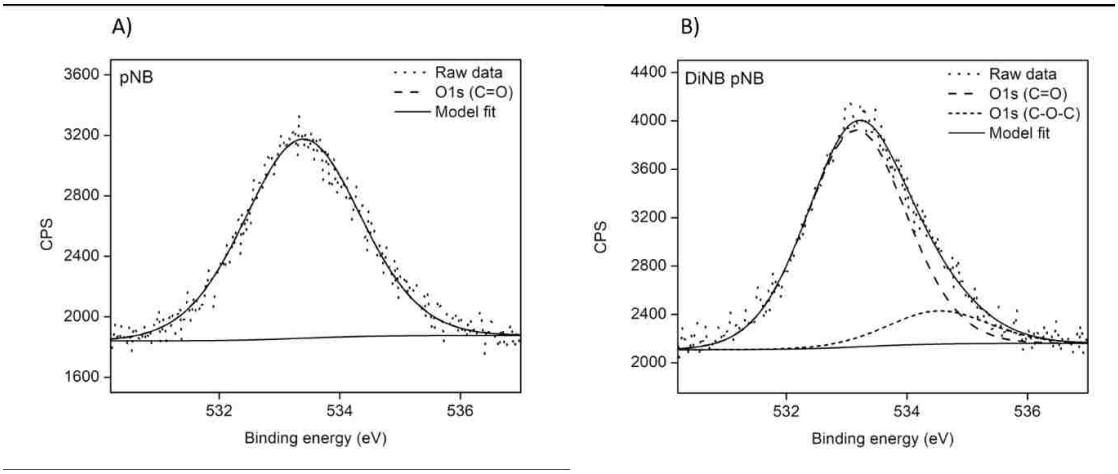

Figure 5.5: O1s region of XPS spectra of (A) non-crosslinked pNB coatings and (B) DiNB-pNB coatings.

The rate of film growth is dramatically decreased by the addition of the DiNB crosslinking monomer. While a 0.5 M solution of NB in dichloromethane yields a coating of ~ 1 μm in 15 minutes, the addition of 0.25 mol % DiNB to the same solution of NB only yields a 30 nm coating. To determine if the decrease in film growth rate is related to chemical attributes of the crosslinker or steric hindrance from the presence of solvated polymer chains, 0.25 mol% methylene terminated PEG (Mn 2000) or 0.25 mol% polystyrene (Mn 2000) was added to the 0.5 M NB solution during polymerization. While the addition of the PEG limited the film growth to 16 nm, the polystyrene and NB solution still supported film growth > 500 nm. These polymer additives both decrease the rate of pNB film growth, but the PEG chain has a stronger negative effect on the film growth rate than the polystyrene. In all, the PEG backbone for the crosslinker is not ideal for supporting the rapid growth of thicker films using Grubbs first generation catalyst. Critically, the polystyrene and other commonly available polymer backbones are more challenging to end functionalize. As a result, we use the PEG backbone here to demonstrate the proof of concept for coating stabilization. For applications requiring thicker films, alternative catalysts or crosslinker chemistries may be warranted.

Table 5.1: Coating thickness following immersion of a Grubbs catalyst coated substrate in the indicated solution for 15 minutes.

Solution	Thickness (nm)
0.5 M NB in dichloromethane	1046 ± 506
0.5 M NB and 0.25 mol % DiNB in dichloromethane	33 ± 12
0.5 M NB and 0.25 mol % methylene terminated PEG 2000 in dichloromethane	16 ± 7
0.5 M NB and 0.25 mol % polystyrene (Mn 2200)	534 ± 93

Advancing and receding water contact angles for pNB coating are ~98º and ~77º, and these values are consistent with prior studies [128, 210]. For DiNB-pNB films, the advancing water contact angle is similar (95º) to that of the pNB film. There is a significant decrease in the receding water contact angle (~65º) with the incorporation of the DiNB crosslinker when compared to the pNB film. The decrease in the contact angles is attributed to the introduction of hydrophilic PEG chains in the DiNB crosslinker [223]. Additionally, the larger change in the receding contact angle than for the advancing contact angle is expected, owing to the receding contact angle's greater dependency on the hydrophilic content of the surface [227, 228].

Table 5.2: Advancing and receding contact angle for water on SI ROMP coating. Data represent mean ± standard deviation.

Coating	Thickness (nm)	Θ_A (º)	Θ_R (º)
pNB	46 ± 6	98 ± 2	77 ± 3
DiNB-pNB	40 ± 5	95 ± 3	65 ± 6

Electrochemical impedance spectroscopy was used to evaluate changes in coating structuring upon the addition of the DiNB crosslinker. Figure 5.6 displays representative Bode plots for ~37 nm pNB coatings and DiNB-pNB coatings. A modified Randle's equivalent circuit with Warburg's impedance term for mass transport resistance was fit to the experimental data. Based on these fits, the film capacitance of the pNB coating (623 ±

514 nF/cm^2) was similar to that of the crosslinked film (210 ± 108 nF/cm^2). This supports a similar dielectric and thickness for the two coatings. Interestingly, the crosslinked coating had a slightly higher mean film resistance ($10^{5.9}$ Ω•cm^2) than that of the native pNB coating ($10^{4.7}$ Ω•cm^2). While this potentially supports greater coating uniformity in the crosslinked film, this minimal difference in mean resistance will not significantly alter the practical application of a functional SI ROMP coating.

Table 5.3: Film resistance and interfacial capacitance for SI ROMP coating

Film	**Thickness (nm)**	**Log (R_f) (Ω•cm^2)**	**C_f (nF/cm^2)**
pNB	38.5 ± 12.4	4.66 ± 0.44	623 ± 514
DiNB-pNB	36 ± 10.5	5.93 ± 0.39	210 ± 108

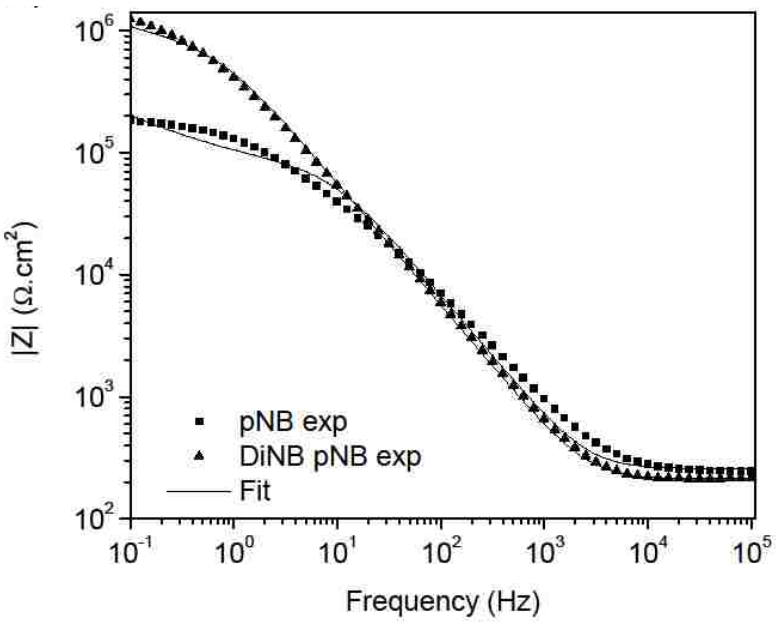

Figure 5.6: Electrochemical impedance spectroscopy of SI ROMP polynorbornene coatings. Bode plot of representative experimental data from SI ROMP polynorbornene (▪) and SI ROMP crosslinked polynorbornene (▲) coatings. Lines represent fitting of an equivalent circuit to experimental data

5.5.2 The influence of crosslinking on coating stability in solvent

To determine the effectiveness of a 0.25 mol% crosslinker in stabilizing an SI ROMP coating, we measured the thickness of pNB and DiNB-pNB coatings after rinsing sequentially with dichloromethane, ethanol, and water (Figure 5.7). All the samples were rinsed in the same ambient atmospheric conditions to minimize the variation in temperature and oxygen content in the atmosphere. Each sample was immersed in the DCM for 5 seconds, removed into ambient air, and gently shaken to remove excess solvent. Samples were then immediately rinsed with ethanol and then water in the same fashion. After rinsing with water, the sample was dried under a stream of nitrogen. Thicker coatings were utilized in this study to allow greater resolution in the fractional coating loss, and polymerization times were adjusted to achieve coatings approximately 90 nm in thickness. The stability of SI ROMP coating increased significantly with the addition of the DiNB crosslinker for the first rinse and each subsequent rinse ($p<0.05$). The film loss after 10 rinses decreased from ~73% to ~28% after introducing crosslinker. The relative film loss for the pNB coating compares favorably with a prior study by Lerum and Chen, where 93 % of a polybutadiene film was lost after 10 rinses of dichloromethane in an ambient environment. A small decrease in the coating thickness upon rinsing still occurs in the DiNB sample and this film loss is expected due to the persistence of olefin functionality in the polymer backbone.

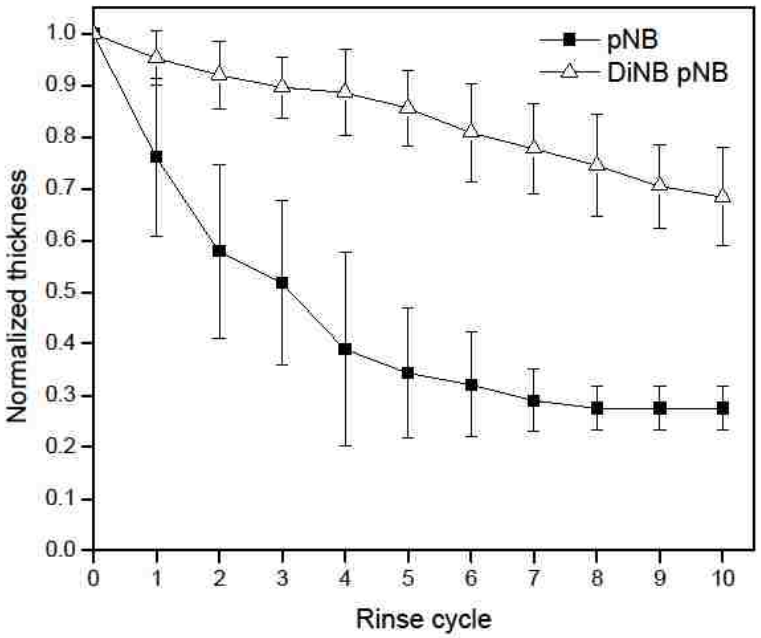

Figure 5.7: SI ROMP coating stability data. The profilometric thickness of a polynorbornene or crosslinked polynorbornene coating is measured following the indicated number of rinse cycles. Each rinse cycle is the sequential exposure to DCM, ethanol, and water.

The microstructure of the rinsed and unrinsed coatings further informs the role of coating crosslinking in the solvent stability of SI ROMP films. Figure 5.8 shows the topographical images of pNB and DiNB-pNB coatings obtained by atomic force microscopy (AFM). Immediately after film formation, the pNB and DiNB-pNB coatings look similar to other polymer brush coatings found in literature, including examples of other SI ROMP coatings[85, 90, 210]. For the pNB film, the surface morphology changes dramatically after exposure to 10 cycles of dichloromethane, ethanol, and water. The rinsed pNB coatings (Figure 5.8B) have nanoscale pits indicative of a uniform loss of material throughout the coating. Additionally, the rinsed pNB coatings have circular, micron-scale defects Figure 5.8B and regions where the pits are interconnected. The DiNB-pNB also forms nanoscale pits from the loss of polymer, but the overall coating morphology is still similar to that of an as-grown pNB and the DiNB-pNB coating. The rinsed DiNB-pNB coating does not have large regions of widespread film loss seen in the pNB rinsed coatings. In all, the film loss in the rinsed pNB coatings supports a rapid, uniform loss of coating material, with localized regions of accelerated film loss. The crosslinked DiNB-pNB coatings still exhibit

uniform loss of material on the submicron scale, but the macroscale loss of films is not observed.

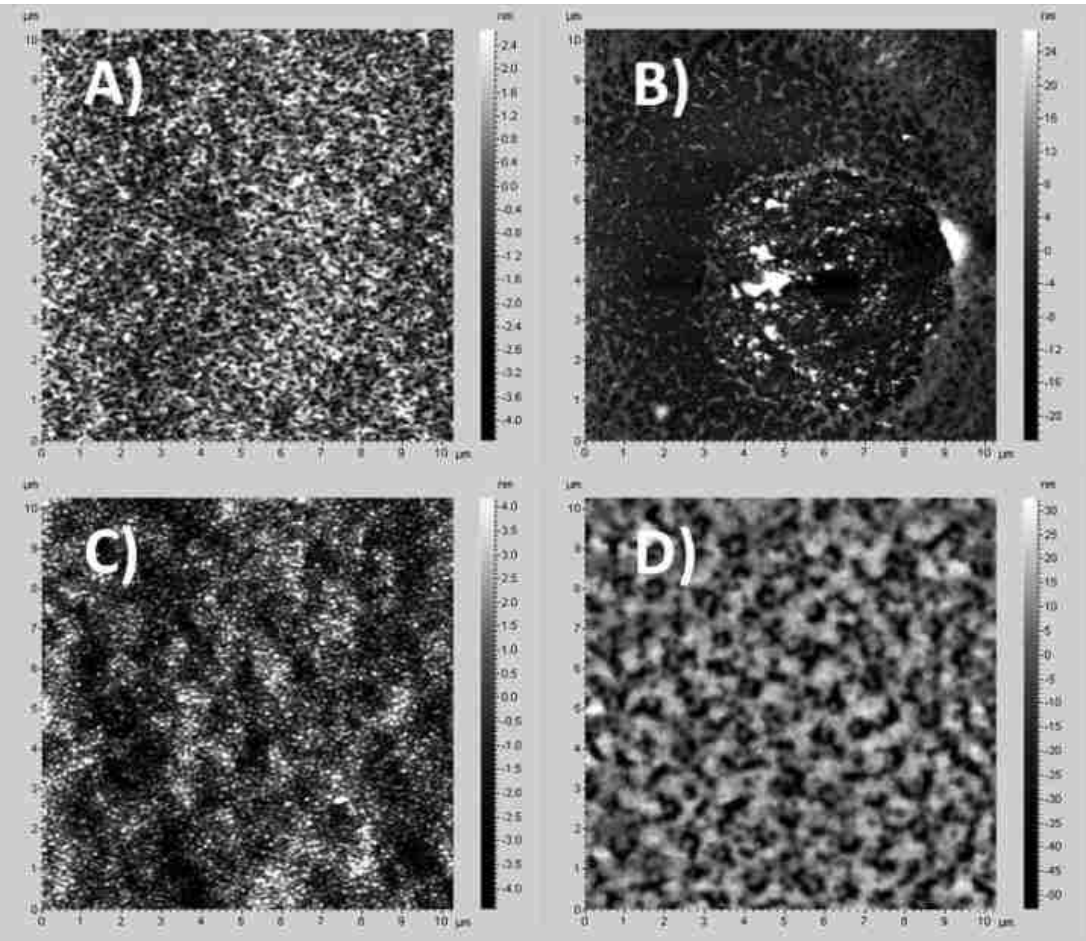

Figure 5.8: AFM image of SI ROMP coatings; A) Non-crosslinked i.e. pNB and unrinsed, B) Non-crosslinked i.e. pNB and rinsed, C) Crosslinked i.e. DiNB-pNB and unrinsed, D) Crosslinked i.e. DiNB-pNB and rinsed

5.6 Conclusions

We hypothesized that *in situ* crosslinking is a straightforward approach to stabilize SI ROMP coatings. We found that the stability of pNB coating against organic solvents in an ambient environment is increased significantly with the addition of a dinorbornene crosslinker at 0.25 mol%. Additionally, we report the first spectral data supporting the oxidative degradation of these SI ROMP coatings in ambient environments. To date, processing in a deoxygenated environment is the only published approach to limit solvent-associated degradation [212]. Interestingly, ROMP with Grubbs catalyst is largely tolerant of oxygen [75, 229], where many competing grafting-from chemistries have stricter

purging requirements [230, 231]. A processing requirement of an oxygen-free environment would significantly decrease the attractiveness of ROMP-based surface modification over slower techniques like SI-ATRP and other radical chain-growth strategies[232, 233].

The crosslinker design described here is based on a PEG-dinorbornene molecule of sufficient length to bridge adjacent active sites on the catalyst primed surface. The PEG chemistry was selected primarily for ease of functionalization but was discovered to actively decrease the rate of polymerization for the pNB coatings. Additionally, the total amount of crosslinker was limited to 0.25 mol% of the NB in solution due to the lower growth rate in the presence of PEG. In future work, the use of catalysts with greater functional group tolerance is expected to enable the use of this PEG dinorbornene crosslinker with a less detrimental impact on the film growth rate. Alternatively, the crosslinker may be redesigned to utilize a backbone more compatible with Grubbs first generation catalyst. While we expect greater stability with higher crosslinker loadings, we also demonstrated that the crosslinker alters the wettability of the polymer coating. A higher crosslinker loading is expected to have a more significant impact on the surface properties of the coating. As a result, future studies in functional SI ROMP coatings should carefully consider the crosslinker's interaction with the catalyst, the crosslinker's impact on the desired surface properties, and the desired solvent stability of the coating.

6 A novel design of photoresponsive ring monomer for light-mediated ROMP

6.1 Introduction

Stimuli-responsive or smart materials that actively respond to environmental changes in temperature[234], light[235, 236], pH[237, 238], humidity[239, 240], electromagnetic fields[241-243], enzyme concentration[244, 245], or mechanical force[246, 247] are poised to have a significant impact on everyday life in the 21st century. However, light as a type of stimuli has attracted researchers because its precise spatiotemporal control (coherence and laser pulse), intensity and energy control, prerequisite of no other reagent in the system to trigger or assist the light absorbance, and very limited by-products during this process[248-251]. Light- or Photoresponsive polymers change their physical or chemical properties when exposed to the light or radiations of the appropriate wavelength. There are plentiful applications of photoresponsive polymers in the field of electronics as temporary storage[252-254], biosensors[224, 255], surface relief gratings[13, 14], and many more. The response of photoresponsive polymers depends on the type of photoresponsive moiety and the way it is incorporated in the polymer chain/matrix. For instance, an ortho-nitrobenzyl ester functional group on the absorption of UV radiations undergoes irreversible cleavage of covalent bond[256]. Whereas, the azobenzene (AB) molecule experiences geometrical isomerization on exposure to UV or visible radiation, also called as photoisomerization[257] (Figure 6.1). Photoresponsive moiety can be present in the polymer chain or matrix as a branch or crosslinker or in the backbone[258, 259]. This research is focused on the photoresponsive polymers with AB as photoresponsive moiety in the backbone, responsible for the reversible light-mediated changes of the polymer properties. AB is one of the most commonly used photoresponsive moiety in research and commercial applications. When irradiated with UV light (λ_{max}), its structure changes due to photoisomerization from its thermodynamically stable *trans* conformation (AB *trans*) to thermodynamically unstable *cis* conformation (AB *cis*). The *cis* to *trans* transition can be driven either using visible light or thermally[257].

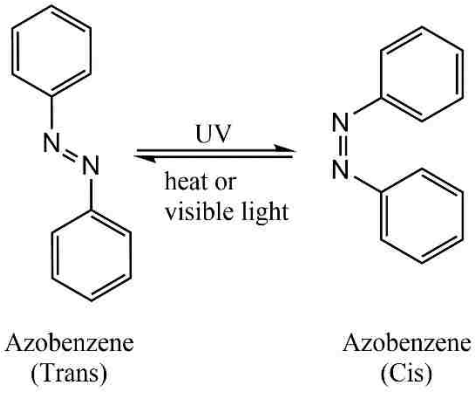

Figure 6.1: Isomerization of photoresponsive moiety; azobenzene (AB)

Another important entity that directly defines the degree of response of photoresponsive polymers is the structural location of the photoresponsive moiety. The photoresponsive unit can either be in the main chain of the polymer or as a crosslinker or as a pendant group to polymer chain[258, 259], and this choice imparts a different degree of mechanical response. For instance, Chang-Dae Keum and group have shown that the photodeformation due solid-state mass transport of polymers with AB in the main chain is slower than when it is present as a pendant. This is attributed to a decrease in the rate of photoisomerization of the AB in the main chain[260]. Hence, the position of AB with respect to the main-chain is very crucial while designing the polymer structure. Currently, extensive research conducted on photoresponsive polymer coatings with AB incorporated as a branch off of the polymer backbone, and significantly fewer with AB in the main chain. The main reason is a lack of robust synthetic tools for making polymers with AB in the backbone.

Typically, photoresponsive polymers are synthesized in the solution by the free radical polymerization of acrylates, which are then spin coated onto the target substrate to make physiosorbed coating of the desired thickness. The complete fabrication process is not ideal with respect to polymer usage, stability, and coating uniformity on complex substrate topography. Common defects found in spin-coated polymer coatings are pinhole defects, swirl patterns, bubbles, streaks and chuck marks due to the viscosity of polymer solution, temperature, angular velocity and other factors[20, 261, 262]. Also, the polymer surface density cannot be controlled in this approach. As each chain is not chemically grafted to the substrate, mechanical shear force easily damages such coatings[263]. The major

limitation of spin coating is that it cannot be used to make the uniform coating on non-planar surfaces but works for only planar substrates.

The development of 'grafting from' or surface initiated polymerization (SIP) has mitigated the major drawbacks of spin-coated films. SIP produces covalently bound uniform polymer coatings/ brushes from the substrate. The covalent bond between polymer chains and substrate provides high robustness to the coatings against damage due to mechanical shear force. Controlled radical polymerization (atom transfer radical polymerization or ATRP), ring opening metathesis polymerization (ROMP), living cationic and anionic polymerization, and reversible addition-fragmentation chain transfer (RAFT) polymerization are few types of SIP techniques[163]. However, most of these methods need controlled conditions for polymerization and are limited to coating growth rates of few nanometers per hour. For pragmatic application, properties such as polymerization in ambient atmosphere, high rate of polymerization, polymerizable in the aqueous or organic environment[264], tunable surface chain density, and conformal coating over complex surfaces are essential[43]. Among all SIP techniques, ring opening metathesis polymerization (ROMP) provides all above properties to polymers, polymer coatings, and polymerization process[42]. Metathesis reactions are the metal catalyst mediated rearrangement of carbon-carbon double bond to form new alkylidene[265]. ROMP is a type of metathesis reaction where a strained ring monomer opens up with the help of transition metal based carbene initiators, and rate of polymerization is directly proportional to the ring strain energy of monomer.

When ROMP is initiated from the surface with the help of surface-bound initiators, then it is called as surface initiated ring opening metathesis polymerization (SI ROMP). The thickness of SI ROMP coatings is related to the ring strain energy of the ROMP monomer[48] (Figure 6.2). It is the living type of polymerization because the polymerization continues in chain growth fashion to generate polymers till the solution has strained cyclic monomer and active catalyst[42].

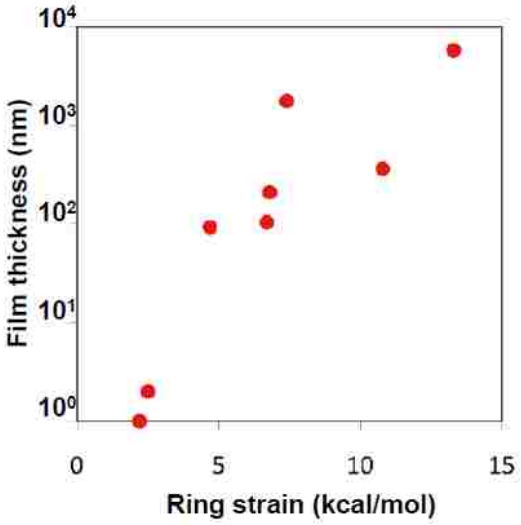

Figure 6.2: Film thickness vs. ring strain energy of monomer[48]

In brief, currently, there is no polymerization technique better than spin coating, to prepare photoresponsive polymer coatings with a photoresponsive moiety in the polymer backbone. This chapter covers the design of a system/monomer capable of preparing photoresponsive SI ROMP coatings with azobenzene groups in the polymer backbone. Moreover, the designed monomer will provide control over the rate of polymerization of ROMP using light by attuning the ring strain energy of monomer. This will be achieved by incorporating the azobenzene into the cyclic ring structure of monomer. When this monomer is exposed to the radiations with a wavelength in its absorption range, azobenzene in the ring monomer will tend to undergo geometrical structural changes thereby affecting the strain energy of the molecule. This will allow remote, non-invasive and instantaneous spatiotemporal control over SI ROMP process.

6.2 Design

We propose the design of the monomer by following the generic design of ROMP monomer and photoresponsive polymers having the azobenzene in the main chain. ROMP is an enthalpic driven polymerization, and hence, monomer needs internal ring strain energy that acts as driving force for the opening of the ring[42]. To initiate the polymerization by a catalyst, binding itself to the olefinic functionality is very essential and the same mechanism is used for propagation of polymerization. Lastly, for AB to be present in the main chain of the polymer, it needs to be present in the ring structure of

cyclic monomer. Hence, the monomer design was divided into two pieces, half part as a linker with alkene functionality and other half part being azobenzene (Figure 6.3 A). As a result, on ROMP of the designed monomer, the AB will be in the backbone of the polymer chain or polymer brushes.

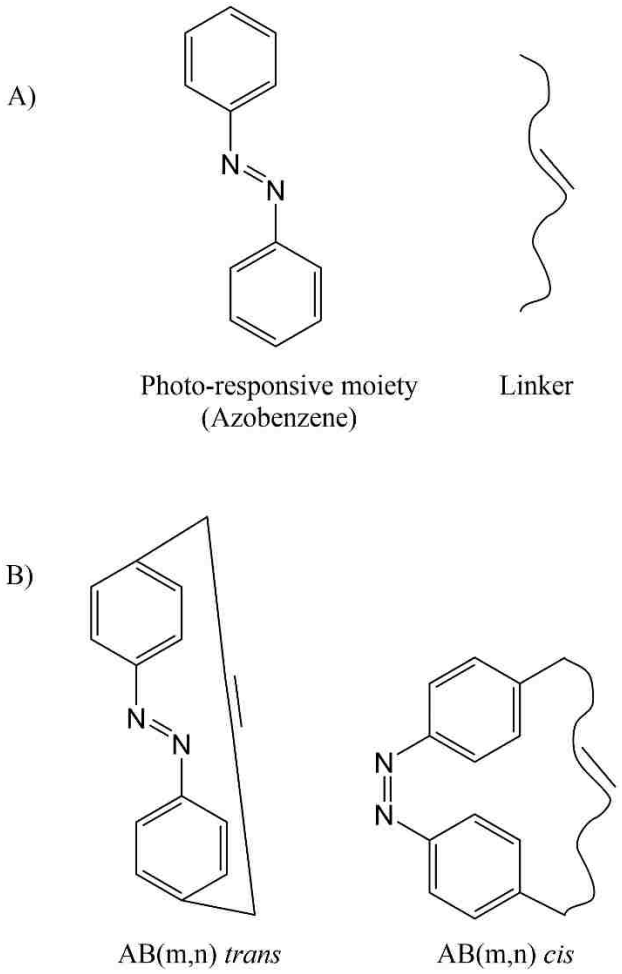

Figure 6.3: A) Parts of monomer; B) AB(m,n) in *trans* and *cis* conformation

We hypothesize that locking the AB in its thermodynamically unfavorable *cis* geometry using a linker with specific length will yield a closed ring monomer with ring strain energy. As a result of AB continually trying to relax back to its thermodynamically stable *trans* state, ring strain energy will be generated in the closed cyclic structure (AB(m,n)). On irradiation with suitable wavelength radiations, it will be feasible to change the geometrical conformation of AB(m,n) between *trans* and *cis* thereby changing the internal ring strain energy (Figure 6.3 B). Hence in this design, the light can be used to control the ring strain

of monomer, and ultimately ring strain of monomer will dictate the rate of its polymerization.

We used 4,4'-Diaminoazobenzene (ABn) as the photoresponsive moiety, i.e., first half part of AB(m,n) and second part, i.e., linker was a chain of methylene groups; L(m,n) with an internal carbon-carbon double bond. 'm' and 'n' are the numbers of methylene groups on either side of carbon-carbon double bond as shown in (Figure 6.4).

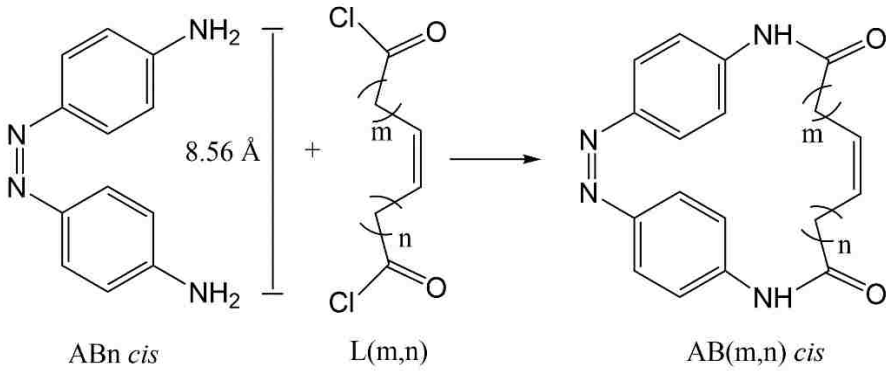

Figure 6.4: Design of AB(m,n) with photoresponsive moiety (ABn) and linker (L(m,n))

The linker with suitable functional groups at the terminals was selected for the convenience of reaction with primary amine groups on ABn. Number of methylene groups ('m' or 'n') define the length of the linker (L(m,n)) (Figure 6.5) and length of the linker defines the size of the cyclic ring; AB(m,n).

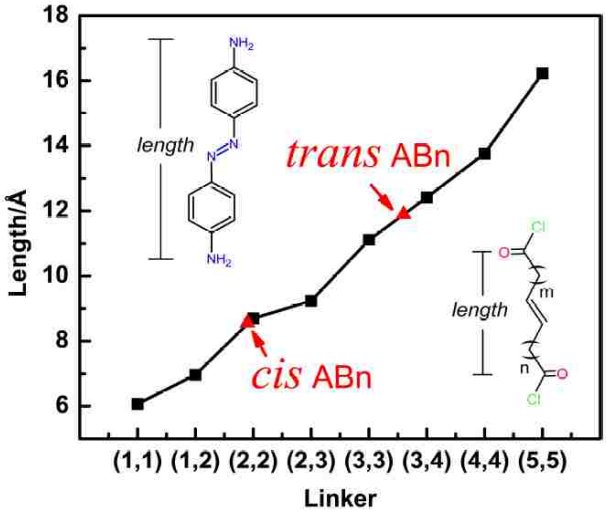

Figure 6.5: Length of linker vs L(m,n)[266]

Our collaborators in the Beck Lab (UKy) calculated the ring strain energies for different sizes of AB(m,n) cyclic monomers in *cis* (RSE_*cis*) and *trans* (RSE_*trans*) conformations[266]. Bigger cyclic molecules AB(m,n) have lower internal ring strain (Figure 6.6). The bigger molecular ring structure will have more freedom for its bonds to rearrange in 3D space in order to achieve the lowest energy possible. The ring strain for two separate states of a same molecule, i.e., *cis* and *trans* was found to be significantly different below a ring size of AB(5,5). Hence, AB(5,5) and any molecule bigger than AB(5,5) cannot be used to demonstrate the light-mediated ring strain of cyclic monomers. The minimum distance between amine functional group of ABn in *cis* conformation is 8.56 Å. As a result, the linker with length less than 8.56 Å will not be capable of connecting the two sides of the azobenzene molecule (Figure 6.4) [266]. This geometrical requirement eliminates AB(1,1) and AB(1,2) from the target set of synthesizable linkers. In all, these criteria focused the monomer design to structures between AB(2,2) and AB(4,5).

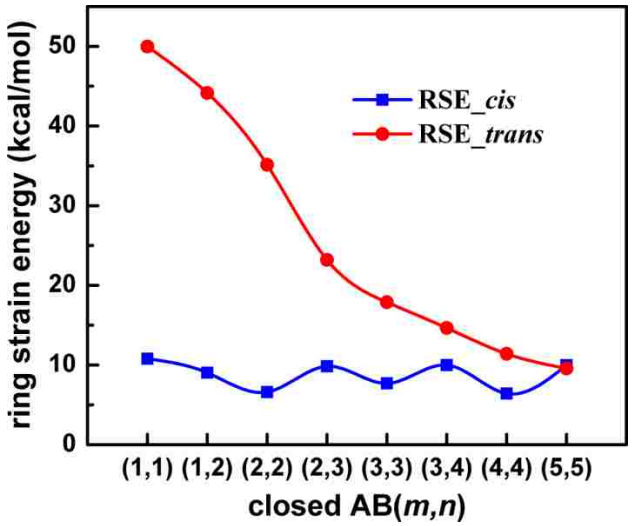

Figure 6.6: Ring strain energy of AB(m,n) in *cis* and *trans* conformation vs. size [266]

It is convenient with the separation and purification point of view to synthesize symmetrical molecule or AB(m,n) where m is same as n. Also, it would be easy to demonstrate the difference in the rate of polymerization of these monomers if the difference in the ring strain is large. Hence, we chose to synthesize AB(2,2) for further experiments. From Figure 6.6 we can see that the difference in the ring strains of AB(2,2) in *cis*

conformation and in *trans* conformation is significantly large to experimentally perform the light-mediated change in ring strain and ultimately rate of polymerization.

6.3 Synthesis approach

We hypothesize that these molecules can be synthesized by forming an AB containing diene (AB(m,n) *trans* open), and closing the ring while it is in the *cis* conformation; AB(m,n) *cis* open to AB(m,n) *cis* closed. We used ring closing metathesis (RCM) reaction to close the diene, yielding the desired cyclic monomer; AB(m,n) *cis* closed. RCM is one of such methodology that is used exclusively for making cyclic organic compounds from dienes. In RCM reaction, a new internal carbon-carbon double bond is formed by joining the two carbon-carbon double bonds of the same linear molecule by eliminating simple molecules like ethylene as a byproduct. Experimentally, RCM is not a single reaction but a fully reversible set of [2+2] cycloaddition-cycloreversion equilibria (Figure 6.7). All metathesis reaction pathways are reversible, and the extent of reversibility depends on the reaction conditions, type of catalyst, and type of monomer. Different products are obtained depending on reaction parameters and conditions among RCM, ROMP, Cyclodepolymerization (CDP), Acyclic diene metathesis polymerization (ADMET)[105]. Equilibrium needs to be shifted to achieve higher yield of desired final cyclic ring product by RCM by optimizing the reaction parameters. Oligomerization and formation of macrocyclic rings are the main competing reactions against RCM. The removal of the ethylene by purging with inert gas prevents the reverse reaction to the diene and promotes RCM and ADMET products[267]. A low concentration of monomer reduces the likelihood of intramolecular reactions and suppresses the ADMET and ROMP polymerization products. Temperature, type of catalyst, catalyst concentration, and time of reaction also play very crucial role in maximizing conversion for RCM[105]. Grubbs catalysts are most commonly used metathesis catalysts, and they can be used in the variety of solvents, at any temperature ranging from ambient temperature to reflux temperature of the solvent. They are stable against polar functional groups in reactant molecules. Many different derivatives of Grubbs catalyst are available according to the reaction conditions, and type of diene[268]. Typically, RCM is carried out at the reflux temperature of the solvent used for the reaction to achieve maximum conversion. But if reactants are heat sensitive then it can

also be performed at lower temperatures. Time of reaction ranges from few minutes to hours, which is very specific to the type of monomer[100, 269, 270].

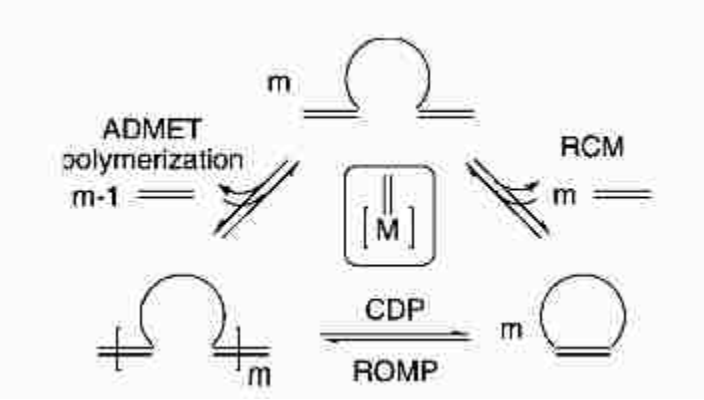

Figure 6.7: Reaction equilibriums in RCM[105]

To synthesize AB(m,n) *cis* closed using RCM, first AB(m,n) *trans* open needs to be synthesized with the half linker in each aromatic ring of azobenzene (Figure 6.8). AB(m,n) *trans* open is a diene that we photoisomerized into AB(m,n) *cis* open and used further for RCM.

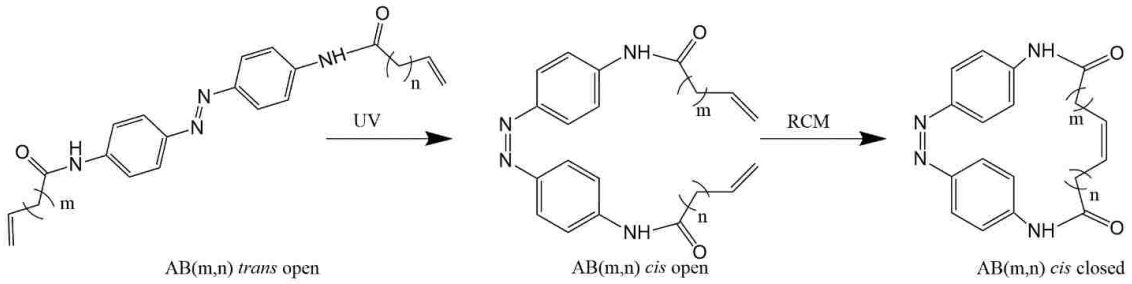

Figure 6.8: Schematic representation of RCM to synthesize AB(m,n) *cis* closed

6.4 Materials

Para-aminoacetanilide, sodium perborate tetrahydrate, boric acid, glacial acetic acid, methanol, hydrochloric acid, 4-Pentenoic acid, thionyl chloride, dry dichloromethane, triethylamine, sodium bicarbonate, Chloroform-*d,* Grubbs catalyst 1st generation, and Grubbs catalyst 2nd generation. All the reagents and solvents were purchased from Sigma-Aldrich and were used as received.

6.5 Results and discussion

For the synthesis of AB(2,2) *cis* closed, total synthesis procedure is divided into 4 steps (Figure 6.9). Synthesis of 4,4'-diaminoazobenzene (ABn), 4-pentenoyl chloride i.e. half of linker with acid chloride functional groups, AB(2,2) *trans* open and AB(2,2) *cis* close using RCM.

6.5.1 Synthesis of 4,4'-Diaminoazobenzene (ABn)

For synthesis of 4,4'-diaminoazobenzene procedure from organic syntheses was referred[271]. Para-aminoacetanilide (29g, 0.19 mol), sodium perborate tetrahydrate (40g, 0.26 mol) and boric acid (10g, 0.16 mol) were mixed in glacial acetic acid (500 ml). 2 necked round bottom flask (RBF) of volume 1l with provision of thermometer, magnetic stirrer, and reflux condenser was used. The mixture was reacted for about 8 hours at 60ºC during which mixture starts phasing out after 50 minutes. After the reaction was complete, the mixture was cooled down to room temperature, and the muddy yellow colored precipitate was collected by filtration under reduced pressure. This solid product was washed with water till the filtrate had neutral pH and the residue product was dried in an oven overnight at 90ºC till most of the water was evaporated, and dry product was obtained. The dry product was dissolved in methanol (150 ml) and hydrochloric acid (150 ml, 6 N) in 500 ml of round bottom flask with reflux condenser and stirrer. This mixture was heated at 110ºC for about 2 hours and was cooled immediately to collect purple-brown solid product using filtration under reduced pressure. It was washed with water till filtrate was neutral in pH. After washing a brown product was obtained and it was dried at 85ºC to get the final dry product of 4,4'-Diaminoazobenzene (ABn) with yield of 50%. The structure was confirmed by Nuclear Magnetic Resonance spectroscopy (^{1}H NMR) and Electrospray ionization mass spectroscopy (ESI-MS). ^{1}H NMR (400 MHz, Chloroform-*d*) δ 7.80 – 7.71 (4H, m, =N-C-C*H*=), 6.80 – 6.72 (4H, m, =CH-C*H*-C), 3.96 (4H, s, -NH_2).

6.5.2 Synthesis of 4-pentenoyl chloride

4-Pentenoic acid (325 µl, 0.0032 mol) was heated in RBF at 55ºC for 15 minutes and the thionyl chloride (243 µl, 0.0033 mol) was added to this heated 4-pentenoic acid slowly. Then this mixture was heated at 65ºC for 4 hours. After 4 hours, the mixture was heated at 75ºC - 80ºC to distill off the excess of thionyl chloride (b.p. 74ºC). Once the mixture was

cooled down to room temperature, the dry dichloromethane (DCM) (5 ml) was added to this 4-pentenoyl acid chloride closing it immediately with a septum.

6.5.3 Synthesis of AB(2,2) trans open

ABn (0.112 g, 0.0005 mol) and triethylamine (TEA) (222 µl, 0.0015 mol) was mixed in DCM (175 ml) and stirred under nitrogen for about 1 hour to completely mix ABn in solvant. A solution of 4-pentenoyl chloride in DCM was added to the solution of ABn and TEA in DCM dropwise. The reaction was allowed to continue overnight under inert atmosphere and stirring conditions. After the reaction was complete, the organic solution was washed with 5% aqueous solution of sodium bicarbonate 5 times. the product solution was passed through silica gel column to completely remove unreacted pentenoic acid and ABn. The structure of final product; AB(2,2) *trans* open was confirmed by ESI-MS and ^{1}H-NMR. ^{1}H NMR (400 MHz, Chloroform-*d*) δ 7.96 – 7.85 (4H, m, =N-C-C*H*=), 7.67 (4H, m, =CH-C*H*-C), 5.91 (2H, m, -CH_2-C*H*=CH_2), 5.18 – 5.03 (4H, -CH=CH_2), 2.56 – 2.43 (8H, m, -CH_2-)

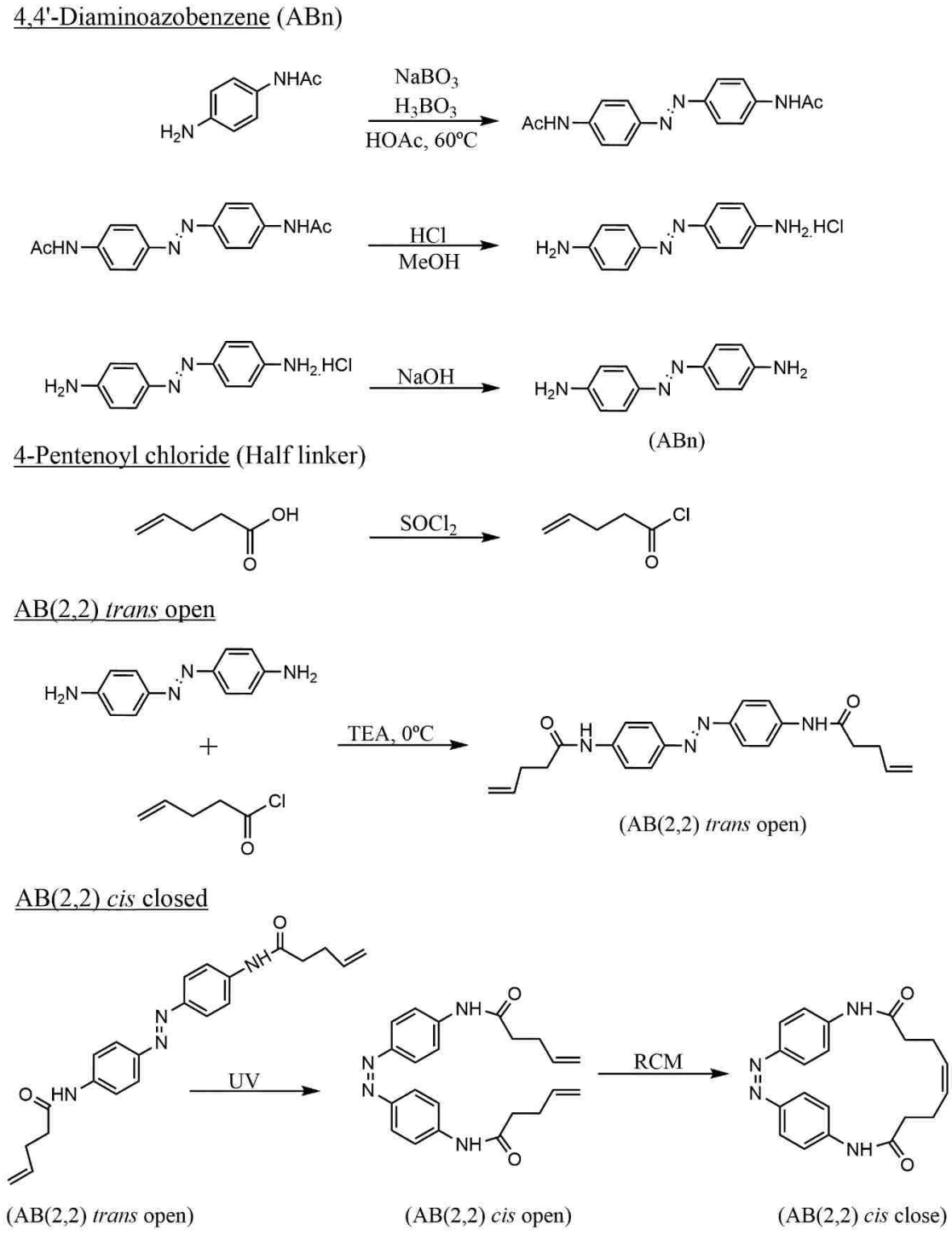

Figure 6.9: Synthesis scheme for AB(2,2) *cis* closed

In order to complete the last step of the synthesis, i.e., closing the AB(2,2) open by RCM reaction, the requirement of absorption properties of AB(2,2) open like λ_{max} and time for *trans* to *cis* photoisomerization are very essential. Because we hypothesize that

photoisomerization of AB(2,2) open to *cis* conformation will bring the terminal unsaturated functional groups closer or decrease the distance between them as in case of pure azobenzene, rendering it easy for the catalyst to close the open molecular structure into a closed ring. Also, it will support the selection of light source that covers the absorption range of AB(2,2). Hence, the absorption properties were studied in DCM using UV-Vis spectroscopy. Single scans of ABn and AB(2,2) are shown in Figure 6.10 in *trans* and *cis* confirmation. λ_{max} for ABn in *trans* and *cis* conformation is 393 nm and 452 nm respectively. Whereas for AB(2,2), the λ_{max} in *trans* and *cis* conformation is 366 nm and 446 nm respectively. Change in the λ_{max} also confirms the modification of ABn to AB(2,2). The kinetic studies of photoisomerization of ABn and AB(2,2) from *trans* to *cis* and *cis* to *trans* were studied too. Solution of AB(2,2) in DCM was first irradiated with UV 365 nm LED light for 10 minutes till equilibrium between *trans* and *cis* molecules was shifted towards *cis* conformation molecules. Then the solution was irradiated with blue light (455 nm) as it is the closest to the absorption required for *cis* to *trans* isomerization. But when the same solution was irradiated with the green light (530 nm) which is in the absorption spectrum of AB(2,2) responsible for *cis* to *trans* isomerization, it shifted the equilibrium of *cis* to *trans* isomerization more towards cis.

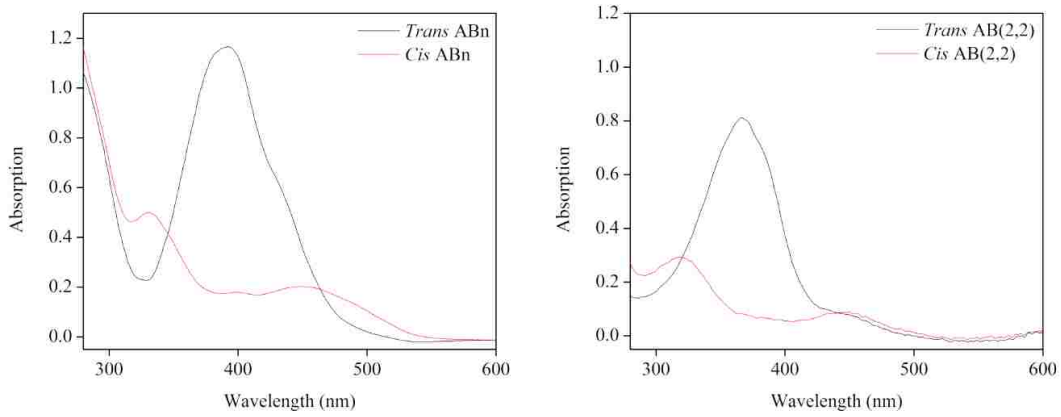

Figure 6.10: UV-Vis absorption spectrum of ABn and AB(2,2) in *trans* and *cis* conformation

Figure 6.11 show increase in the absorption of λ_{max} by AB(2,2) with time under different irradiation conditions. Photoisomerization of AB(2,2) under two different light exposures at their highest intensity (~30 mW/cm^2) were studied because both could photoisomerize

AB(2,2) from *cis* to *trans*. The rate of photoisomerization by blue light (0.3 minutes) was faster than by green light (0.8 minutes), as it matches exactly with the wavelength needed by AB(2,2) for isomerization (452 nm). But the population of *trans* AB(2,2) achieved by green light exposure is higher than by blue light.

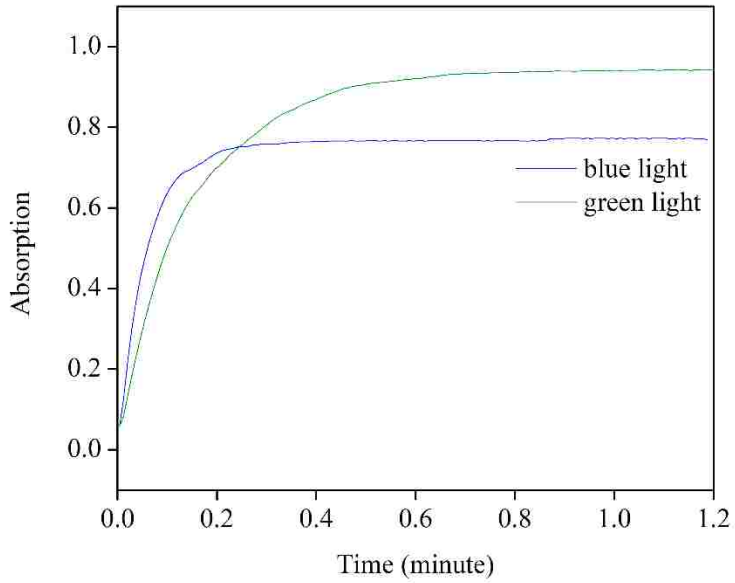

Figure 6.11: Kinetics of absorption of AB(2,2) under blue light and green light separately

This is because LED light sources emit photons with a distribution of wavelength. Figure 6.12 (from https://www.thorlabs.com/) shows an emission spectrum of light sources used for the experiment. The wavelength distribution for the LED lamps is a single peak centered at a specific λ_{max} for each light source. Although the blue light source has λ_{max} of 455 nm, it also emits light with wavelength till 420 nm which helps *trans* to *cis* isomerization. Whereas, even though green light emits λ_{max} of 530 nm which is not closest to 452 nm (exact wavelength for *cis* to *trans* isomerization), it does not participate in *trans* to *cis* isomerization. Hence, using green light compromises the rate of photoisomerization, but it generates a higher population of molecules in *trans* conformation. This study very crucial for the selection of light source when AB(2,2) open is closed to AB(2,2) *cis* closed. After synthesis of closed ring monomer, if the absorption spectrum of AB(2,2) does not change then, experimentally, the green light source will be perfect for demonstrating

AB(2,2) *cis* closed to AB(2,2) *trans* closed isomerization which is essential for light-mediated ROMP.

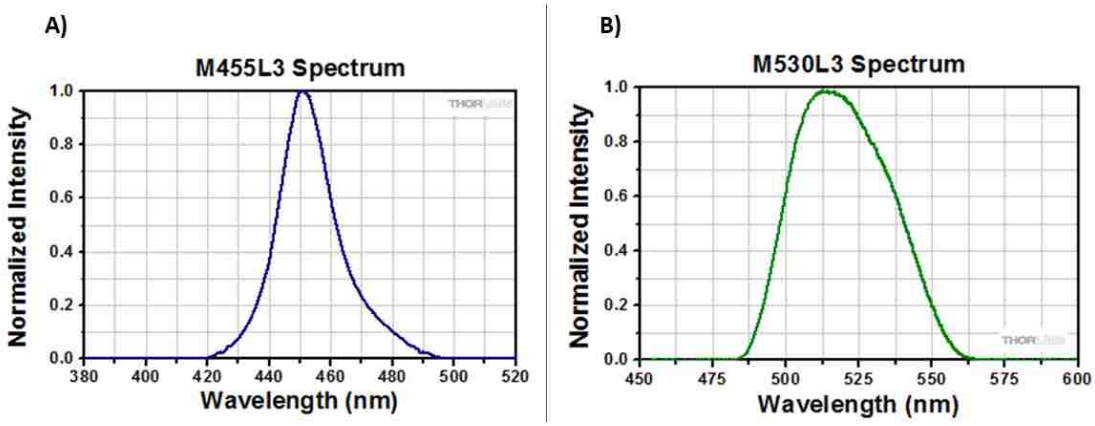

Figure 6.12: Emission spectra of LED light sources; A) Royal blue light (455 nm); B) Green light (530 nm)

6.5.4 Synthesis of AB(2,2) cis closed

Reaction setup for ring closing metathesis was consists of heating at reflux temperature, continuous removal of ethylene gas, UV irradiation, and stirring. The temperature during the reaction, monomer concentration, grubbs catalyst concentration, reaction time and UV light for irradiation during the reaction are the parameters directly affecting the yield of the reaction. We used maximum intensity (~15 mW/cm^2) of light provided by THORLABS UV LED lamp for photoisomerization to *cis*. Reactions were performed at room temperature and also at the reflux temperature of solvent, i.e., 40ºC for DCM. Two different monomer concentrations of AB(2,2) open were used, i.e., 2 mM and 2 μm concentration, and reactions were performed for the time span from 5 minutes to 48 hours. And lastly, the concentration of catalyst (1st or 2nd generation) was varied between 1, 2, 5 and 10 mol% with respect to monomer concentration.

As shown in the Figure 6.13 below, the reactor vessel (50 ml, 3 necked round bottom flask) was continuously irradiated with UV light for 30 minutes before and during the reaction. Using a hot plate, the reaction vessel was heated, and the solution was stirred continuously. Above the reaction vessel, a dropping funnel was attached to ensure slow and dropwise addition of catalyst to the monomer solution. The reaction was purged and bubbled with nitrogen intermittently to remove dissolved ethylene from the reaction solution.

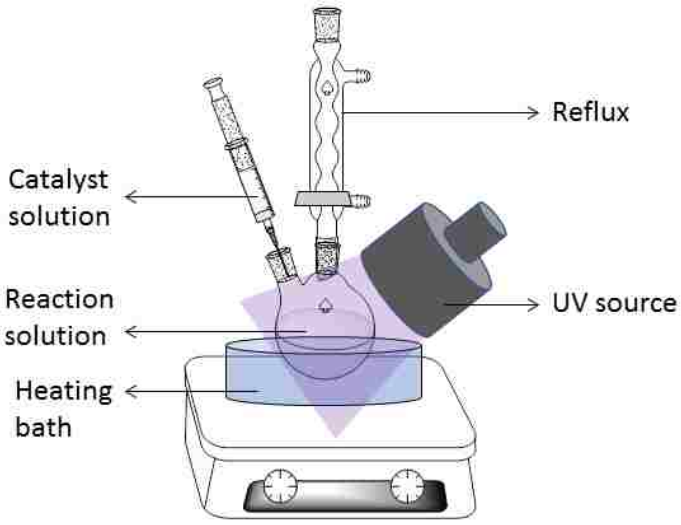

Figure 6.13: Reaction setup used for RCM

Using any combination of reaction parameters discussed above, RCM did not yield any cyclic ring product of AB(2,2) *cis* closed. ^{1}H-NMR of reaction solution before and after RCM was same for all the reactions. ADMET reaction was also performed to confirm the metathesis activity of the catalyst. In ADMET reaction, oligomers are formed by cross metathesis between diene AB(m,n) open units. No oligomers were obtained as the product of ADMET reaction of AB(2,2) open. Based on the literature, presence of metathesis catalyst in diene solution should yield either oligomers or closed ring product to some extent. Hence, we hypothesize that the catalyst is getting deactivated during the reaction. As there was only monomer present in the reaction solution except the catalyst, we hypothesize that monomer is deactivating the catalyst. We tested this hypothesis by designing experiments using a reaction performed in literature. We found that amide functional group is the root cause for the deactivation of the catalyst.

6.5.5 Catalyst deactivation investigation

A control reaction from literature was used to troubleshoot and investigate the root cause of zero yield for closed ring product or AB(2,2) *cis* closed from the RCM reaction. Diethyl diallyl malonate (DEDAM), a diene monomer was used for control RCM reaction with 99% conversion to closed ring product in 4 hours of reaction[106]. To determine which functional group out of amide, amine, and azo was the reason for deactivation of the

catalyst, all the precursor compounds of AB(m,n) i.e. azobenzene, diaminoazobenzene, and AB(2,2) were used as additives during RCM reaction of DEDAM.

In brief, RCM of DEDAM (0.5 mM) was performed in DCM at room temperature using grubbs 2nd generation catalyst (0.2 mM) (Figure 6.14), giving 99% conversion of DEDAM to ring product. This was confirmed from ^{1}H-NMR and no peaks for ethylene were present as it is a gaseous product. The progress of the reaction can be seen in the NMR profile (Figure 6.15) of reaction where at 4th hour reaction is almost complete.

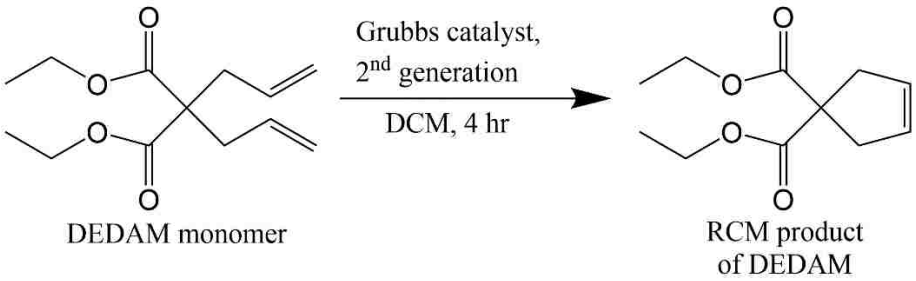

Figure 6.14: Reaction scheme of RCM of DEDAM using Grubbs catalyst 2nd generation

Structures of DEDAM monomer and RCM product were confirmed by ^{1}H-NMR. ^{1}H NMR of DEDAM (400 MHz, Chloroform-*d*) δ 5.64 (2H, m, CH_2=C*H*-CH_2), 5.14 – 5.03 (4h, tm, C*H*$_2$=), 4.16 (4H, qt, -O-C*H*$_2$-CH_3), 2.62 (4H, dd, =CH-C*H*$_2$-C), 1.23 (6H, m, -C*H*$_3$). ^{1}H-NMR of RCM product of DEDAM (400 MHz, Chloroform-*d*) δ 5.61 (2H, s, =C*H*-CH_2), 4.19 (4H, qt, -O-C*H*$_2$-CH_3), 3.01 (4H, s, =CH-C*H*$_2$-C), 1.25 (6H, m, -C*H*$_3$).

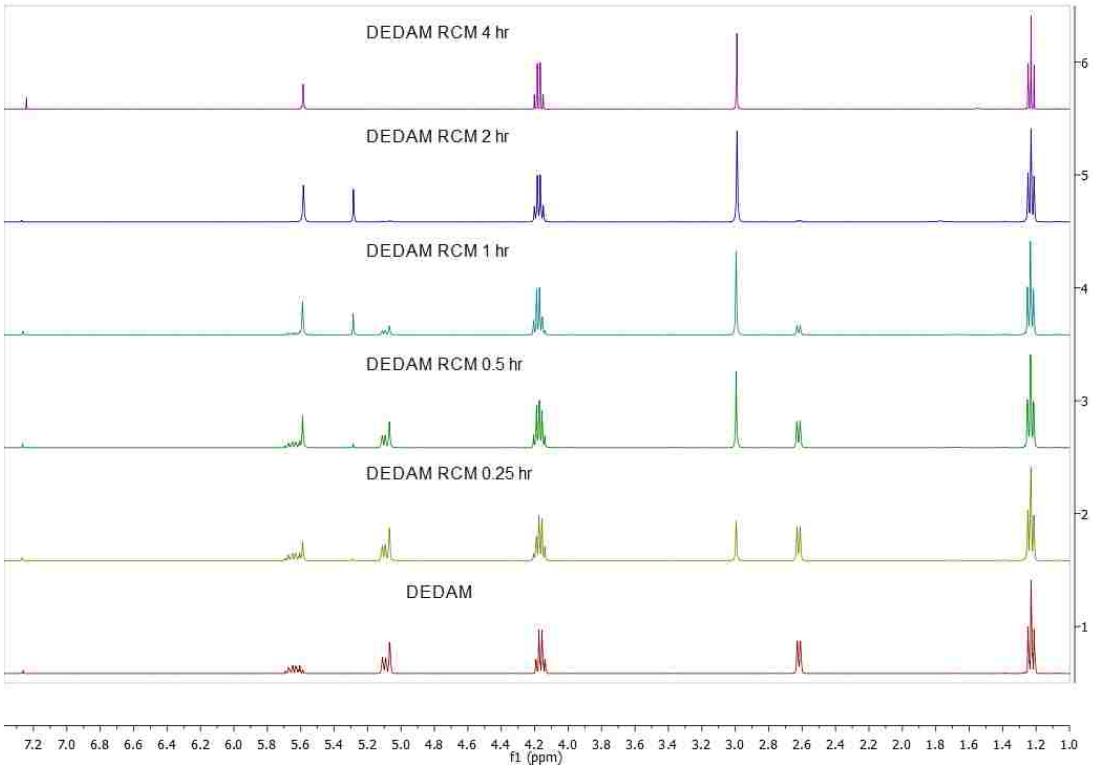

Figure 6.15: ^{1}H-NMR profile of RCM of DEDAM

Using this control reaction, first, the effect of UV irradiation on the activity of grubbs catalyst 2nd generation was checked by performing two RCM reaction with same concentrations and atmospheric conditions but one reaction was performed under continuous UV irradiation, and other was performed in room light and not external UV exposure. From ^{1}H-NMR of the products (Figure 6.16) it was confirmed that there is no significant difference in the conversion, i.e., 99% conversion is achieved with no UV exposure and 98% conversion with UV exposure.

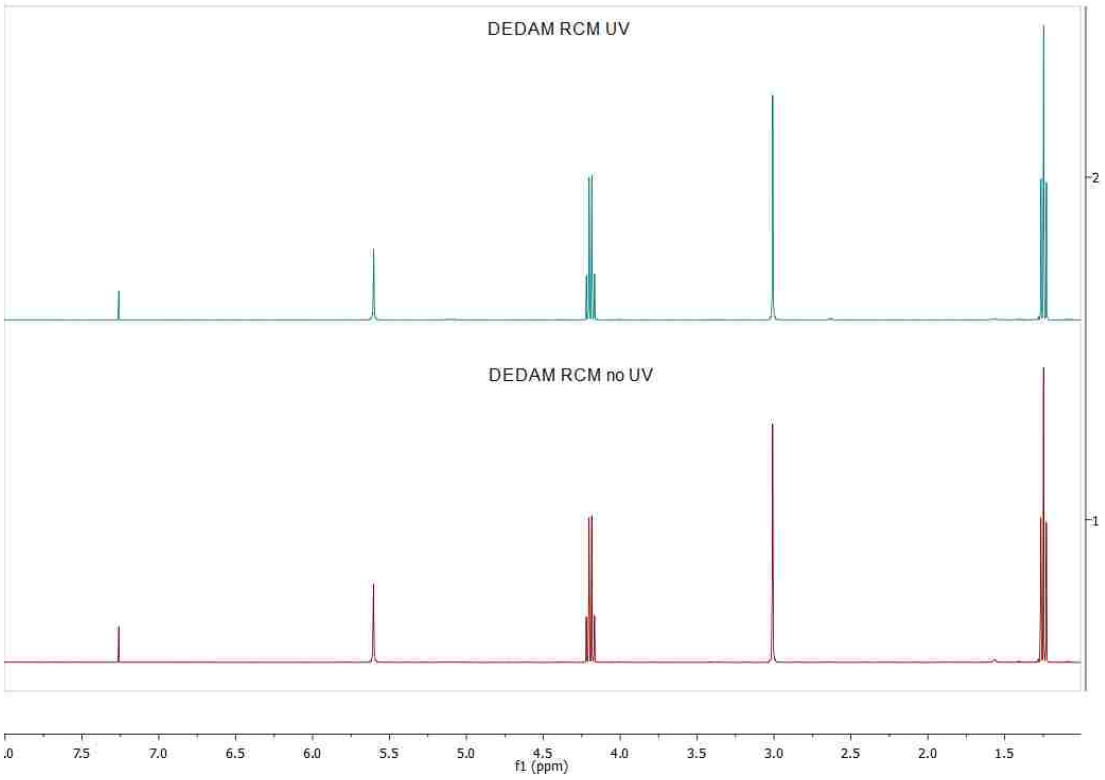

Figure 6.16: ^{1}H-NMR of RCM of DEDAM with and without UV exposure

With the exclusion of light deactivation pathway, we hypothesized the monomer functional groups were responsible for the deactivation of the catalyst during RCM.

To evaluate the deactivation by functional groups in AB(2,2); azobenzene (AB), and AB(2,2) were added in the control reaction. Azobenzene was present in an equimolar concentration to the catalyst, and AB(2,2) was present in two different concentrations; equimolar and 10x to the catalyst concentration. All three control reactions along with a reaction with no additives were set up and allowed to react for 4 hours in same atmospheric conditions. No irradiation was done to the reaction solutions during the reaction.

The RCM reactions of AB(2,2) were performed for different length of times but the average time was around 2 hours. Hence, experiments were done where catalyst was first dissolved in DCM and DEDAM was added after 2 hours (Figure 6.17). This let us find out actual decrease in the activity of catalyst after 2 hours. Still 92% conversion was achieved for the reaction with only DEDAM. This RCM of DEDAM could achieve only 7% conversion of reactants to product where AB (2,2) and catalyst were present in same concentration.

Whereas, when concentration of AB(2,2) was 10 times excess to catalyst and only 3 % conversion could be reached. And the last reaction was carried out by dissolving catalyst and azobenzene (AB) together in DCM for 2 hours and then DEDAM was added for RCM. Here the experimental conversion was 88% which confirmed negligible effect of azo functional group (N=N) on catalyst in 2 hours. Hence, based on these results, it was concluded that the amide functional group is the cause for catalyst deactivation. Other potential reason would be the deactivation by primary amine if diaminoazobenzene was present. But the AB(2,2) was purified and purity was confirmed by 1H-NMR and ESI, which eliminates the possibility by amine group. Hence, the cause of deactivation is attributed to amide functional group in AB(2,2).

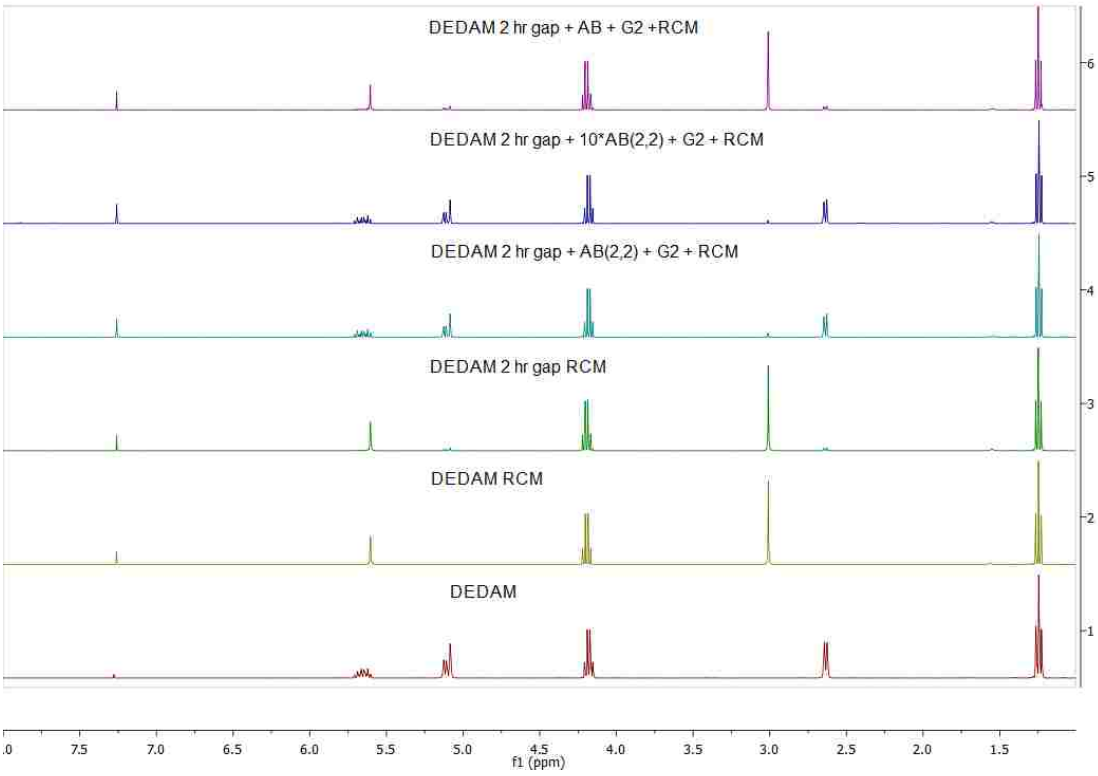

Figure 6.17: ^{1}H-NMR of RCM product of DEDAM in presence of different compounds after 2 hour exposure of grubbs catalyst to those molecules

But, some literature examples document the use of Grubbs catalyst 2nd generation in RCM reactions with amide functionality[272-275]. Unfortunately, this study strongly supports a drastic decrease in the activity of Grubbs 2nd generation catalyst in the presence of an amide functional group. As a result, we are motivated to redesign the responsive ring to eliminate

amide bonds, and promote the reactivity of Grubbs 2nd generation catalyst for our target RCM reactions.

6.6 Conclusions

In this work, detail design of a class of photoresponsive monomer capable of light-mediated modulation of ring strain energy and thus ring opening metathesis polymerization is presented. Synthesis and characterization of a representative monomer is exploited in depth. AB(2,2) open, a photoresponsive diene derivative of azobenzene is synthesized to obtain AB(2,2) closed using ring closing metathesis polymerization. Absorption properties of AB(2,2) were studied using UV-Vis spectroscopy under different irradiation conditions. Unfortunately, cyclic closed ring product could not be obtained from AB(2,2) open using any combination of reaction condition. The problem was carefully analyzed using a control RCM reaction of diethyl diallylmalonate from literature. The experiments led to the conclusion that UV irradiation did not alter the activity of the catalyst in action, but the prolonged exposure of grubbs catalyst (2nd generation) to AB(2,2) was deactivating the catalyst, more specifically, amide functional group was the root cause for the deactivation of the catalyst. Nonetheless, the concept of light-mediated ring opening metathesis polymerization was still explored using an alternative monomer with the different structure. Details are discussed in chapter 7.

7 Light-mediated ring opening metathesis polymerization

7.1 Introduction

Photo-responsive polymer surface coatings have gained huge acceleration in its research since last decade. Photo-responsive polymers typically have alkane chains as the backbone with azobenzene molecules as a branch [2, 3] or in the main chain of the polymer itself[4]. On exposure to particular radiations, these polymers change their physical and chemical properties. Azobenzene is the most commonly used photo-responsive moiety to impart photo-responsive nature to polymers or macromolecules. Azobenzene undergoes 'photoisomerization' changing its structure from *trans* to *cis* when exposed to UV radiations and back from *cis* to *trans* by 'photo or thermally assisted isomerization' when exposed to visible light or heated, respectively. There are numerous applications in the form of a surface patterned photoresponsive polymers coatings in microfluidics[276], biosensors[276, 277], dry etching[278, 279], and patterns for reactive ion etching resist[280]. Variety of studies has been published regarding the different monomers for photoresponsive polymers, and creative applications using conventional methods to prepare photoresponsive polymers or coatings. Very less focus has been on the actual development of the method for controlling or improving the existing polymerization techniques. For instance, some research groups have introduced a monomer for making photoresponsive polymers with ring opening metathesis polymerization (ROMP)[4, 171]. Whereas, Aaron Teator and co-workers have developed a photo-switchable olefin metathesis catalyst with the ability to 'switch ON' and 'switch OFF' ROMP using light as stimuli. We combined these two ideas into one to develop a monomer with the ability to 'switch ON' and 'switch OFF' the ROMP using light. This novel photoresponsive monomer allows spatiotemporal control on the process of polymerization using light, which is very crucial in tailoring the block co-polymers by sequential addition of monomers and switching polymerization ON and OFF as required during polymerization in solution phase. This will also provide freedom of spatiotemporal control on the surface polymerization during surface initiated ring opening metathesis polymerization (SI ROMP) to create surface architectures. SI ROMP is a type of surface initiated polymerization (SIP) technique to prepare surface coatings, comparatively stable than by

spin coating, with better control over the process of surface polymerization to tune the properties of coatings as desired.

In this work, we have introduced a light-mediated temporal control over its ROMP by designing a photoresponsive monomer for ROMP. The ROMP of the designed monomer can be switched ON and OFF using UV and visible light as required without deactivating the olefin metathesis catalyst.

7.2 Design

We hypothesize that introducing chromophore very near to the main structure of strained ring will create stearic protection for the unsaturated site between the catalyst and growing chain, on photoisomerization of the chromophore to *cis* conformation. When chromophore is photoisomerized back to *trans* conformation, it will be possible to resume the polymerization as the propagation site will be again accessible to the next monomer. Hence, the fundamental requirement for the practicality of this mechanism is the proximity of chromophore to the cyclic ring monomer as much as possible. On photoisomerization of the chromophore to *cis* conformation, the distance between the open phenyl ring and the metal center of the bound catalyst should decrease enough to reduce the accessibility to the catalyst metal center. This is the first of a kind where the process of polymerization will be controlled using light without irreversible deactivation of the catalyst by addition of terminating agent like ethyl vinyl ether.

Our approach to design this monomer is based on the combinations of two chemistries: photoisomerization and ROMP. More specifically, we merged a photoresponsive group (azobenzene, chromophore) and a ROMP polymerizable group (norbornene). Azobenzene and its derivations isomerize when irradiated with UV light, changing its conformation from thermodynamically stable *trans* to unstable *cis* conformation. Norbornene is the most commonly used monomer for the study of ROMP because of its high ring strain energy, thermal stability, and easy to modify or synthesize derivatives. Figure 7.1 shows norbornene (NB) and polynorbornene (pNB) formed by ROMP.

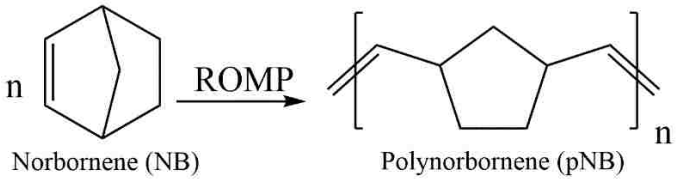

Figure 7.1: Norbornene and its polymerization to polynorbornene

For the facile synthesis of norbornene monoazobenzene (NMA), derivatives of norbornene and azobenzene with functional groups were used for the synthesis of representative monomer. The essential requirement was to keep azobenzene as close to cyclic ring structure as possible, so that, photoisomerization of azobenzene (*trans* to *cis*) creates a stearic hindrance (stearic protection) around the catalyst-intermediate, preventing the monomer access to the catalyst-intermediate during ROMP.

We used an azobenzene with the hydroxyl functional group at *para*- position and a norbornene derivative with carboxylic acid functional group substituted at the 2- or 3-position. Norbornene derivatives are categorized as isomers with different orientations of the functional groups. Functional group pointing towards the carbon-carbon double bond of the cyclic ring is called endo isomer, and if it is pointing away from carbon-carbon double bond, then it is called exo isomer. After tagging chromophore at this location, it produces two conformations of new monomer, endo, and exo. In addition, when we tag chromophore to norbornene it introduces two more sub conformations, i.e., *trans* and *cis* for each type of orientation, i.e., endo and exo (Figure 7.2) (See appendix for simulated 3D structures). The 3D images in appendix help for better imagination of accessibility of benzene ring of azobenzene in cis conformation after photoisomerization. It has been shown previously, that typically exo isomer of norbornene derivatives is more reactive than endo isomer mainly due to a steric hindrance to the catalyst by endo functional group trying to form metallocyclobutane intermediate (2+2 cycloaddition) for initiation and propagation of polymerization[175, 179].

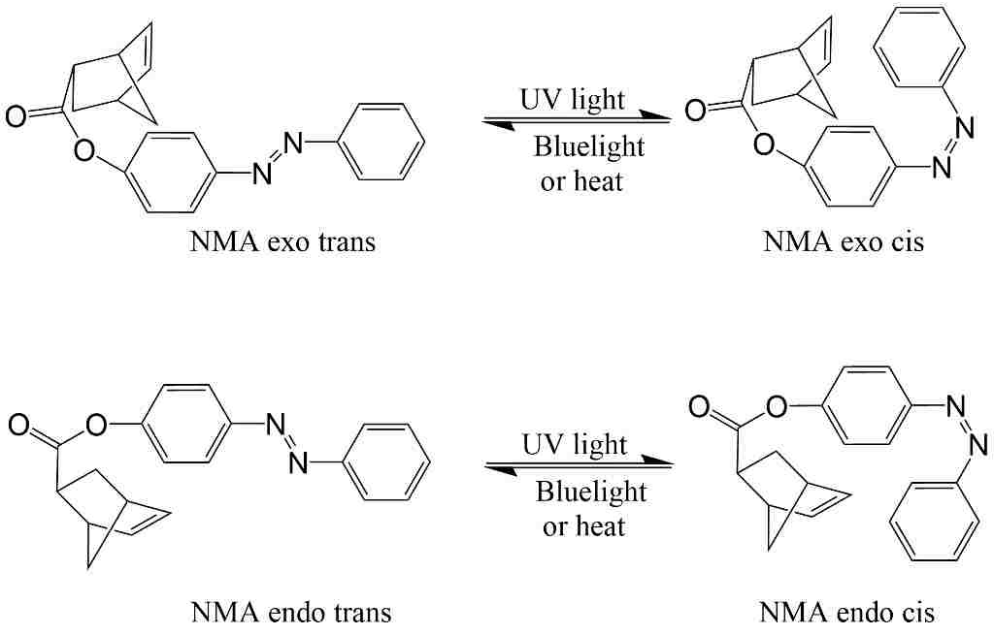

Figure 7.2: Photoisomerization of NMA exo & endo

7.3 Materials

All the reagents were purchased from Sigma Aldrich and were used as received. Exo-5-Norbornenecarboxylic acid (NCA exo) (97%), 5-norbornene-2-carboxylic acid (NCA endo) (98%) (mixture of endo and exo but predominantly endo, 80%), 4-phenylazophenol (ABOH) (98%), thionyl chloride reagent plus (>99.0%), triethylamine (>99.5%), Grubbs catalyst 3rd generation (G3), ethyl vinyl ether (EVE) (99%), tetrahydrofuran HPLC grade (THF, from Pharmco-aaper), dichloromethane anhydrous (DCM) (>99.8%), chloroform anhydrous (>99%), dichloromethane-d_2 (>99.5%, 0.03% v/v TMS).

7.4 Synthesis

For the synthesis of NMA endo & exo, commercially available 5-norbornene-2-carboxylic acid predominantly endo (NCA endo) and 5-norbornene carboxylic acid exo (NCA exo) were used. As the carboxylic acid group was available in two stereoisomers, endo & exo, we synthesized both endo & exo form of NMA to study the effect of stereoisomerization and photoisomerization simultaneously. Solution of azo-4-phenylazophenol and triethylamine (TEA) solution was prepared in anhydrous chloroform and stirred under nitrogen environment till azo-4-phenylazophenol was dissolved completely. In a second flask, carboxylic acid functional group in NCA was converted to the carbonyl chloride

functional group using highly reactive thionyl chloride. NCA was reacted with 15 times molar excess of thionyl chloride at 60 ºC for 3 hours[281]. The residual thionyl chloride after the reaction was distilled under reduced pressure at 40ºC. The freshly synthesized acid chloride, still under nitrogen environment was dissolved in anhydrous chloroform and transferred immediately to the solution of ABOH and TEA very slowly using dropping funnel. The reaction was allowed to continue for 14 hours and monitored by TLC for completion. The reaction solution was then washed with water and brine solution to completely remove the TEA salts. The product was purified by running the product mixture through silica gel column multiple times with 10% acetone as mobile phase and recrystallized to get solid orange crystals. Synthesis route is shown in Figure 7.3. The structure of the final product was confirmed by proton nuclear magnetic resonance spectroscopy (^{1}H-NMR) and electron spray ionization mass spectroscopy (ESI-MS). NMA endo and NMA exo were synthesized separately. NMA endo product was synthesized using NCA endo (mixture of endo and exo with 80% endo) and hence it was not purified further as it needs special distillation setup for separation of stereoisomers with a small difference in boiling points.

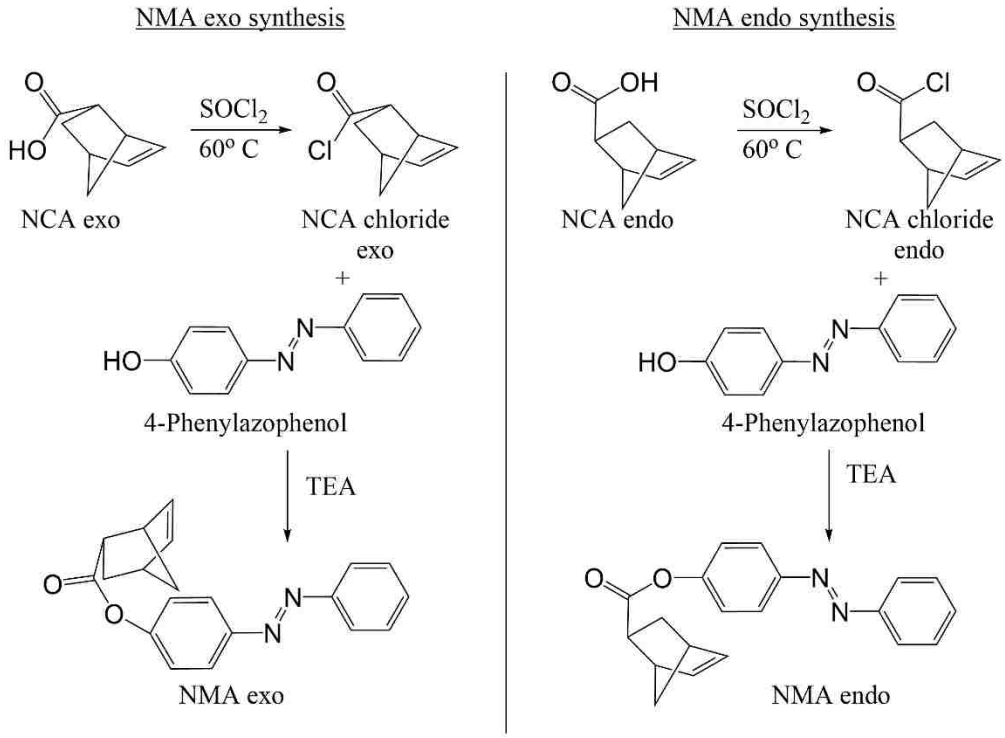

Figure 7.3: Synthesis scheme for NMA exo and endo

7.5 Characterization

The purity of the synthesized product was confirmed by electrospray ionization mass spectrometry (ESI-MS). The molecular ion was obtained at 319 m/z which corresponds to the MW of NMA endo or exo singly charged ion. Figure 7.4 is the MS spectrum for NMA endo (same for NMA exo). The ion at 199 is a fragment ion of 319, confirmed by forced ionizing 319 ions with suitable energy reproducing the same 199 ions by complete fragmentation.

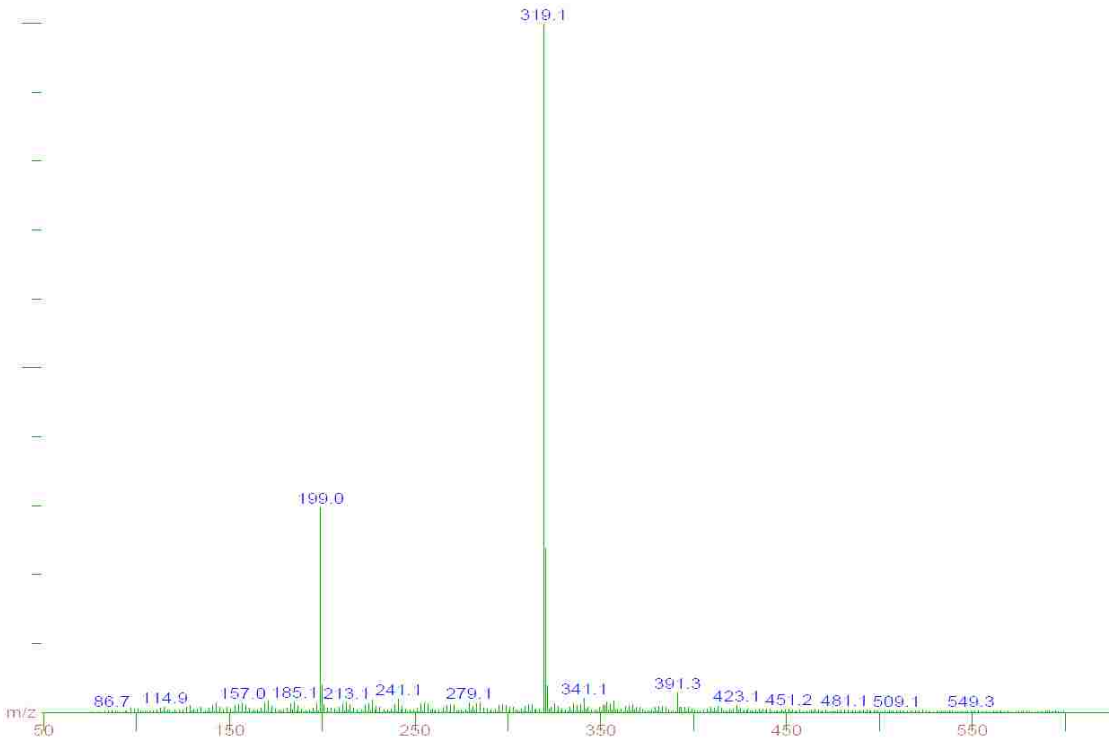

Figure 7.4: ESI-MS spectrum for NMA endo

^{1}H-NMR of NMA exo was collected in DCM-d_2 when the solution had negligible NMA *cis*. NMA exo *trans* (Figure 7.5 B): 7.95 (m, 4H, Ar-*H*), 7.54 (m, 3H, Ar-*H*), 7.28 (dt, 2H, Ar-*H*), 6.23 (m, 2H, C*H*=C*H*), 3.26 (s, 1H, =CH-C*H*-*CH*), 3.01 (s, 1H, =CH-C*H*-CH_2), 2.54 (m, 1H, CH-CH_2-CH), 2.07 (m, 1H, -CO-C*H*), 1.66-1.38 (m, 3H, CH-CH_2-CH). The same solution was then exposed to UV 365 nm light for 30 minutes, and ^{1}H-NMR was collected immediately without exposing it to room light. This spectrum has both *trans* and *cis* conformation isomers as it is practically impossible to shift the equilibrium between the two isomers completely towards one type of stereoisomer. NMA exo *cis* and *trans* (Figure 7.5 A): 8.01-6.82 (m, 9H, Ar-*H*), 6.35-6.00 (m, 2H, C*H*=C*H*), 3.26 & 3.17 (s, 1H, =CH-C*H*-*CH*), 3.01 & 2.97 (s, 1H, =CH-C*H*-CH_2), 2.54 & 2.44 (m, 1H, CH-CH_2-CH), 2.07 & 2.00 (m, 1H, -CO-C*H*), 1.66-1.38 (m, 3H, CH-CH_2-CH)

When NMA exo *trans* solution in DCM-d_2 is irradiated with UV 365 nm radiations, new peaks are observed in NMR at chemical shifts different than the original. This is due to the changes in the electronic environment of protons or the photoinduced anisotropy in

azobenzene structure[282-284]. Photoisomerization of NMA *trans* to *cis* conformation affects the electronic spin of almost all the protons in the molecule which is detected in ^{1}H-NMR shown below in Figure 7.5. New peaks generated between 8.01 to 6.82 are for protons in the aromatic ring and between 6.35 to 1.38 are for protons in norbornene cyclic structure. There is a noticeable change in the splitting of peaks at 6.25 for CH=CH. Even tiny change or addition in the proton peaks are the result of photoinduced anisotropy.

Similarly, ^{1}H-NMR was obtained for NMA with predominantly endo (80%) when it had negligible NMA *cis* molecules. Hence, the spectrum in Figure 7.5 D is the ^{1}H-NMR spectrum for NMA endo (80%) & exo (20%) *trans* in DCM. NMA endo (& exo) *trans*: 7.95 (m, 4H, Ar-*H*), 7.53 (m, 3H, Ar-*H*), 7.28 (d, 1H, Ar-*H*), 7.21 (d, 1H, Ar-*H*), 6.34-6.07 (m, 2H, C*H*=C*H*), 3.41 (s, 1H, =CH-C*H*-CH_2), 3.27 (d, 1H, CH-CH_2-CH), 3.01 (s, 1H, =CH-C*H*-CH_2), 2.53 (m, 1H, CH-CH_2-CH), 2.04 (m, 1H, -CO-C*H*), 1.66-1.34 (m, 3H, CH-CH_2-CH). The NMR spectrum of the same solution after exposing it to UV radiations for 30 minutes has both *trans* and *cis* conformation molecules of NMA endo (80%) and exo (20%). NMA endo (& exo) *cis* and *trans* (Figure 7.5 C): 8.02-6.76 (m, 9H, Ar-*H*), 6.34-5.98 (m, 2H, C*H*=C*H*), 3.41 & 3.33 (s, 1H, =CH-C*H*-CH_2), 3.27 & 3.18 (d, 1H, CH-CH_2-CH), 3.01 & 2.97 (s, 1H, =CH-C*H*-CH_2), 2.53 & 2.44 (m, 1H, CH-CH_2-CH), 2.02 (m, 1H, -CO-C*H*), 1.66-1.30 (m, 3H, CH-CH_2-CH).

As for NMA exo, NMA endo too generated new peaks at different chemical shifts than original when ^{1}H-NMR was collected after photoisomerization. New peaks between 8.02 to 6.76 are for protons in the aromatic ring of azobenzene and peaks between 6.34 to 1.30 are for protons in cyclic norbornene ring. For NMA endo, very significant changes are observed around the original CH=CH peak, i.e., 2 new peaks are generated. Similarly, new peaks are seen around old peaks of norbornene cyclic ring. This confirms that on photoisomerization the phenyl ring on azobenzene in NMA endo comes closer to the unsaturated functionality of norbornene even more than in case of NMA exo *cis*.

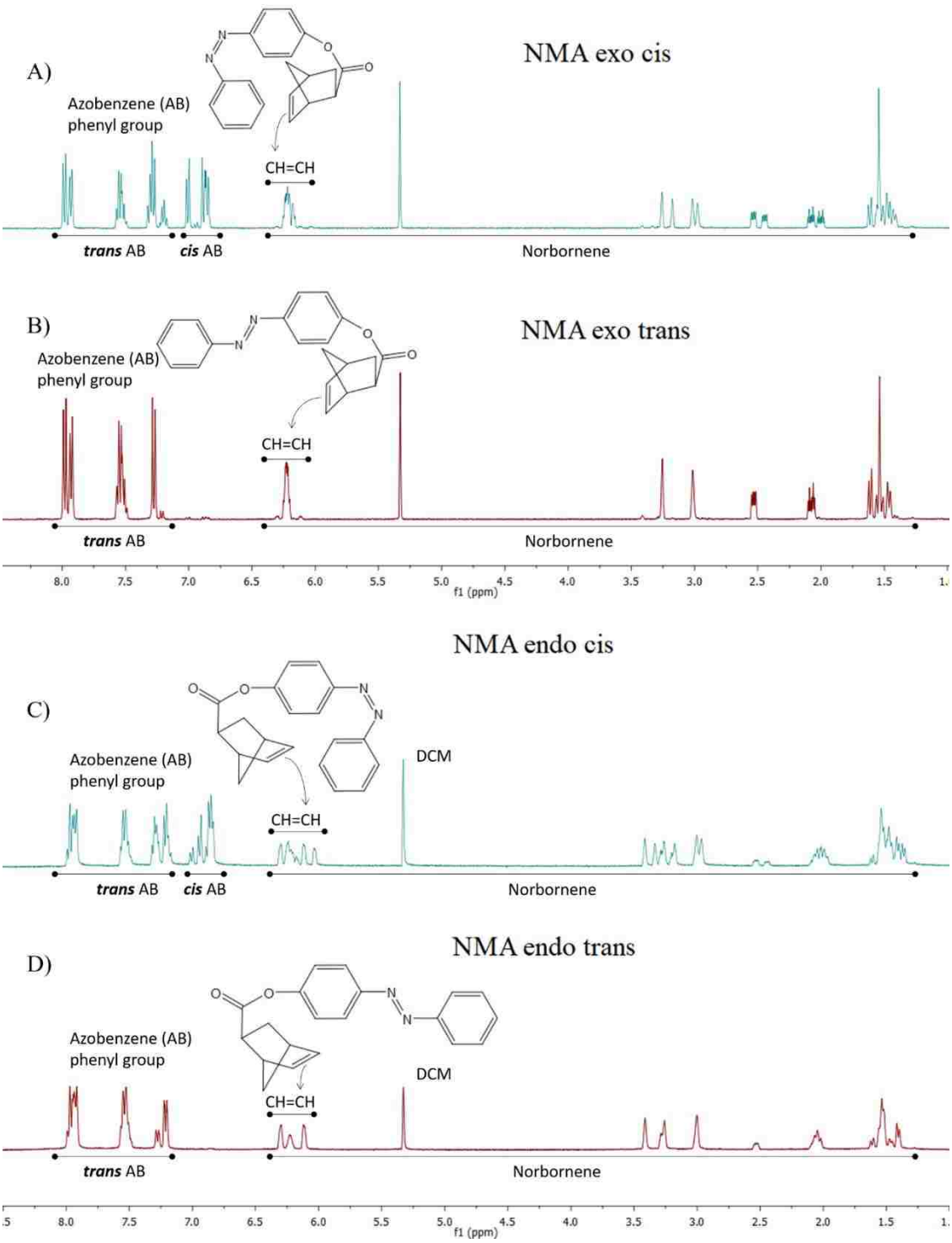

Figure 7.5: ^{1}H-NMR of NMA under different irradiation conditions; A) NMA exo *cis*, B) NMA exo *trans*, C) NMA endo *cis*, D) NMA endo *trans*

The light absorption properties of NMA endo & exo were studied by recording UV-Vis spectrum using UV-Vis spectrophotometer to find out their λ_{max} and rate of

photoisomerization in DCM by recording real-time photoisomerization spectrum. Figure 7.2 shows changes in the geometrical structure of NMA due to photoisomerization. Figure 7.6 A) shows single scan UV-Vis spectrum of molecules dissolved in DCM. In *trans* conformation (π-π^* transition), ABOH has λ_{max} at 343 nm whereas NMA exo & endo have λ_{max} at 325 nm. When irradiated with their λ_{max}, they change their geometry to *cis* conformation and their λ_{max} changes to 436 nm (n-π^* transition). On irradiating solution of *cis* molecules with 436 nm radiations, the molecules photoisomerize back to *trans* conformation. The time taken by molecules for photoisomerization under different irradiation conditions is shown in Figure 7.6 B, C, D. About 0.8 minutes are required by ABOH for *trans* to *cis* transition, whereas NMA exo & endo require approximately 3.5 minutes. This is due to the bulky group attached to ABOH at para position[285]. The isomer population in *cis* conformation can also be thermally relaxed to *trans* conformation either by keeping it in the dark/away from any radiation in its absorption spectrum or heating it. UV led lamp with 365 nm and royal blue led lamp with 455 nm light sources were used for photoisomerization as they are nearest to $\lambda_{max,}$ i.e., 325 nm, 343 nm, and 436 nm. The thermal transition for ABOH is much faster than NMA endo & exo. Similarly, *cis* to *trans* photoisomerization time for ABOH (~0.7 minute) is also comparatively faster than NMA endo & exo (~1 minute). This information is used further in experiments during polymerization.

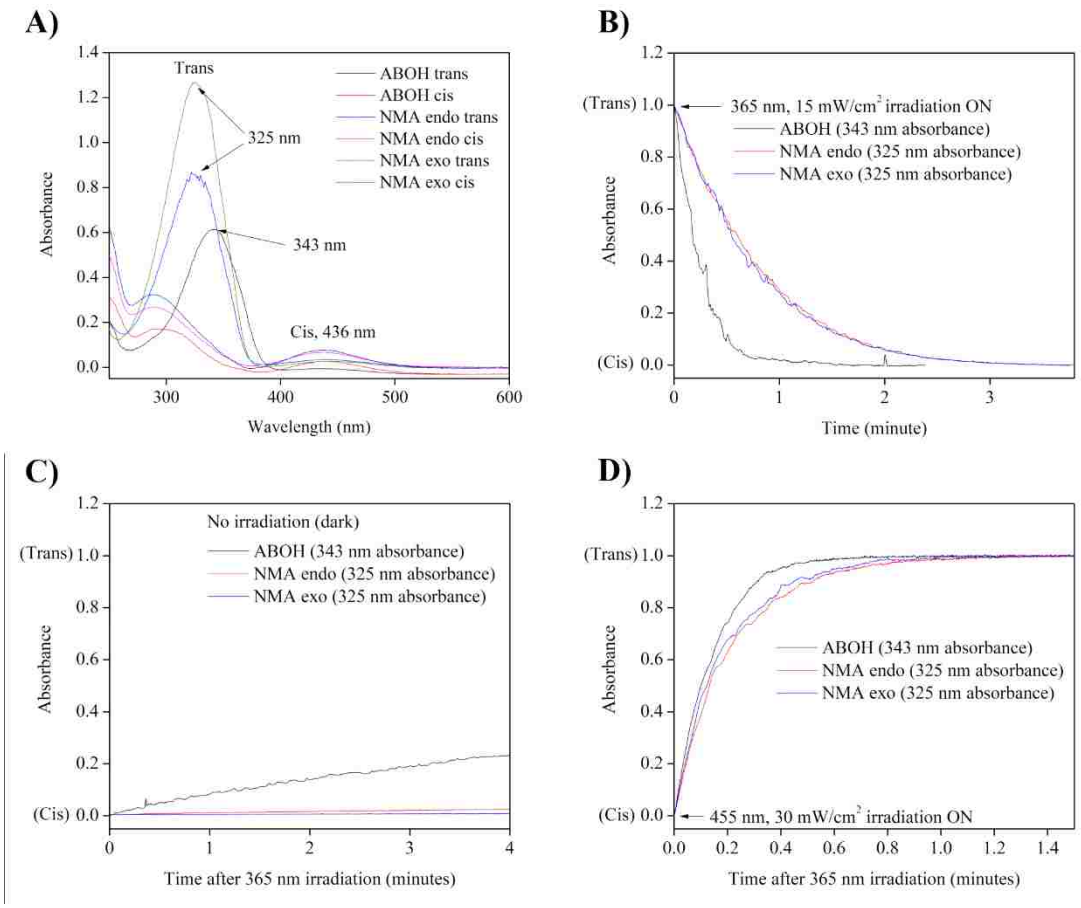

Figure 7.6: UV-Vis spectrum of ABOH, NMA exo & endo; A) Single scan of *trans* and *cis* conformation, B) *trans* to *cis* photoisomerization, C) *cis* to *trans* isomerization (thermal), D) *cis* to *trans* photoisomerization

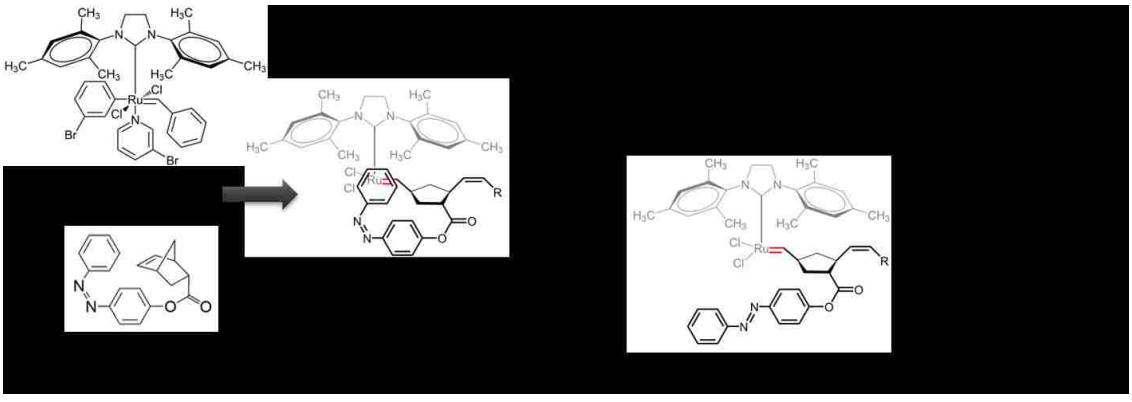

Figure 7.7: Proposed mechanism for reversible, light-mediated catalyst activity (G3 represents the main body of catalyst)

7.6 Polymerization: Results and discussion

The polymerization studies were mainly divided into 3 sets and results were focused on the conversion of monomer to polymer. In the first set, light-mediated ROMP of NMA endo & exo is demonstrated. Following that, the second set contains the supporting experiments for the first set, where it is confirmed that the light switching of ROMP is not the property of the only monomer but it is the conformation of monomer which turns off the activity of the catalyst. In the last set, i.e., set 3, experiments and results to demonstrate the reactivation of catalyst to resume ROMP are discussed. All the monomers were polymerized using G3 at room temperature, and their conversion to polymer was determined using GPC with tetrahydrofuran (THF) as an eluent. See section 3.2.9 for the instrument details. G3 is a fast initiating catalyst, used for polymerization studies of similar monomers[286].

In a typical polymerization experiment, the desired amount of NMA (exo or endo) was charged in a 2ml vial. Dry DCM was added to the vials via syringe and was mixed till monomer was completely soluble. Similarly, catalyst (G3) solution was prepared in another 2 ml vial using the desired amount of catalyst and DCM. A fresh new solution of catalyst was used before every sample of polymerization. To initiate polymerization, catalyst solution was added to monomer solution quickly, and the reaction vial was shaken not to vigorously till reaction was terminated by adding 2 drops of ethyl vinyl ether. The solvent was evaporated at atmospheric pressure to replace it by dry THF for GPC measurements. Various monomer to the catalyst concentration ratios was used to obtain optimum values for future experiments (see appendix). In the experiments with the two monomers, the concentration of primary monomer and catalyst was 5 mM and 2 mM respectively. The concentration of primary monomer was kept lower than the concentration of secondary monomer (100 mM) but higher than catalyst concentration. All the reactions were terminated after polymerization for 5 minutes of the last monomer added to the solution.

Table 7.1 summarizes all the experiments, sequence of compounds addition and their conversion results. Boxes with light violet color indicate UV irradiation of the initial monomer solutions for 5 minutes and all the procedures in that experiment till next step of irradiation (if any) were carried out in the absence of any light i.e. dark. Boxes with light

blue color indicate 1 minute of irradiation and any procedure followed by blue light exposure was performed in the daylight. Boxes with no color represent experiments in the daylight.

Table 7.1: ROMP of NMA and NCA under different irradiation conditions.

Exp #	Initial solution in DCM	@ t=0 – 1 min	t = 1 - 2 min	t = 2 min	Conversion for 5 min of polymerization
1	NMA endo	G3	-	-	97.60 %
2	NMA exo	G3	-	-	100.00 %
3	NMA endo	G3	-	-	3.85 %
4	NMA exo	G3	-	-	6.54 %
5	NCA endo	G3	-	-	65.50 %
6	NCA exo	G3	-	-	80.05 %
7	NMA endo	G3	NCA	-	17.00 %
8	NMA exo	G3	NCA	-	19.00 %
9	NMA endo	G3 + NCA	-	-	37.00 %
10	NMA exo	G3 + NCA	-	-	51.00 %
11	NMA endo	G3	NCA	-	0.00 %
12	NMA exo	G3	NCA	-	0.00 %
13	NMA endo	G3 + NCA	-	-	1.80 %
14	NMA exo	G3 + NCA	-	-	2.40 %
15	NMA endo	G3	NCA	-	25.92 %
16	NMA exo	G3	NCA	-	22.58 %
17	NMA endo	G3	-	NCA	19.13 %
18	NMA exo	G3	-	NCA	18.66 %

7.6.1 Set 1: Light-mediated ROMP

The four experiments in this set demonstrate the light-mediated ROMP. Total four experiments were conducted in this experiment, two for the polymerization of NMA *trans* and two for NMA *cis*. If NMA *cis* (endo & exo) do not yield any polymer, then it confirms the switching OFF of ROMP. Both NMA endo & exo were capable of polymerization in *trans* conformation by G3, and their conversion was confirmed by GPC. 5 minutes of polymerization resulted in 97.60% and 100.00% conversion for NMA endo and NMA exo respectively (exp # 1,2). The monomers were not irradiated with any radiations before the polymerization, i.e., a negligible number of *cis* isomers of NMA endo & exo were present. From the basic geometry of these monomers (Figure 7.8), it is understood that the orientation of non-substituted phenyl ring in azobenzene is away from the polymerizable carbon-carbon double bond in cyclic norbornene ring, introducing no interference in the polymerization. But polymerization of NMA endo & exo in *cis* confirmation yielded no polymer which confirmed the switching OFF of ROMP after UV irradiation of NMA. Only 3.85% and 6.54% of NMA endo *cis* and NMA exo *cis* were converted to the polymer (exp # 3,4). This polymerization can be attributed to the polymerization of residual NMA *trans* molecules even after photoisomerization. It is practically challenging to achieve 100% photoisomerization of azobenzene/derivatives to *cis* conformation.

If the switching off of ROMP was due to the monomer or due to catalyst was confirmed in the next set of experiment.

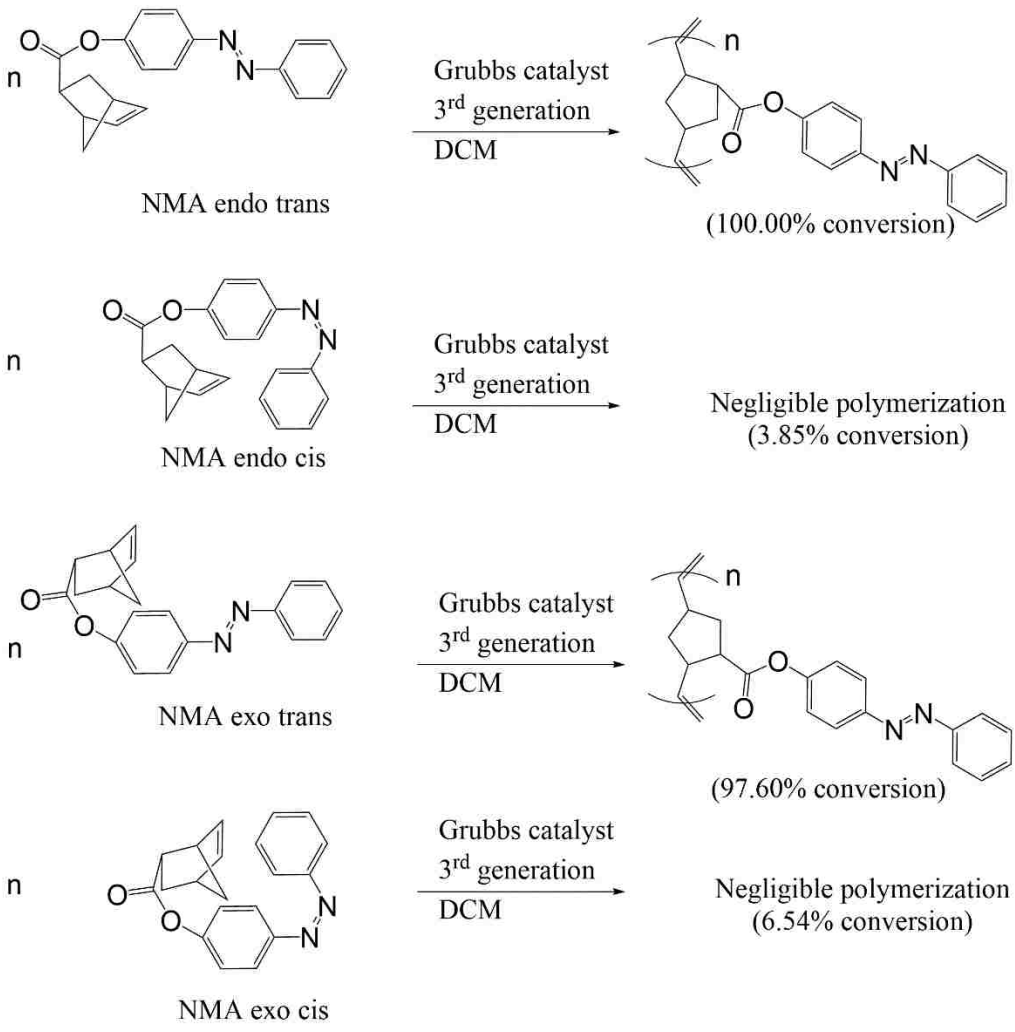

Figure 7.8: Polymerization of NMA exo & endo *trans* (monomer conversion values are experimentally determined using gel permeation chromatography)

7.6.2 Set 2: Temporary catalyst deactivation

This set of experiments is to determine the reason for the deactivation of G3 in the presence of NMA *cis* as seen in previous experiments. When the solutions of NMA endo & exo were irradiated with UV 365 nm radiations, and then G3 was introduced, very negligible conversion of monomer to polymer was detected. We hypothesize the temporary deactivation of the catalyst is due to the stearic hindrance/protection created by non-substituted phenyl group of *cis* azobenzene after initiation reaction of NMA *cis* molecule and a catalyst molecule (Figure 7.7).

As a reference in these experiments, NCA was used as the secondary monomer as it is not a light-sensitive monomer. We introduced NCA in the reaction solution of NMA (endo & exo) *cis* after initiation by G3 to determine the activity status of the catalyst after its interaction with NMA. If NCA yields any polymer after its introduction in NMA *cis* solution, then it confirms the inert nature of NMA *cis* monomer to polymerization. But if NCA does not yield any polymer, then it confirms the deactivation of the catalyst.

To compare the difference between the endo and exo isomer of NCA, both the isomers were homopolymerized separately. A significant difference was observed in the conversion of monomers between NCA endo (65.5%) and NCA exo (80.05%) (Exp#5,6). But, NCA endo was used in all further reactions as a secondary monomer (further referred as only 'NCA') to detect the activity of the catalyst after its reaction with NMA endo or exo (primary monomer). It forms co-polymer of NMA and NCA when polymerized together, but we have focused only on total quantitative conversion of both the monomers to polymer.

Before introducing NCA in NMA *cis* solutions, we first confirmed the co-polymerization of NMA *trans* and NCA. We know NMA trans and NCA are capable of homopolymerization in the presence of G3 yielding almost complete conversion of monomer, but we also determined the quantitative conversion of monomers (NMA *trans* and NCA) together when co-polymerized. For co-polymerization, NCA was added in the reaction solution (NMA *trans* and G3) either immediately or after 1 minute of addition of G3 in the solution of NMA *trans*. The two ways of sequential addition of NCA is to find out the difference in co-polymerization.

When NMA endo or exo was in *trans* conformation and NCA was added after 1 minute of the addition of G3, conversion detected in GPC was 17% for co-polymerization of NMA endo & NCA and 19 % for NMA exo & NCA reaction solutions (exp # 7,8). But when NCA was added immediately after addition of G3, the final conversion was 37% and 51% in the NMA endo *trans* and NMA exo *trans* reaction solutions respectively (exp # 9,10). This confirms the co-polymerization of NMA *trans* and NCA.

When NMA monomer was in *cis* confirmation, we detected no polymerization in either NMA endo or exo on the addition of NCA endo after 1 minute of addition of G3 (Exp # 11,12). Even when NCA was added immediately after G3, negligible polymerization was observed in NMA endo (1.8%) & exo (2.4%) reaction solution (Exp # 13,14). Hence, if catalyst had not even initiated the polymerization of NMA *cis*, then it would have resulted in the relatively higher conversion of NCA (homopolymerization of NCA). But the negligible activity of the catalyst was detected with NMA *cis*, which supports our proposed hypothesis that catalyst initiates the polymerization with NMA *cis* (endo or exo) but does not propagate it with NCA making copolymer. Figure 7.7 shows schematically represents the reaction products of NMA endo *cis* and G3 under two different light conditions. Whereas in the presence of NMA *trans* (endo or exo), it initiates the polymerization with either NMA *trans* or NCA and propagates to give a significantly higher conversion to a copolymer of NMA and NCA. Thus, G3 forms an intermediate complex/caged intermediate product with NMA *cis* stopping it to react with the next monomer molecule due to the steric protection by *cis* azobenzene in the caged intermediate. This mechanism deactivates the catalyst and above results support our hypothesis.

7.6.3 Set 3: Catalyst reactivation

In this set of experiments, reactivation of catalyst is demonstrated. Reactivation of catalyst will spontaneously resume the ROMP using available monomer molecules in the solution. We hypothesize that photoisomerization of azobenzene in caged intermediate from *cis* to *trans* would reactivate the catalyst by making its reactive site available to the next monomer for the propagation of polymerization.

Figure 7.9 shows the absorption spectrum of the caged intermediate with λ_{max} to be around 455 nm. This confirms the presence of azobenzene derivative bound to catalyst molecule.

We used a blue led lamp (455 nm) for the photoisomerization of the *cis* intermediate molecule to *trans* intermediate molecule.

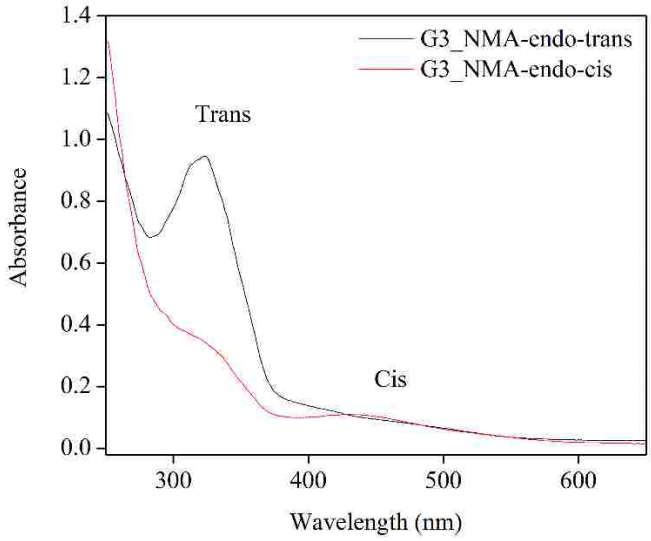

Figure 7.9: UV-Vis absorption spectrum of G3 and NMA endo intermediate molecule

Similar to experiments in set 2, NMA endo & exo *cis* were used with G3. First, NMA solution in dry DCM was irradiated with the UV 365 nm radiations for 5 minutes to photoisomerize NMA from *trans* to *cis*, and then the G3 solution was added to it for polymerization. After 1 minute, the solution of the caged intermediate of G3 and NMA was irradiated with blue light (455 nm) for 1 minute followed by the addition of NCA. After addition of NCA endo immediately as soon as the solution was exposed to blue light, 25.92% and 22.58% conversion was observed for NMA endo and NMA exo samples respectively (exp # 15,16). Whereas, when NCA endo was added after 1 minute of blue light irradiation, 19.13% and 18.66% conversion of monomers was observed in NMA endo and NMA exo respectively (exp # 17,18). The lower conversion of monomer can be attributed to the decrease in the activity of the catalyst on forming an intermediate caged molecule and repeated photoirradiation. The reactivation of catalyst activity and continuing polymerization demonstrates the switching ON of ROMP using blue light successfully. The higher conversions in the exp #15-18 than conversions in exp #11-14 confirms the co-polymerization of NMA and NCA after reactivation of the catalyst. If there was no polymerization following photoisomerization by blue light, then it would support

irreversible deactivation of the catalyst by the *cis* NMA. But these experiments confirm the successful reactivation of catalyst on irradiation with blue light.

7.7 Conclusions

In conclusion, monomers (NMA endo & exo) for light-mediated ROMP in solution were designed, synthesized, and characterized using UV-Vis spectrophotometer, ^{1}H-NMR, and ESI MS. ^{1}H-NMR spectrum confirmed the increase in the proximity of non-substituted phenyl ring in azobenzene on photoisomerization from NMA *trans* to NMA *cis*. Three sets of polymerization experiments were conducted to successfully demonstrate the light-mediated ROMP of NMA endo and exo, temporary deactivation of G3 using UV irradiation, and reactivation using blue light irradiation. The hypothesis of temporary deactivation and reactivation of catalyst (G3) was confirmed by sequential addition of secondary monomer (NCA endo) to the reaction solution of primary monomer (NMA *trans* or *cis*). Homopolymerization and co-polymerization of NCA with NMA *trans* was confirmed before demonstrating deactivation and reactivation of G3. UV irradiation blocks the activity of catalyst by forming a caged intermediate with NMA (endo or exo) *cis* and creating stearic protection around it against incoming monomer. But when the intermediate molecule is photoisomerized back to *trans* conformation using blue light, the stearic protection decreases and polymerization propagate again.

This study establishes a novel concept of light-mediated ROMP and opens up the field that can be continued in many directions for improvement. Future work for this study is mentioned in more details in the next chapter.

8 Conclusions and future work

8.1 Conclusions

In conclusion, this dissertation has aimed towards the development of a technique for the light-mediated ROMP to synthesize photo-responsive polymers, coatings with higher resistance to organic solvents and a versatile surface photochemistry to modify the coating functionality as per the end use.

The results in chapter 4 demonstrate the successful grafting of derivatized alkanethiol molecules across the unsaturated functionality in the polymer brushes of polynorbornene on a gold substrate. The polymer brushes made by SI ROMP of norbornene in DCM and were modified by surface click chemistry. Irgacure-184 photoinitiator was used for thiol-ene click chemistry on polynorbornene surface for the addition of thiyl radicals across the alternate carbon-carbon double bonds on irradiation with UV 365 nm light. Thiol-ene click reaction is a very rapid and versatile chemistry that adds free radicals of any molecule to carbon-carbon double bond. The technique was tested by grafting three different types of thiol molecules, differing to each other regarding molecular size and tail group functionality. We believe that this method can be extended to modify the SI ROMP coating of any polyolefinic polymer brushes or coating of the functionalized derivative of norbornene, and even be used with photomask for photopatterning in order to graft selected regions of the coating. Although strong evidence to support the findings are presented here, significant loss in the film thickness was also recorded for most of the samples. With objective to find the solution, a crosslinker is designed and incorporated to increase the solvent resistance of pNB coatings.

Chapter 5 contains the details of synthesis, experiments, and results for the introduction of crosslinker in the SI ROMP coating of pNB. Oxidative degradation of polyolefinic coatings is a common problem, and the same problem was encountered in the experiments of grafting thiol molecules in pNB coatings. Huge decrease in the film thickness was observed during the grafting reaction which is attributed to the soluble oxygen in the organic solvent, i.e. DCM used during the photochemical reaction. Hence, a crosslinker is designed and incorporated into the pNB coating during the SI ROMP process. As a result, the film loss of pNB coating against the DCM, ethanol, and water dropped from 73% to 28%. The

solvent resistance to the crosslinked coatings is tested by repeating the rinse cycle 10 times. As an additional advantage to the *in situ* crosslinking, the olefinic functionality of the coating is also preserved for further modification. This crosslinker can be used with any ROMP monomer during the SI ROMP process for in situ crosslinking.

Lastly, chapter 6 and 7 contain the details of two different class of monomer with the common aim of undergoing light-mediated ROMP of photoresponsive monomers. Chapter 6 provides the details of a monomer design whose rate of ROMP can be controlled via modulating its ring strain energy by illuminating the monomer with UV radiations. The photoresponsive moiety is incorporated into the cyclic ring structure of ROMP monomer that tends to change its structural geometry when irradiated with the particular wavelength radiations, changing the ring strain energy of monomer. When the irradiation is performed during the ROMP process, it would directly control the rate of polymerization in a non-invasive manner because the rate of ROMP is directly proportional to the ring strain energy of monomer in the solution. The synthesis of the designed monomer encountered the solubility and catalyst incompatibility issue, and hence the monomer is not synthesized at this stage. Whereas, chapter 7 is focused on the alternative design of a monomer for the same goal of light-mediated ROMP. The underlying fundamental principle of this design is to create a temporary steric hinderance/protection around monomer-catalyst caged intermediate after initiation of polymerization of monomer in *cis* conformation, against the incoming monomer to pause the propagation of polymerization. This basically deactivates the catalyst temporarily, switching OFF the ROMP temporarily. Switching ON of the paused ROMP in solution phase is done by irradiating the solution with blue light which reactivates the caged catalyst intermediate. We have obtained comprehensive results demonstrating the switching OFF and switching ON of polymerization of monomer using UV and blue light exposure successfully. This is a powerful and innovative tool for surface patterning of photoresponsive polymer which is still a challenge in this research field.

8.2 Future work

The direction and achievements of this doctoral research are towards the development of surface initiated ring opening metathesis polymerization of norbornene for preparing stable and multi-functional photoresponsive polymer coatings. The three goals achieved in this

doctoral research work; surface modification, crosslinking and technique of light-mediated ROMP, when used together can produce photoresponsive surface patterns with provision for further modification.

Below are some proposed ideas for new research projects as application and extension of techniques developed in this work.

8.2.1 Photo-patterning

A very exciting application of light mediated ROMP would be making SI ROMP coatings of NMA monomer and using its photo-switching property for surface patterning. Variety of applications in microfluidics[276], biosensors[276, 277], dry etching[278, 279] and patterns for reactive ion etching resist[280] are there for photoresponsive polymers in the form of surface nano/microarchitectures. Currently, most common method of making surface architectures of photoresponsive polymers is exposing a region of the photoresponsive coating to the interference pattern of polarized light. On exposure to polarized light, the photoresponsive moiety undergoes solid-state mass transport displacing the polymer chains either in bright or in dark regions of interference pattern[287]. Either a linear or a circularly polarized light can be used[287-289]. But they do not have the flexibility to be used for making complex surface architectures. Other methods used for surface patterning are dip-pen lithography for nanoscale lithography [84, 290], and directional photofluidization imprint lithography[291] for creating vertical structures of photoresponsive polymer brushes. But they are very complicated, and the later method also needs a mold of the desired pattern. Light-mediated ROMP can be extended to the surface polymerization by SI ROMP. In brief, a chrome based photomask can be used for selectively irradiating the regions on the surface exposed to monomer solution with UV 365 nm, thereby holding a spatial control over the activity of surface-bound catalyst for photo-patterning.

8.2.2 Liquid crystal aggregates with tunable density

After confirming amide functional groups as the root cause for the deactivation of catalyst in chapter 6, the synthesis route was modified to make similar diene molecule but with ester functional group instead of amide functional group. The stability of grubbs catalyst in the presence of ester functional group was already known and checked as DEDAM had

ester functional group in it. Hence, we synthesized AB(m,n) open with ester functional group (Figure 8.1).

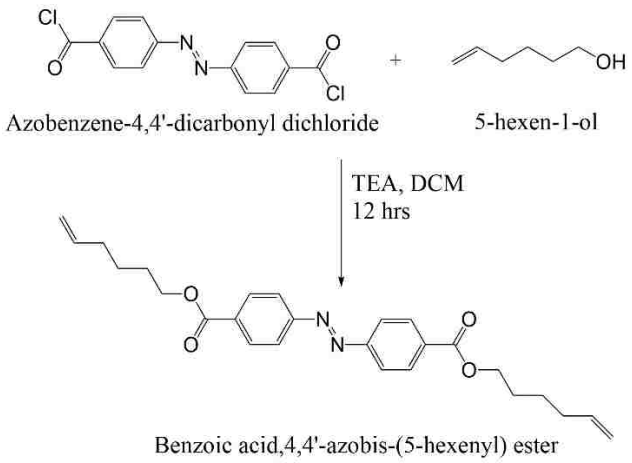

Figure 8.1: Synthesis scheme for AB(2,2) with ester functional group

Interestingly, after synthesis, the solubility of the pure final product in most of the organic solvents dropped extensively forming supramolecular aggregates in DCM (Figure 8.2). Also, upward motion of these aggregates was noted in solution under irradiation by various energy radiations. These aggregates have very large volume to mass ratio. When they were irradiated with UV (365 nm) or blue (455 nm) or green (530 nm) LED light, they moved in the upward direction. As a future work, this phenomenon can be explored further to understand the light-mediated rearrangement of these liquid crystals in an organic solvent at the molecular scale. Literature reveals that solid-state motion of azobenzene derivative molecules are actively researched by many scientists, but the behavior of liquid crystals like these in liquids/solvents is still a remarkably unexplored research field. Some progress has already been made in this project; please contact the author of this dissertation for more details.

Figure 8.2: Insoluble liquid crystals of azobenzene in DCM

8.2.3 NMA monomer for biomedical application

The monomer designed in chapter 7 can be creatively exploited to make monomer with specific biomedical applications. For instance, azobenzene and β-cyclodextrin form a supramolecular complex when azobenzene is in *trans* conformation[292]. This phenomenon is currently being explored for the photo-controlled release of protein loaded in the hydrogel formed by interaction between azobenzene and β-cyclodextrin[293, 294]. Another application of norbornene in biomedical field (drug delivery and tissue engineering) is in the form of thiol-norbornene (thiol-ene) photo-click hydrogels[295, 296]. These hydrogels are diverse in gelation and highly biocompatible. As one of the future project, above two methodologies where azobenzene and norbornene are used separately, can be combined for one potential application. An optimized incorporation of NMA molecules in thiol-norbornene hydrogel can efficiently be used to formulate hydrogels mixture capable of the photo-controlled release of proteins loaded in them. An additional advantage in this approach would be a modification of azobenzene to tetra-ortho-methoxy-substituted azobenzene which can photoisomerize between *trans* and *cis* conformation under visible light. It can isomerize from *trans* to *cis* under red light exposure and from cis to trans under blue light exposure. *Trans* to *cis* isomerization under red light is beneficial due to its higher penetration depth in tissues[293].

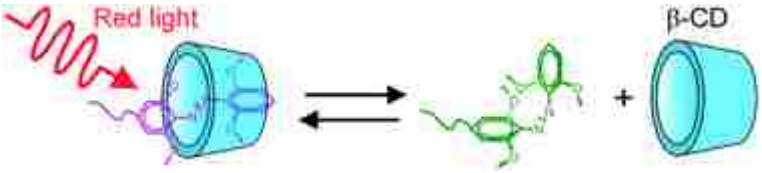

Figure 8.3: Schematic representation of photoinduced supramolecular complex formation between azobenzene derivative molecule and β-cyclodextrine[293]

Appendix

SI ROMP stability data all samples

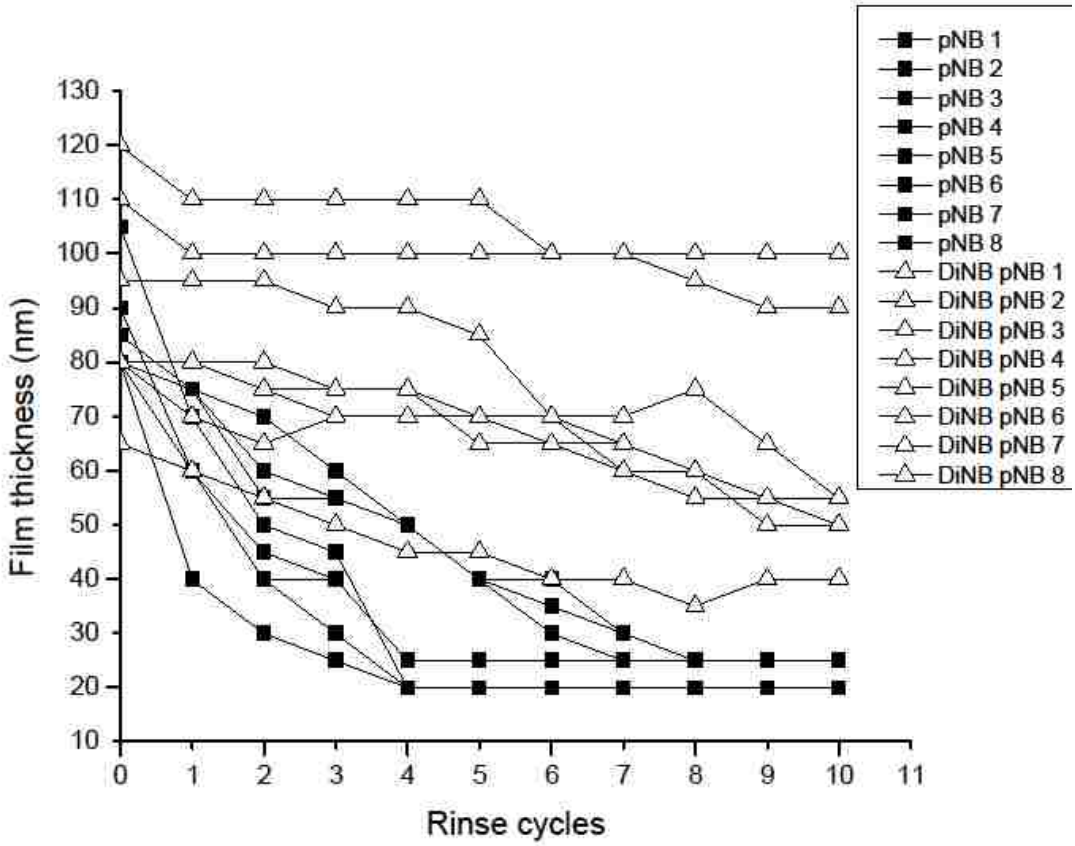

Film thickness vs number of rinses for each sample of pNB and DiNB-pNB

DiNB ^{1}H-NMR

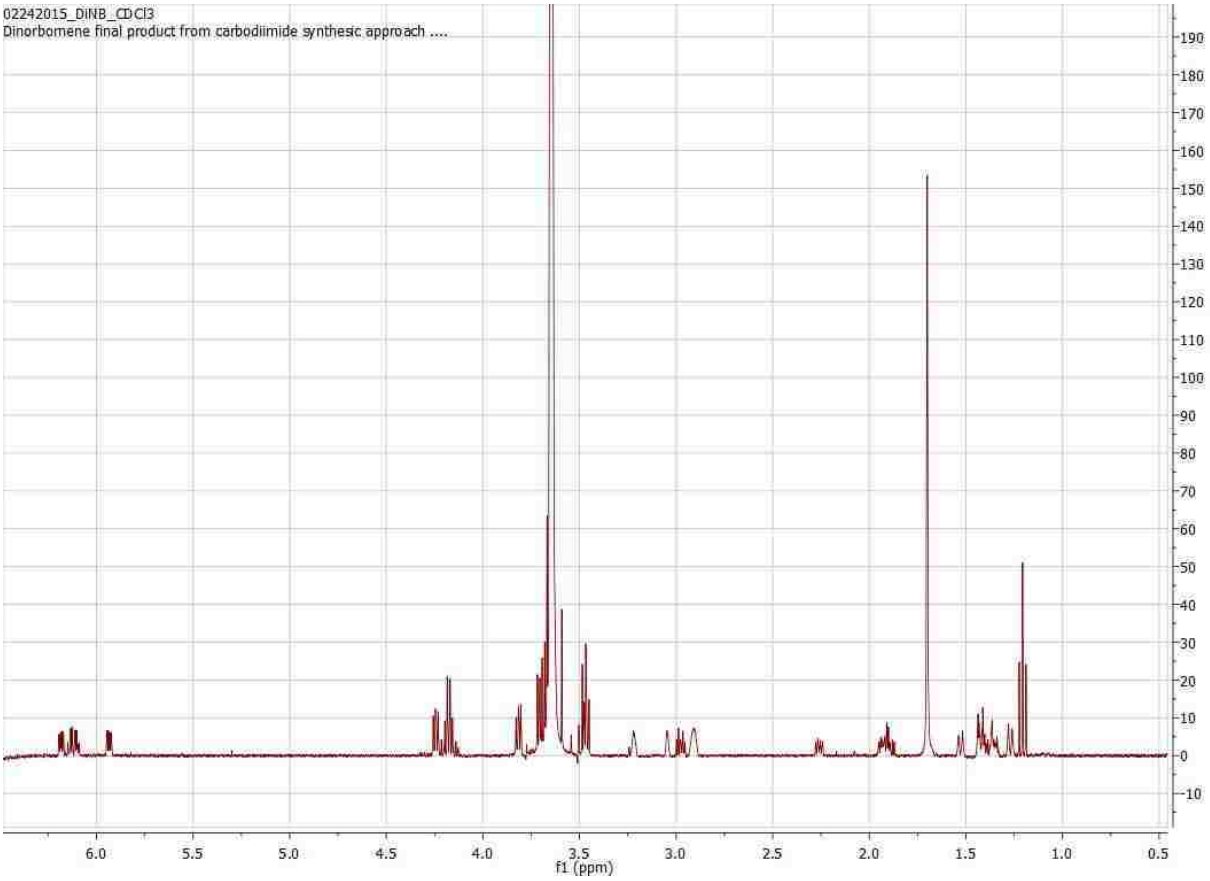

^{1}H-NMR of DiNB in $CDCl_3$

Crosslinker dimensions calculation

Calculations to estimate the minimum average distance between the polynorbornene chains tethered to the surface. Following calculations are based on the values based on SI ROMP coatings with amplified grafting density of surface initiator. Hence, the actual grafting density is same or less than calculated.

- Average density of Self assembled monolayer [223]= 0.18 nm^2 /molecule
- Area for 100 molecules = 100 molecules/ 18 nm^2

- Maximum 5 % of hydroxyl groups reacts 1:1 with norbornenyl groups, 33% of the hydroxyl groups react 2:1 with norborneneyl groups [93]= 0.215 x 100 molecules / 18 nm^2
- 21.5% of monolayer reacts with norbornenyl molecules = 21.5 molecules / 18 nm^2
- Maximum 7 % of norbornenyl react to for Grubbs catalyst surface[93] = 0.07 x 21.5 molecules / 18 nm^2
- 7 % of norbornenyl react to for Grubbs catalyst surface = 1.5 molecule/18 nm^2
- Area per active/surface bound catalyst molecule on the surface = 12 nm^2
- Average chain to chain distance = 3.5 nm

The length of crosslinker was estimated by finding the radius of gyration as the crosslinker will be in the collapsed state in solution[218].

- Radius of gyration; $Rg = 0.02 \times M^{0.58}$ nm
- M = 3590 g/mol
- $Rg = 0.02 \times (3590)^{0.58} = 2.3$ nm

^{1}H-NMR of ABn trans in $CDCl_2$

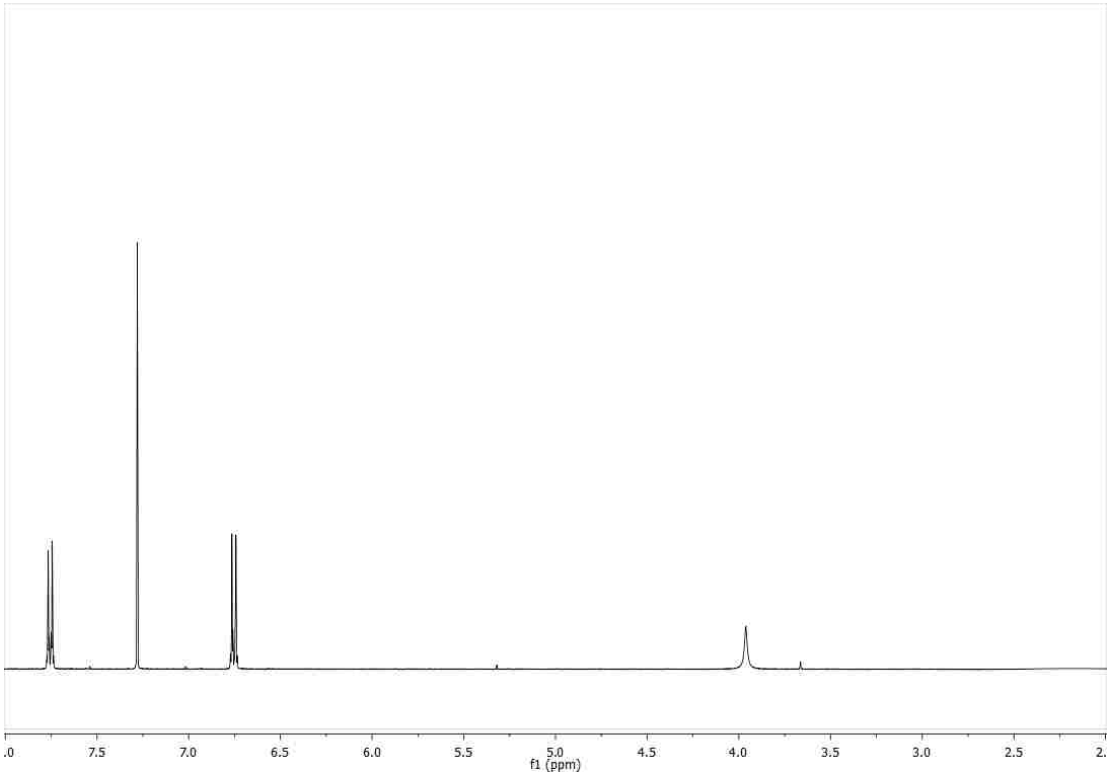

^{1}H-NMR of ABn *trans*

[1]H-NMR of AB(2,2) trans open

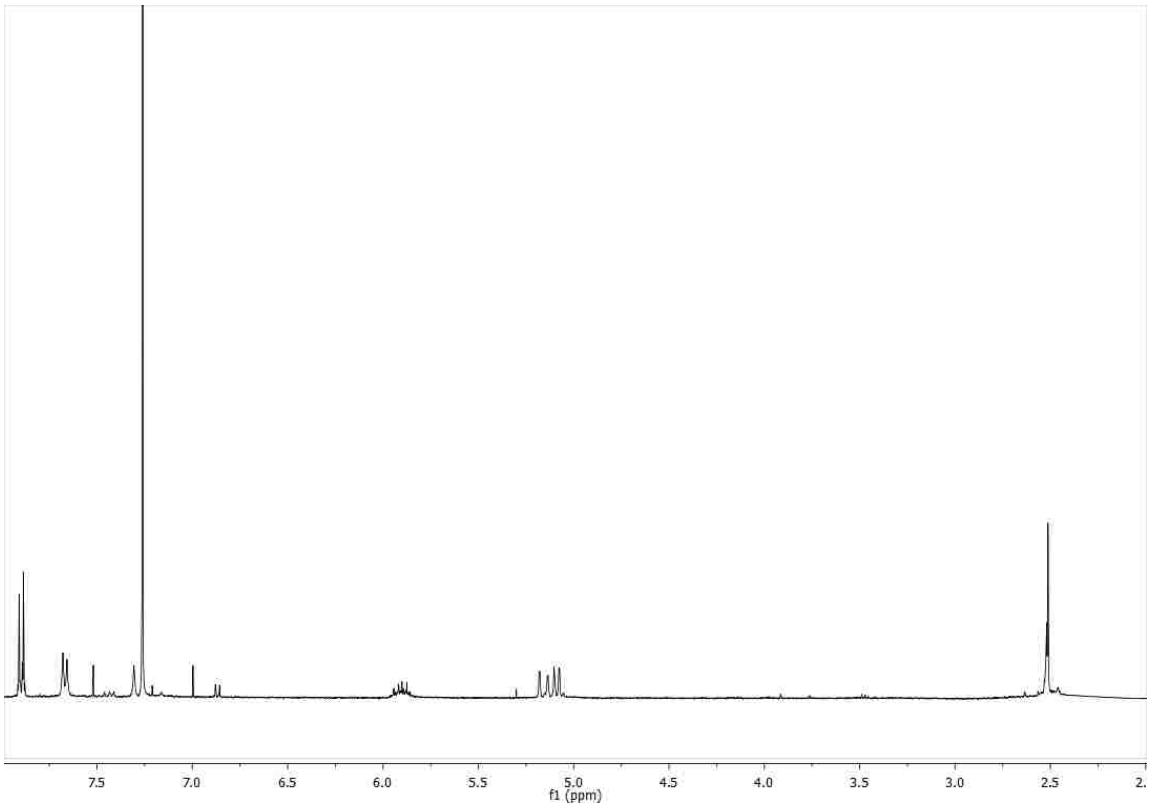

[1]H-NMR of AB(2,2) *trans* open

[1]H-NMR of AB(3,3) trans open

[1]H NMR (400 MHz, Chloroform-*d*) δ 7.94 – 7.86 (m, 1H), 7.67 (d, *J* = 8.5 Hz, 1H), 7.26 (s, 2H), 5.90 – 5.71 (m, 2H), 5.05 – 4.96 (m, 2H), 2.39 (dt, *J* = 13.1, 7.5 Hz, 3H), 2.25 – 2.07 (m, 3H), 1.88 (p, *J* = 7.4 Hz, 1H), 1.75 (p, *J* = 7.5 Hz, 1H)

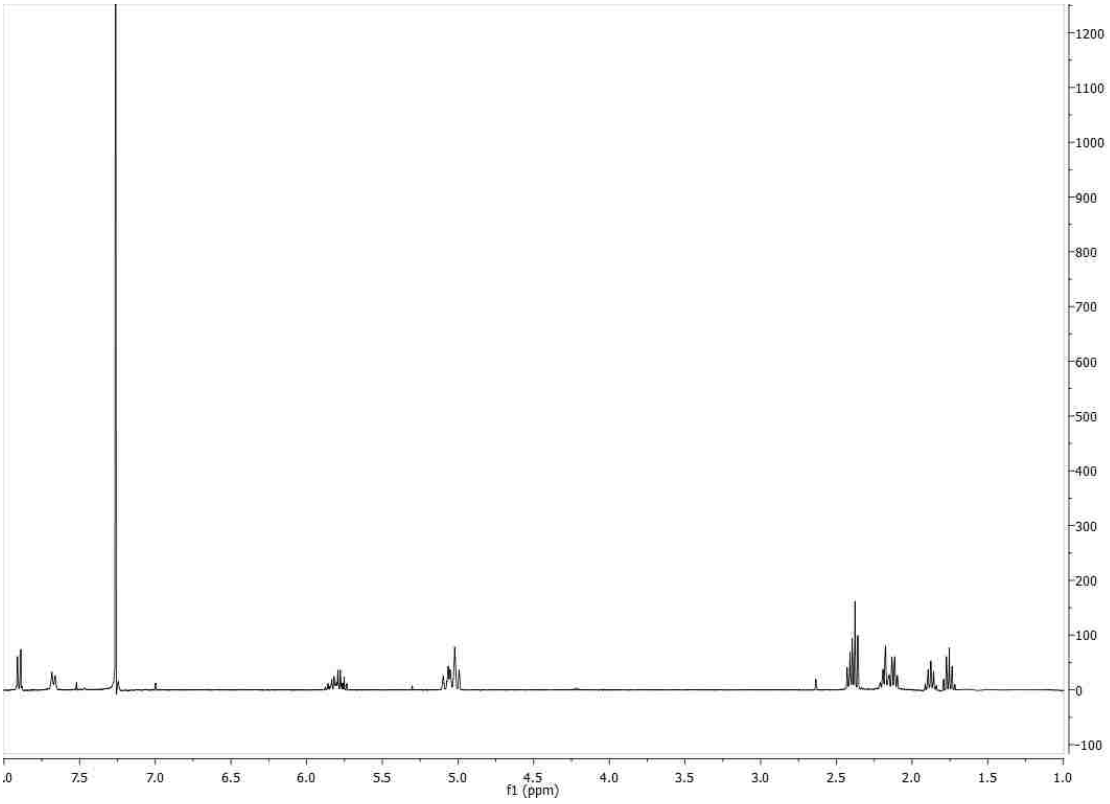

^{1}H-NMR of AB(3,3) *trans* open

Concentration optimization results using Gel permeation chromatography

NMA endo concentration	**Grubbs (2nd generation) catalyst concentration**	**Conversion**
50mM	0.5mM	3.28%
50mM	0.25mM	0.89%
25mM	0.5mM	3.38%
50mM	1mM	91.89%
100mM	1mM	52.08%

3D images of Norbornene monoazobenzene isomers and intermediate complex with G3.

A) Norbornene monoazobenzene (NMA) exo in trans and cis
B) Norbornene monoazobenzene (NMA) endo in trans and cis
C) Norbornene monoazobenzene exo intermediate complex with Grubbs catalyst 3rd generation in trans and cis
D) Norbornene monoazobenzene endo intermediate complex with Grubbs catalyst 3rd generation in trans and cis

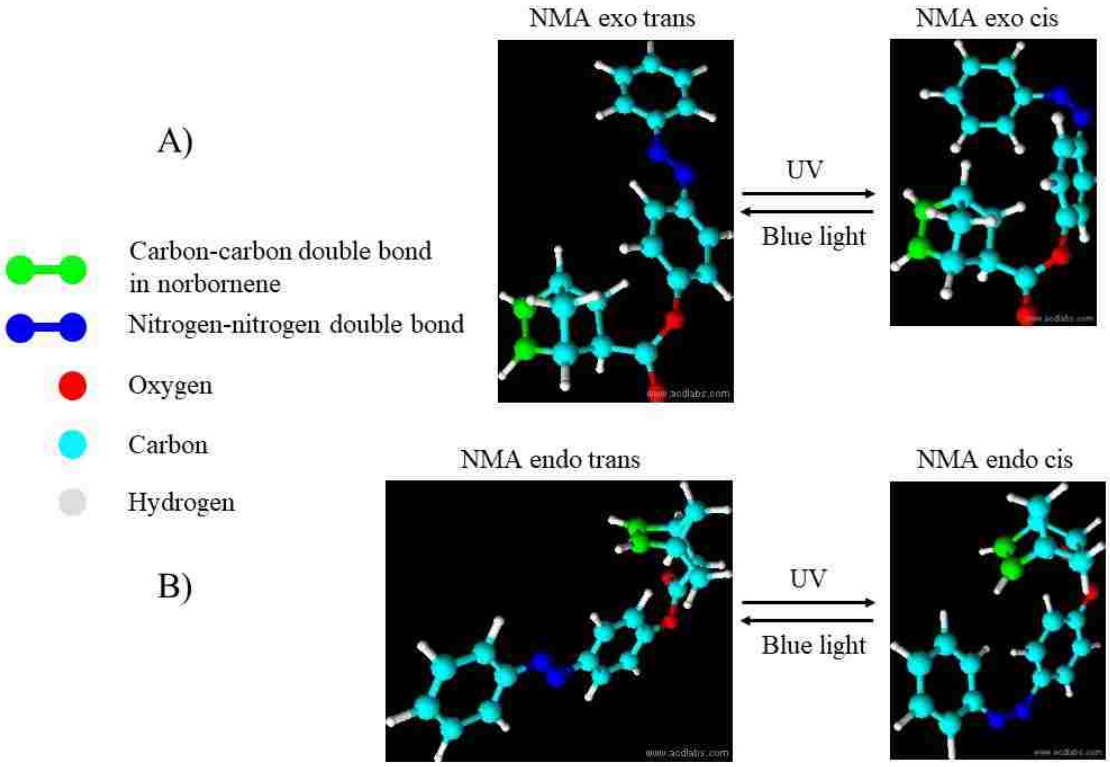

C)

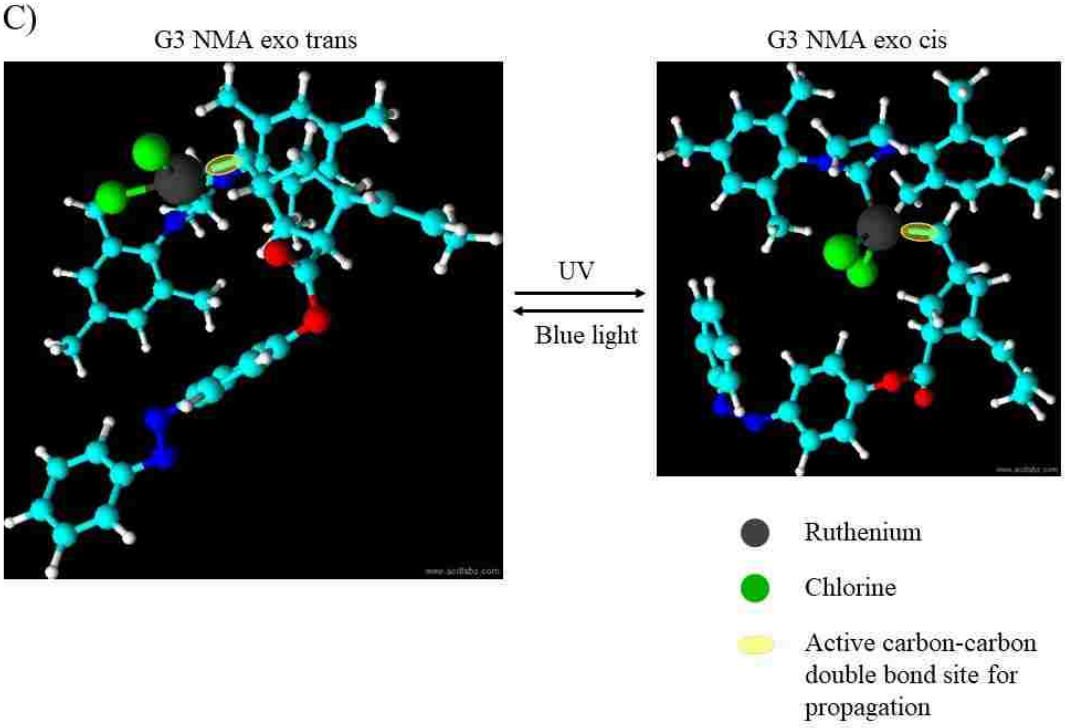
G3 NMA exo trans
G3 NMA exo cis
UV
Blue light
Ruthenium
Chlorine
Active carbon-carbon double bond site for propagation

D)

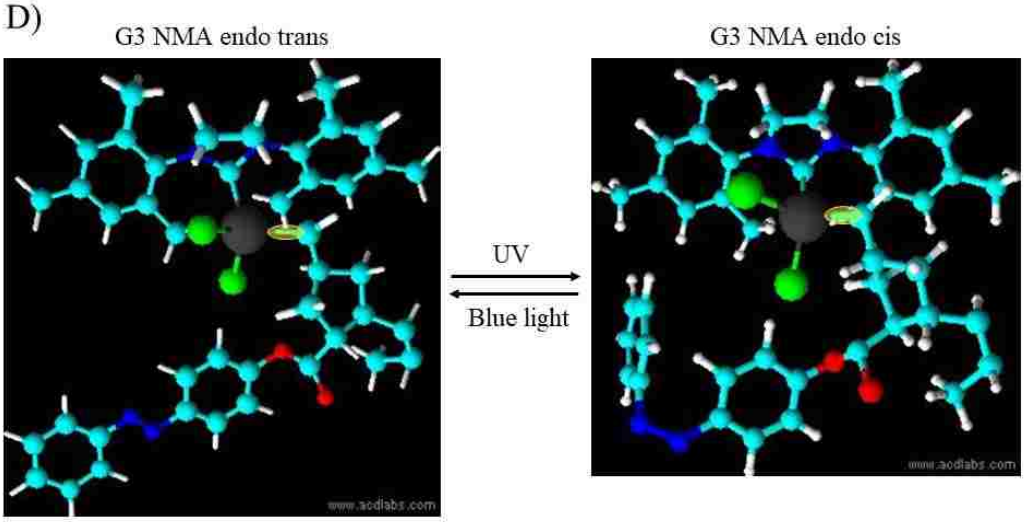
G3 NMA endo trans
G3 NMA endo cis
UV
Blue light

References

1. Nelson, A., *Stimuli-responsive polymers: engineering interactions.* Nature materials, 2008.
2. Tenkovtsev, A.V., O.N. Piraner, and A.Y. Bilibin, *Thermotropic polyesters, 7.. Liquid-crystalline polymers with meta-phenylene units in the mesogenic moiety.* Macromolecular Chemistry and Physics, 1991. **192**(6): p. 1275-1283.
3. Iimura, K., et al., *Syntheses of thermotropic liquid crystalline polymers, 1. Azoxy and azo type polyesters.* Macromolecular Chemistry and Physics, 1981. **182**(10): p. 2563-2568.
4. Kang, S.H., et al., *Synthesis and photoisomerization properties of polynorbornenes with azobenzene chromophores.* BULLETIN-KOREAN CHEMICAL SOCIETY, 2002. **23**(7): p. 957-963.
5. Riul, A., et al., *Artificial Taste Sensor: Efficient Combination of Sensors Made from Langmuir−Blodgett Films of Conducting Polymers and a Ruthenium Complex and Self-Assembled Films of an Azobenzene-Containing Polymer.* Langmuir, 2002. **18**(1): p. 239-245.
6. Lim, H.S., et al., *Photoreversibly switchable superhydrophobic surface with erasable and rewritable pattern.* Journal of the American …, 2006.
7. Narita, M., et al., *Photoinduced Immobilization of Biomolecules on the Surface of Azopolymer Films and Its Dependence on the Concentration and Type of the Azobenzene Moiety.* Macromolecules, 2007. **40**(3): p. 623-629.
8. Osella, S., P. Samorì, and J.r.m. Cornil, *Photoswitching azobenzene derivatives in single molecule junctions: A theoretical insight into the I/V characteristics.* The Journal of Physical Chemistry C, 2014. **118**(32): p. 18721-18729.
9. Henzl, J., et al., *Photoisomerization for a molecular switch in contact with a surface.* Physical Review B, 2012. **85**(3): p. 035410.
10. Na, S.I., et al., *Efficient polymer solar cells with surface relief gratings fabricated by simple soft lithography.* Advanced Functional Materials, 2008. **18**(24): p. 3956-3963.
11. Schubert, S., et al., *Oxide Sandwiched Metal Thin-Film Electrodes for Long-Term Stable Organic Solar Cells.* Advanced Functional Materials, 2012. **22**(23): p. 4993-4999.
12. Lee, J.-T., et al., *Multiphoton writing of three-dimensional fluidic channels within a porous matrix.* Journal of the American Chemical Society, 2009. **131**(32): p. 11294-11295.
13. Rochon, P., E. Batalla, and A. Natansohn, *Optically induced surface gratings on azoaromatic polymer films.* Applied Physics Letters, 1995. **66**(2): p. 136-138.
14. Kim, D., et al., *Polarized laser induced holographic surface relief gratings on polymer films.* Macromolecules, 1995. **28**(26): p. 8835-8839.
15. Zhao, Y., et al., *Holographic recording in a photoactive elastomer.* Advanced Functional Materials, 2003. **13**(10): p. 781-788.
16. Yamada, M., et al., *Photomobile polymer materials: towards light-driven plastic motors.* Angewandte Chemie International Edition, 2008. **47**(27): p. 4986-4988.

17. Huang, J., et al., *Light driving force for surface patterning on azobenzene-containing polymers.* Physical Chemistry Chemical Physics, 2011. **13**(36): p. 16150-16158.
18. Paik, M.Y., et al., *Surface organization, light-driven surface changes, and stability of semifluorinated azobenzene polymers.* Langmuir, 2007. **23**(9): p. 5110-5119.
19. Palffy-Muhoray, P., T. Kosa, and E. Weinan, *Dynamics of a light driven molecular motor.* Molecular Crystals and Liquid Crystals, 2002. **375**(1): p. 577-591.
20. Birnie III, D.P., B.J. Zelinski, and D.L. Perry, *Infrared observation of evaporative cooling during spin-coating processes.* OPTICAL ENGINEERING-BELLINGHAM-INTERNATIONAL SOCIETY FOR OPTICAL ENGINEERING-, 1995. **34**: p. 1782-1782.
21. Assink, R. and R. Schwartz, *Proton and carbon-13 NMR investigations of lead zirconate titanate (Pb (Zr, Ti) O3) thin-film precursor solutions.* Chemistry of materials, 1993. **5**(4): p. 511-517.
22. Lee, S.-S., et al., *Layer-by-layer deposited multilayer assemblies of ionene-type polyelectrolytes based on the spin-coating method.* Macromolecules, 2001. **34**(16): p. 5358-5360.
23. Hinczewski, D.S., et al., *Optical filters from SiO 2 and TiO 2 multi-layers using sol–gel spin coating method.* Solar Energy Materials and Solar Cells, 2005. **87**(1): p. 181-196.
24. Feng, C.L., et al., *Reversible wettability of photoresponsive fluorine-containing azobenzene polymer in Langmuir− Blodgett films.* Langmuir, 2001. **17**(15): p. 4593-4597.
25. Sidorenko, A., et al., *Photoresponsive Langmuir monolayers from azobenzene-containing dendrons.* Langmuir, 2000. **16**(26): p. 10569-10572.
26. Ulman, A., *An Introduction to Ultrathin Organic Films: From Langmuir--Blodgett to Self--Assembly*. 2013: Academic press.
27. Netzer, L., R. Iscovici, and J. Sagiv, *Adsorbed monolayers versus Langmuir-Blodgett monolayers—Why and how? I: From monolayer to multilayer, by adsorption.* Thin Solid Films, 1983. **99**(1-3): p. 235-241.
28. Jennings, G.K. and E.L. Brantley, *Physicochemical Properties of Surface-Initiated Polymer Films in the Modification and Processing of Materials.* Advanced Materials, 2004. **16**(22): p. 1983-1994.
29. Porter, M.D., et al., *Spontaneously organized molecular assemblies. 4. Structural characterization of n-alkyl thiol monolayers on gold by optical ellipsometry, infrared spectroscopy, and electrochemistry.* Journal of the American Chemical Society, 1987. **109**(12): p. 3559-3568.
30. Bain, C.D., et al., *Formation of monolayer films by the spontaneous assembly of organic thiols from solution onto gold.* Journal of the American Chemical Society, 1989. **111**(1): p. 321-335.
31. Advincula, R., *Polymer brushes by anionic and cationic surface-initiated polymerization (SIP)*, in *Surface-initiated polymerization I*. 2006, Springer. p. 107-136.
32. Safazadeh, L. and B.J. Berron, *Photopatterning of Stable, Low-Density, Self-Assembled Monolayers on Gold.* Langmuir, 2015. **31**(9): p. 2689-2696.

33. Berron, B. and K.G. Jennings, *Loosely Packed Hydroxyl-Terminated SAMs on Gold.* Langmuir, 2006. **22**(17): p. 7235-7240.
34. Balachandra, A.M., G.L. Baker, and M.L. Bruening, *Preparation of composite membranes by atom transfer radical polymerization initiated from a porous support.* Journal of membrane science, 2003. **227**(1): p. 1-14.
35. Ulbricht, M., *Advanced functional polymer membranes.* Polymer, 2006. **47**(7): p. 2217-2262.
36. Chiefari, J., et al., *Living free-radical polymerization by reversible addition− fragmentation chain transfer: the RAFT process.* Macromolecules, 1998. **31**(16): p. 5559-5562.
37. Perrier, S. and P. Takolpuckdee, *Macromolecular design via reversible addition–fragmentation chain transfer (RAFT)/xanthates (MADIX) polymerization.* Journal of Polymer Science Part A: Polymer Chemistry, 2005. **43**(22): p. 5347-5393.
38. Barner-Kowollik, C. and S. Perrier, *The future of reversible addition fragmentation chain transfer polymerization.* Journal of Polymer Science Part A: Polymer Chemistry, 2008. **46**(17): p. 5715-5723.
39. Moad, G., E. Rizzardo, and S.H. Thang, *Living radical polymerization by the RAFT process–a second update.* Australian journal of chemistry, 2009. **62**(11): p. 1402-1472.
40. Barbey, R., et al., *Polymer brushes via surface-initiated controlled radical polymerization: synthesis, characterization, properties, and applications.* Chem. Rev, 2009. **109**(11): p. 5437-5527.
41. Duong, H.T., et al., *Organic nitrate functional nanoparticles for the glutathione-triggered slow-release of nitric oxide.* Journal of Polymer Science Part A: Polymer Chemistry, 2014. **52**(15): p. 2099-2103.
42. Bielawski, C.W. and R.H. Grubbs, *Living ring-opening metathesis polymerization.* Progress in Polymer Science, 2007. **32**(1): p. 1-29.
43. Leitgeb, A., J. Wappel, and C. Slugovc, *The ROMP toolbox upgraded.* Polymer, 2010. **51**(14): p. 2927-2946.
44. Buchmeiser, M.R., *Metathesis polymerization to and from surfaces*, in *Surface-Initiated Polymerization I*. 2006, Springer. p. 137-171.
45. Sutthasupa, S., M. Shiotsuki, and F. Sanda, *Recent advances in ring-opening metathesis polymerization, and application to synthesis of functional materials.* Polymer journal, 2010. **42**(12): p. 905.
46. Rutenberg, I.M., et al., *Synthesis of polymer dielectric layers for organic thin film transistors via surface-initiated ring-opening metathesis polymerization.* Journal of the American Chemical Society, 2004. **126**(13): p. 4062-4063.
47. Carlsson, L., E. Malmström, and A. Carlmark, *Surface-initiated ring-opening metathesis polymerisation from cellulose fibres.* Polymer Chemistry, 2012. **3**(3): p. 727-733.
48. Lerum, M.F.Z. and W. Chen, *Surface-Initiated Ring-Opening Metathesis Polymerization in the Vapor Phase: An Efficient Method for Grafting Cyclic Olefins with Low Strain Energies.* Langmuir, 2011. **27**(9): p. 5403-5409.
49. Hornbeck, L.J., *Low surface energy passivation layer for micromechanical devices*. 1997, Google Patents.

50. Zhang, L., Y.-H. Zhao, and R. Bai, *Development of a multifunctional membrane for chromatic warning and enhanced adsorptive removal of heavy metal ions: Application to cadmium.* Journal of membrane science, 2011. **379**(1): p. 69-79.
51. Bai, H., Z. Liu, and D.D. Sun, *A hierarchically structured and multifunctional membrane for water treatment.* Applied Catalysis B: Environmental, 2012. **111**: p. 571-577.
52. Griffini, G., et al., *Multifunctional Luminescent Down-Shifting Fluoropolymer Coatings: A Straightforward Strategy to Improve the UV-Light Harvesting Ability and Long-Term Outdoor Stability of Organic Dye-Sensitized Solar Cells.* Advanced Energy Materials, 2015. **5**(3).
53. Faustini, M., et al., *Hydrophobic, antireflective, self-cleaning, and antifogging sol–gel coatings: an example of multifunctional nanostructured materials for photovoltaic cells.* Chemistry of Materials, 2010. **22**(15): p. 4406-4413.
54. Callow, M.E. and R.L. Fletcher, *The influence of low surface energy materials on bioadhesion—a review.* International Biodeterioration & Biodegradation, 1994. **34**(3-4): p. 333-348.
55. Huang, Y., et al., *Corrosion resistance properties of electroless nickel composite coatings.* Electrochimica Acta, 2004. **49**(25): p. 4313-4319.
56. Li, Z., et al., *Two-level antibacterial coating with both release-killing and contact-killing capabilities.* Langmuir, 2006. **22**(24): p. 9820-9823.
57. Montali, A., *Antibacterial coating systems.* Injury, 2006. **37**(2): p. S81-S86.
58. Yuan, W., et al., *A facile method to construct hybrid multilayered films as a strong and multifunctional antibacterial coating.* Journal of Biomedical Materials Research Part B: Applied Biomaterials, 2008. **85**(2): p. 556-563.
59. Berron, B.J., E.P. Graybill, and G.K. Jennings, *Growth and structure of surface-initiated poly (n-alkylnorbornene) films.* Langmuir, 2007. **23**(23): p. 11651-11655.
60. Hoyle, C.E. and C.N. Bowman, *Thiol–ene click chemistry.* Angewandte Chemie International Edition, 2010. **49**(9): p. 1540-1573.
61. Tsujii, Y., et al., *Structure and properties of high-density polymer brushes prepared by surface-initiated living radical polymerization*, in *Surface-initiated polymerization I*. 2006, Springer. p. 1-45.
62. Bhat, R.R., et al., *Surface-grafted polymer gradients: Formation, characterization, and applications*, in *Surface-initiated polymerization ii*. 2006, Springer. p. 51-124.
63. Dyer, D.J., *Photoinitiated synthesis of grafted polymers*, in *Surface-Initiated Polymerization I*. 2006, Springer. p. 47-65.
64. Bain, C.D. and G.M. Whitesides, *Molecular-level control over surface order in self-assembled monolayer films of thiols on gold.* Science, 1988. **240**(4848): p. 62-64.
65. Balachandra, A.M., G.L. Baker, and M.L. Bruening, *Preparation of composite membranes by atom transfer radical polymerization initiated from a porous support.* Journal of Membrane Science, 2003. **227**(1–2): p. 1-14.
66. Escobar, C.A., et al., *Composite Fluorocarbon Membranes by Surface-Initiated Polymerization from Nanoporous Gold-Coated Alumina.* ACS applied materials & interfaces, 2012. **4**(2): p. 906-915.

67. Brittain, W.J., et al., *Surface rearrangement of diblock copolymer brushes—stimuli responsive films,* in *Surface-Initiated Polymerization II*. 2006, Springer. p. 125-147.
68. Slugovc, C., *The ring opening metathesis polymerisation toolbox.* Macromolecular rapid communications, 2004. **25**(14): p. 1283-1297.
69. Ivin, K.J. and J. Mol, *Olefin metathesis and metathesis polymerization*. 1997: Academic Press.
70. Schwab, P., R.H. Grubbs, and J.W. Ziller, *Synthesis and applications of RuCl2 (CHR ')(PR3) 2: the influence of the alkylidene moiety on metathesis activity.* Journal of the American Chemical Society, 1996. **118**(1): p. 100-110.
71. Trnka, T.M. and R.H. Grubbs, *The development of L2X2Ru CHR olefin metathesis catalysts: an organometallic success story.* Accounts of Chemical Research, 2001. **34**(1): p. 18-29.
72. Jean-Louis Hérisson, P. and Y. Chauvin, *Catalyse de transformation des oléfines par les complexes du tungstène. II. Télomérisation des oléfines cycliques en présence d'oléfines acycliques.* Macromolecular Chemistry and Physics, 1971. **141**(1): p. 161-176.
73. Schrock, R.R., *Alkylidene complexes of niobium and tantalum.* Accounts of Chemical Research, 1979. **12**(3): p. 98-104.
74. Nguyen, S.T., et al., *Ring-opening metathesis polymerization (ROMP) of norbornene by a group VIII carbene complex in protic media.* Journal of the American Chemical Society, 1992. **114**(10): p. 3974-3975.
75. Nguyen, S.T., R.H. Grubbs, and J.W. Ziller, *Syntheses and activities of new single-component, ruthenium-based olefin metathesis catalysts.* Journal of the American Chemical Society, 1993. **115**(21): p. 9858-9859.
76. Grubbs, R.H., *Olefin metathesis.* Tetrahedron, 2004. **60**(34): p. 7117-7140.
77. Feldman, J. and R.R. Schrock, *Recent advances in the chemistry of d° alkylidene and metallacycobutane complexes.* Progress in inorganic chemistry, 1991. **39**: p. 1-74.
78. Grubbs, R.H. and S. Chang, *Recent advances in olefin metathesis and its application in organic synthesis.* Tetrahedron, 1998. **54**(18): p. 4413-4450.
79. Eleuterio, H., *German Pat., 1072811.* Du Pont de Nemours & Co, 1960.
80. Truett, W.L., et al., *Polynorbornene by Coördination Polymerization1.* Journal of the American Chemical Society, 1960. **82**(9): p. 2337-2340.
81. Grubbs, R.H., *Olefin-metathesis catalysts for the preparation of molecules and materials (Nobel lecture).* Angewandte Chemie International Edition, 2006. **45**(23): p. 3760-3765.
82. Schrock, R.R., *Multiple metal–carbon bonds for catalytic metathesis reactions (Nobel lecture).* Angewandte Chemie International Edition, 2006. **45**(23): p. 3748-3759.
83. Buchmeiser, M.R., et al., *Ring-opening metathesis polymerization for the preparation of surface-grafted polymer supports.* Macromolecules, 2000. **33**(1): p. 32-39.
84. Liu, X., S. Guo, and C.A. Mirkin, *Surface and Site-Specific Ring-Opening Metathesis Polymerization Initiated by Dip-Pen Nanolithography.* Angewandte Chemie International Edition, 2003. **42**(39): p. 4785-4789.

85. Kim, N.Y., et al., *Surface-initiated ring-opening metathesis polymerization on Si/SiO2.* Macromolecules, 2000. **33**(8): p. 2793-2795.
86. Harada, Y., G.S. Girolami, and R.G. Nuzzo, *Catalytic Amplification of Patterning via Surface-Confined Ring-Opening Metathesis Polymerization on Mixed Primer Layers Formed by Contact Printing.* Langmuir, 2003. **19**(12): p. 5104-5114.
87. Lapinte, V., et al., *Surface initiated ring-opening metathesis polymerization of norbornene onto Wang and Merrifield resins.* Journal of Molecular Catalysis A: Chemical, 2007. **276**(1): p. 219-225.
88. Liu, Y. and A. Adronov, *Preparation and Utilization of Catalyst-Functionalized Single-Walled Carbon Nanotubes for Ring-Opening Metathesis Polymerization.* Macromolecules, 2004. **37**(13): p. 4755-4760.
89. Buchmeiser, M.R. *Ring-Opening Metathesis Polymerization-Derived Materials for Separation Science, Heterogeneous Catalysis and Tissue Engineering*. in *Macromolecular symposia*. 2010. Wiley Online Library.
90. Ye, Q., et al., *Surface-Initiated Ring-Opening Metathesis Polymerization of Pentadecafluorooctyl-5-norbornene-2-carboxylate from Variable Substrates Modified with Sticky Biomimic Initiator.* Macromolecules, 2010. **43**(13): p. 5554-5560.
91. Buchmeiser, M.R., *Metathesis-based monolithic supports: synthesis, functionalization and applications.* Macromolecular Rapid Communications, 2001. **22**(14): p. 1081-1094.
92. Mayr, B., et al., *Metathesis-based monoliths: influence of polymerization conditions on the separation of biomolecules.* Analytical chemistry, 2001. **73**(17): p. 4071-4078.
93. Escobar, C.A., et al., *Amplification of Surface-Initiated Ring-Opening Metathesis Polymerization of 5-(Perfluoro-n-alkyl)norbornenes by Macroinitiation.* Langmuir, 2013. **29**(40): p. 12560-12571.
94. Seehof, N., S. Grutke, and W. Risse, *Selective reaction with exo-isomers in ring-opening olefin metathesis polymerization (ROMP) of fluoroalkyl-substituted norbornene derivatives.* Macromolecules, 1993. **26**(4): p. 695-700.
95. Villemin, D., *Synthese de macrolides par methathese.* Tetrahedron Letters, 1980. **21**(18): p. 1715-1718.
96. Tsuji, J. and S. Hashiguchi, *Application of olefin metathesis to organic synthesis. Syntheses of civetone and macrolides.* Tetrahedron Letters, 1980. **21**(31): p. 2955-2958.
97. de Weghe, P.V. and J. Eustache, *The application of olefin metathesis to the synthesis of biologically active macrocyclic agents.* Current topics in medicinal chemistry, 2005. **5**(15): p. 1495-1519.
98. Nishida, A., T. Nagata, and M. Nakagawa, *Topics in Heterocyclic Chemistry*. 2006, Springer: Berlin, Heidelberg.
99. Nicolaou, K., P.G. Bulger, and D. Sarlah, *Metathesis reactions in total synthesis.* Angewandte Chemie International Edition, 2005. **44**(29): p. 4490-4527.
100. Deiters, A. and S.F. Martin, *Synthesis of oxygen-and nitrogen-containing heterocycles by ring-closing metathesis.* Chemical reviews, 2004. **104**(5): p. 2199-2238.

101. Collins, S.K., *Preparation of cyclic molecules bearing "strained" olefins using olefin metathesis.* Journal of organometallic chemistry, 2006. **691**(24): p. 5122-5128.
102. Donohoe, T., L. Fishlock, and P. Procopiou, *Chem. sEur. J. 2008, 14, 5716.(b) Donohoe, TJ; Orr, AJ; Bingham, M.* Angew. Chem., Int. Ed, 2006. **45**: p. 2664.
103. Kotha, S. and K. Lahiri, *Synthesis of diverse polycyclic compounds via catalytic metathesis.* Synlett, 2007. **2007**(18): p. 2767-2784.
104. Schmidt, B. and J. Hermanns, *Ring Closing Metathesis of Substrates Containing more than two C-Cdouble Bonds: Rapid Access to Functionalized Heterocycles.* Current Organic Chemistry, 2006. **10**(12): p. 1363-1396.
105. Sebastien, M. and E.F. Deryn, *Equilibrium Ring-Closing Metathesis.* Chemical Reviews, 2009.
106. Adjiman, C.S., et al., *Solvents for ring-closing metathesis reactions.* Solvents for ring-closing metathesis reactions, 2008.
107. Marx, V.M., et al., *Stereoselective access to Z and E macrocycles by ruthenium-catalyzed Z-selective ring-closing metathesis and ethenolysis.* Journal of the American Chemical Society, 2012. **135**(1): p. 94-97.
108. Hein, C.D., X.-M. Liu, and D. Wang, *Click Chemistry, a Powerful Tool for Pharmaceutical Sciences.* Pharmaceutical research, 2008. **25**(10): p. 2216-2230.
109. Kolb, H.C., M.G. Finn, and K.B. Sharpless, *Click Chemistry: Diverse Chemical Function from a Few Good Reactions.* Angew Chem Int Ed Engl, 2001. **40**(11): p. 2004-2021.
110. Kolb, H.C., M. Finn, and K.B. Sharpless, *Click chemistry: diverse chemical function from a few good reactions.* Angewandte Chemie International Edition, 2001. **40**(11): p. 2004-2021.
111. Kolb, H.C. and K.B. Sharpless, *The growing impact of click chemistry on drug discovery.* Drug discovery today, 2003. **8**(24): p. 1128-1137.
112. Tufariello, J., *Dipolar Cycloaddition Chemistry, ed. A. Padwa*. 1984, Wiley Interscience, New York.
113. Lowe, A.B., *Thiol-ene "click" reactions and recent applications in polymer and materials synthesis.* Polymer Chemistry, 2010. **1**(1): p. 17-36.
114. Hoyle, C.E., A.B. Lowe, and C.N. Bowman, *Thiol-click chemistry: a multifaceted toolbox for small molecule and polymer synthesis.* Chemical Society Reviews, 2010. **39**(4): p. 1355-1387.
115. Posner, T., *Beiträge zur Kenntniss der ungesättigten Verbindungen. II. Ueber die Addition von Mercaptanen an ungesättigte Kohlenwasserstoffe.* European Journal of Inorganic Chemistry, 1905. **38**(1): p. 646-657.
116. Kakwere, H. and S. Perrier, *Orthogonal "relay" reactions for designing functionalized soft nanoparticles.* Journal of the American Chemical Society, 2009. **131**(5): p. 1889-1895.
117. Surendra, K., et al., *β-Cyclodextrin promoted aza-Michael addition of amines to conjugated alkenes in water.* Tetrahedron letters, 2006. **47**(13): p. 2125-2127.
118. Moses, J.E. and A.D. Moorhouse, *The growing applications of click chemistry.* Chemical Society Reviews, 2007. **36**(8): p. 1249-1262.

119. Hoyle, C.E., T.Y. Lee, and T. Roper, *Thiol–enes: chemistry of the past with promise for the future.* Journal of Polymer Science Part A: Polymer Chemistry, 2004. **42**(21): p. 5301-5338.
120. Griesbaum, K., *Problems and possibilities of the free-radical addition of thiols to unsaturated compounds.* Angewandte Chemie International Edition in English, 1970. **9**(4): p. 273-287.
121. Hampson, G. and J.M. Robertson, *78. Bond lengths and resonance in the cis-azobenzene molecule.* Journal of the Chemical Society (Resumed), 1941: p. 409-413.
122. Hartley, G., *The cis-form of azobenzene.* Nature, 1937. **140**(3537): p. 281.
123. Mita, I., K. Horie, and K. Hirao, *Photochemistry in polymer solids. 9. Photoisomerization of azobenzene in a polycarbonate film.* Macromolecules, 1989. **22**(2): p. 558-563.
124. Lednev, I.K., et al., *Femtosecond time-resolved UV− visible absorption spectroscopy of trans-azobenzene in solution.* The Journal of Physical Chemistry, 1996. **100**(32): p. 13338-13341.
125. Rau, H. and E. Lueddecke, *On the rotation-inversion controversy on photoisomerization of azobenzenes. Experimental proof of inversion.* Journal of the American Chemical Society, 1982. **104**(6): p. 1616-1620.
126. Paik, C.S. and H. Morawetz, *Photochemical and thermal isomerization of azoaromatic residues in the side chains and the backbone of polymers in bulk.* Macromolecules, 1972. **5**(2): p. 171-177.
127. Louie, J. and R.H. Grubbs, *Metathesis of Electron-Rich Olefins: Structure and Reactivity of Electron-Rich Carbene Complexes.* Organometallics, 2002. **21**(11): p. 2153-2164.
128. Berron, B.J., P.A. Payne, and G.K. Jennings, *Sulfonation of surface-initiated polynorbornene films.* Industrial & Engineering Chemistry Research, 2008. **47**(20): p. 7707-7714.
129. Laibinis, P.E., et al., *Structure and wetting properties of omega-alkoxy-N-alkanethiolate monolayers on gold and silver.* Journal of Physical Chemistry, 1995. **99**(19): p. 7663-7676.
130. Holländer, A., *On the selection of test liquids for the evaluation of acid-base properties of solid surfaces by contact angle goniometry.* Journal of colloid and interface science, 1995. **169**(2): p. 493-496.
131. Yuan, Y. and T.R. Lee, *Contact angle and wetting properties*, in *Surface science techniques*. 2013, Springer. p. 3-34.
132. Nandivada, H., A.M. Ross, and J. Lahann, *Stimuli-responsive monolayers for biotechnology.* Progress in Polymer Science, 2010. **35**(1): p. 141-154.
133. Wang, X., Z. Chen, and Z. Shen, *Dynamic behavior of polymer surface and the time dependence of contact angle.* Science in China Series B: Chemistry, 2005. **48**(6): p. 553-559.
134. Zisman, W.A., *Relation of the equilibrium contact angle to liquid and solid constitution*. 1964, ACS Publications.
135. Nuzzo, R.G., L.H. Dubois, and D.L. Allara, *Fundamental studies of microscopic wetting on organic surfaces. 1. Formation and structural characterization of a self-*

consistent series of polyfunctional organic monolayers. Journal of the American Chemical Society, 1990. **112**(2): p. 558-569.
136. Greenler, R.G., *Infrared study of adsorbed molecules on metal surfaces by reflection techniques.* The Journal of Chemical Physics, 1966. **44**(1): p. 310-315.
137. Huh, Y.S., A.J. Chung, and D. Erickson, *Surface enhanced Raman spectroscopy and its application to molecular and cellular analysis.* Microfluidics and nanofluidics, 2009. **6**(3): p. 285.
138. Indian, J., *A new radiation.* Indian J. Phys, 1928. **2**: p. 387-398.
139. Landsberg, G., *Eine neue Erscheinung bei der Lichtzerstreuung in Krystallen.* Naturwissenschaften, 1928. **16**: p. 558.
140. Singh, R., *C. V. Raman and the Discovery of the Raman Effect.* Physics in Perspective, 2002. **4**(4): p. 399-420.
141. Ayas, S., et al., *Label-free nanometer-resolution imaging of biological architectures through surface enhanced raman scattering.* Scientific reports, 2013. **3**.
142. Bard, A.J. and L.R. Faulkner, *Fundamentals and applications.* Electrochemical Methods, 2001. **2**.
143. Park, S.-M. and J.-S. Yoo, *Peer reviewed: electrochemical impedance spectroscopy for better electrochemical measurements*. 2003, ACS Publications.
144. Skoog, D.A., F.J. Holler, and S.R. Crouch, *Principles of instrumental analysis*. 2007: Thomson Brooks/Cole.
145. Shah, N., et al., *Magnetic resonance spectroscopy as an imaging tool for cancer: a review of the literature.* The Journal of the American Osteopathic Association, 2006. **106**(1): p. 23-27.
146. Bubert, H., et al., *Surface and Thin-Film Analysis*. 2002: Wiley Online Library.
147. Fujiwara, H., *Spectroscopic ellipsometry: principles and applications*. 2007: John Wiley & Sons.
148. Chen, S., et al., *Strong resistance of phosphorylcholine self-assembled monolayers to protein adsorption: insights into nonfouling properties of zwitterionic materials.* Journal of the American Chemical Society, 2005. **127**(41): p. 14473-14478.
149. Woollam, J.A., et al., *VUV and IR spectroellipsometric studies of polymer surfaces.* Nuclear Instruments and Methods in Physics Research Section B: Beam Interactions with Materials and Atoms, 2003. **208**: p. 35-39.
150. Cant, N.E., et al., *Fabrication and characterization of self-assembled nanoparticle/polyelectrolyte multilayer films.* The Journal of Physical Chemistry B, 2003. **107**(49): p. 13557-13562.
151. Wood, J. and R. Redin, *A simple profilometer for film thickness measurement.* Review of scientific instruments, 1993. **64**(8): p. 2405-2406.
152. Niles, D.W., et al., *Na impurity chemistry in photovoltaic CIGS thin films: Investigation with x-ray photoelectron spectroscopy.* Journal of Vacuum Science & Technology A: Vacuum, Surfaces, and Films, 1997. **15**(6): p. 3044-3049.
153. Asami, K. and K. Hashimoto, *X-ray photoelectron spectroscopy for corrosion studies.* Langmuir, 1987. **3**(6): p. 897-904.
154. Sarma, D.D., et al., *X-ray Photoelectron Spectroscopy: A Unique Tool To Determine the Internal Heterostructure of Nanoparticles.* Chemistry of Materials, 2013. **25**(8): p. 1222-1232.

155. Bubert, H., J.C. Rivière, and W.S.M. Werner, *X-Ray Photoelectron Spectroscopy (XPS)*, in *Surface and Thin Film Analysis*. 2011, Wiley-VCH Verlag GmbH & Co. KGaA. p. 7-41.
156. Lehenkari, P., et al., *Adapting atomic force microscopy for cell biology.* Ultramicroscopy, 2000. **82**(1): p. 289-295.
157. Lin, H., D.O. Clegg, and R. Lal, *Imaging real-time proteolysis of single collagen I molecules with an atomic force microscope.* Biochemistry, 1999. **38**(31): p. 9956-9963.
158. Poggi, M.A., L.A. Bottomley, and P.T. Lillehei, *Scanning probe microscopy.* Analytical chemistry, 2002. **74**(12): p. 2851-2862.
159. Martin, Y., C. Williams, and H.K. Wickramasinghe, *Atomic force microscope–force mapping and profiling on a sub 100-Å scale.* Journal of Applied Physics, 1987. **61**(10): p. 4723-4729.
160. Zhong, Q., et al., *Fractured polymer/silica fiber surface studied by tapping mode atomic force microscopy.* Surface Science, 1993. **290**(1): p. L688-L692.
161. Wägli, P., A. Homsy, and N. de Rooij, *Norland optical adhesive (NOA81) microchannels with adjustable wetting behavior and high chemical resistance against a range of mid-infrared-transparent organic solvents.* Sensors and Actuators B: Chemical, 2011. **156**(2): p. 994-1001.
162. Eckenrode, H.M. and H.-L. Dai, *Nonlinear optical probe of biopolymer adsorption on colloidal particle surface: Poly-L-lysine on polystyrene sulfate microspheres.* Langmuir, 2004. **20**(21): p. 9202-9209.
163. Edmondson, S., V.L. Osborne, and W.T. Huck, *Polymer brushes via surface-initiated polymerizations.* Chemical society reviews, 2004. **33**(1): p. 14-22.
164. Bielawski, C.W. and R.H. Grubbs, *Highly efficient ring-opening metathesis polymerization (ROMP) using new ruthenium catalysts containing N-heterocyclic carbene ligands.* Angewandte Chemie International Edition, 2000. **39**(16): p. 2903-2906.
165. Buchmeiser, M.R., *Polymeric monolithic materials: syntheses, properties, functionalization and applications.* Polymer, 2007. **48**(8): p. 2187-2198.
166. Jordi, M.A. and T.A. Seery, *Quantitative determination of the chemical composition of silica-poly (norbornene) nanocomposites.* Journal of the American Chemical Society, 2005. **127**(12): p. 4416-4422.
167. Hilf, S. and A.F. Kilbinger, *Functional end groups for polymers prepared using ring-opening metathesis polymerization.* Nature chemistry, 2009. **1**(7): p. 537-546.
168. Zhang, Q., et al., *Covalent modification of graphene oxide with polynorbornene by surface-initiated ring-opening metathesis polymerization.* Polymer, 2014. **55**(23): p. 6044-6050.
169. Xu, Y., et al., *Growing Multihydroxyl Hyperbranched Polymers on the Surfaces of Carbon Nanotubes by in Situ Ring-Opening Polymerization.* Macromolecules, 2004. **37**(24): p. 8846-8853.
170. Gómez, F.J., et al., *Ring opening metathesis polymerization on non-covalently functionalized single-walled carbon nanotubes.* Chemical Communications, 2003(2): p. 190-191.

171. Haque, H.A., et al., *High-Density Liquid-Crystalline Azobenzene Polymer Brush Attained by Surface-Initiated Ring-Opening Metathesis Polymerization.* Langmuir, 2013. **29**(25): p. 7571-7575.
172. Faulkner, C.J., P. Andrew Payne, and G.K. Jennings, *Surface-initiated ring-opening metathesis polymerization of 5-(perfluorohexyl)norbornene on carbon paper electrodes.* Journal of Colloid and Interface Science, 2010. **351**(1): p. 248-253.
173. Weck, M., et al., *Ring-Opening Metathesis Polymerization from Surfaces.* Journal of the American Chemical Society, 1999. **121**(16): p. 4088-4089.
174. Li, X.-M., J. Huskens, and D.N. Reinhoudt, *Towards in-plane metathesis polymerization at self-assembled monolayers of norbornene adsorbates on gold surfaces.* Nanotechnology, 2003. **14**(10): p. 1064.
175. Pasquale, A.J., A.R. Fornof, and T.E. Long, *Synthesis of Norbornene Derivatives by Diels-Alder Cycloaddition and Subsequent Copolymerization with Maleic Anhydride.* Macromolecular Chemistry and Physics, 2004. **205**(5): p. 621-627.
176. Khoury, P.R., J.D. Goddard, and W. Tam, *Ring strain energies: substituted rings, norbornanes, norbornenes and norbornadienes.* Tetrahedron, 2004. **60**(37): p. 8103-8112.
177. Hatjopoulos, J.D. and R.A. Register, *Synthesis and Properties of Well-Defined Elastomeric Poly(alkylnorbornene)s and Their Hydrogenated Derivatives.* Macromolecules, 2005. **38**(24): p. 10320-10322.
178. Feast, W.J., M. Gimeno, and E. Khosravi, *Approaches to highly polar polymers with low glass transition temperatures: 2. fluorinated polymers via ring-opening metathesis copolymerisation and hydrogenation.* Journal of Molecular Catalysis A: Chemical, 2004. **213**(1): p. 9-14.
179. Sauer, J. and R. Sustmann, *Mechanistic Aspects of Diels-Alder Reactions: A Critical Survey.* Angewandte Chemie International Edition, 1980. **19**(10): p. 779-807.
180. Lowe, A.B., *Thiol–ene "click" reactions and recent applications in polymer and materials synthesis: a first update.* Polymer Chemistry, 2014. **5**(17): p. 4820-4870.
181. Morgan, C., F. Magnotta, and A. Ketley, *Thiol/ene photocurable polymers.* Journal of Polymer Science: Polymer Chemistry Edition, 1977. **15**(3): p. 627-645.
182. Li, G.L., et al., *Binary Polymer Brushes on Silica@ Polymer Hybrid Nanospheres and Hollow Polymer Nanospheres by Combined Alkyne− Azide and Thiol− Ene Surface Click Reactions.* Macromolecules, 2010. **43**(24): p. 10275-10282.
183. Uygun, M., M.A. Tasdelen, and Y. Yagci, *Influence of type of initiation on thiol–ene "click" chemistry.* Macromolecular Chemistry and Physics, 2010. **211**(1): p. 103-110.
184. Goldmann, A.S., et al., *Surface Modification of Poly (divinylbenzene) Microspheres via Thiol− Ene Chemistry and Alkyne− Azide Click Reactions.* Macromolecules, 2009. **42**(11): p. 3707-3714.
185. Planche, J., A. Revillon, and A. Guyot, *Chemical modification of polynorbornene. I. Sulfonation in dilute solution.* Journal of Polymer Science Part A: Polymer Chemistry, 1988. **26**(2): p. 429-444.

186. de Silva, D.S.M., et al., *Chain tilt and surface disorder in lamellar crystals. A FTIR and SAXS study of labeled long alkanes.* Macromolecules, 2002. **35**(20): p. 7730-7741.
187. Silverstein, R.M., et al., *Spectrometric identification of organic compounds*. 2014: John Wiley & Sons.
188. Desbief, S., et al., *Superhydrophobic aluminum surfaces by deposition of micelles of fluorinated block copolymers.* Langmuir, 2009. **26**(3): p. 2057-2067.
189. Wang, J., et al., *Liquid crystalline, semifluorinated side group block copolymers with stable low energy surfaces: synthesis, liquid crystalline structure, and critical surface tension.* Macromolecules, 1997. **30**(7): p. 1906-1914.
190. Andruzzi, L., et al., *Control of surface properties using fluorinated polymer brushes produced by surface-initiated controlled radical polymerization.* Langmuir, 2004. **20**(24): p. 10498-10506.
191. Zhou, F. and W.T. Huck, *Surface grafted polymer brushes as ideal building blocks for "smart" surfaces.* Physical Chemistry Chemical Physics, 2006. **8**(33): p. 3815-3823.
192. Li, B., et al., *Chemical reactivity of C–F bonds attached to graphene with diamines depending on their nature and location.* Physical Chemistry Chemical Physics, 2016. **18**(26): p. 17495-17505.
193. Sandford, G., *Perfluoroalkanes.* Tetrahedron, 2003. **59**(4): p. 437-454.
194. Lerum, M.F.Z. and W. Chen, *Acute Degradation of Surface-Bound Unsaturated Polyolefins in Common Solvents under Ambient Conditions.* Langmuir, 2009.
195. Rabek, J.F., *Polymer photodegradation: mechanisms and experimental methods*. 2012: Springer Science & Business Media.
196. Wikipedia, *Polymer degradation.*
197. CH, O. and C.C. CH, *Photodegradation of polymers.* 1998.
198. *Ozonolysis*. Available from: https://en.wikipedia.org/wiki/Ozonolysis.
199. Wu, S.K., et al., *Photo-oxidative degradation of polynorbornene (part I).* Polymer Photochemistry, 1982. **2**(1): p. 73-85.
200. Sriram, S.R., *Development of self-healing polymer composites and photoinduced ring-opening metathesis polymerization*. 2002.
201. Briscoe, B., L. Fiori, and E. Pelillo, *Nano-indentation of polymeric surfaces.* Journal of Physics D: Applied Physics, 1998. **31**(19): p. 2395.
202. Grove, N.R., et al., *Functionalized polynorbornene dielectric polymers: adhesion and mechanical properties.* Journal of Polymer Science Part B Polymer Physics, 1999. **37**(21): p. 3003-3010.
203. Bai, Y., et al., *Photosensitive polynorbornene based dielectric. I. Structure–property relationships.* Journal of Applied Polymer Science, 2004. **91**(5): p. 3023-3030.
204. Bai, D., B.M. Habersberger, and G.K. Jennings, *pH-Responsive Copolymer Films by Surface-Catalyzed Growth.* Journal of the American Chemical Society, 2005. **127**(47): p. 16486-16493.
205. Ayres, N., S.G. Boyes, and W.J. Brittain, *Stimuli-Responsive Polyelectrolyte Polymer Brushes Prepared via Atom-Transfer Radical Polymerization.* Langmuir, 2007. **23**(1): p. 182-189.

206. Voccia, S., et al., *Sequential Electrografting and Ring-Opening Metathesis Polymerization: a Strategy for the Tailoring of Conductive Surfaces.* Macromolecular rapid communications, 2005. **26**(10): p. 779-783.
207. Boyes, S.G., et al., *Synthesis, characterization, and properties of ABA type triblock copolymer brushes of styrene and methyl acrylate prepared by atom transfer radical polymerization.* Macromolecules, 2002. **35**(13): p. 4960-4967.
208. Liu, Y.L., et al., *Surface-initiated atom transfer radical polymerization from porous poly (tetrafluoroethylene) membranes using the C□ F groups as initiators.* Journal of Polymer Science Part A: Polymer Chemistry, 2010. **48**(10): p. 2076-2083.
209. Berron, B.J., et al., *Surface-Initiated Growth of Ionomer Films from Pt-Modified Gold Electrodes.* Langmuir, 2009. **25**(21): p. 12721-12728.
210. Berron, B.J., E.P. Graybill, and G.K. Jennings, *Growth and Structure of Surface-Initiated Poly(n-alkylnorbornene) Films.* Langmuir, 2007. **23**(23): p. 11651-11655.
211. Bielawski, C.W. and R.H. Grubbs, *Increasing the initiation efficiency of ruthenium-based ring-opening metathesis initiators: effect of excess phosphine.* Macromolecules, 2001. **34**(26): p. 8838-8840.
212. Lerum, M.F.Z. and W. Chen, *Acute Degradation of Surface-Bound Unsaturated Polyolefins in Common Solvents under Ambient Conditions.* Langmuir, 2009. **25**(19): p. 11250-11254.
213. Sipinen, A.J. and D.R. Rutherford, *A study of the oxidative degradation of polyolefins.* Journal of environmental polymer degradation, 1993. **1**(3): p. 193-202.
214. Faulkner, C.J., R.E. Fischer, and G.K. Jennings, *Surface-Initiated Polymerization of 5-(Perfluoro-n-alkyl)norbornenes from Gold Substrates.* Macromolecules, 2010. **43**(3): p. 1203-1209.
215. Hoyle, C.E., T.Y. Lee, and T. Roper, *Thiol-enes: Chemistry of the past with promise for the future.* Journal of Polymer Science Part a-Polymer Chemistry, 2004. **42**(21): p. 5301-5338.
216. Hoyle, C.E. and C.N. Bowman, *Thiol-Ene Click Chemistry.* Angewandte Chemie-International Edition, 2010. **49**(9): p. 1540-1573.
217. Rehmann, M.S., A.C. Garibian, and A.M. Kloxin. *Hydrolytically degradable thiol–ene hydrogels for protein release*. in *Macromolecular symposia*. 2013. Wiley Online Library.
218. Ziebacz, N., et al., *Crossover regime for the diffusion of nanoparticles in polyethylene glycol solutions: influence of the depletion layer.* Soft Matter, 2011. **7**(16): p. 7181-7186.
219. Sahlin, J.J. and N.A. Peppas, *Near-field FTIR imaging: a technique for enhancing spatial resolution in FTIR microscopy.* Journal of applied polymer science, 1997. **63**(1): p. 103-110.
220. Roberts, M., M. Bentley, and J. Harris, *Chemistry for peptide and protein PEGylation.* Advanced drug delivery reviews, 2012. **64**: p. 116-127.
221. Singh, T.J. and S. Bhat, *Morphology and conductivity studies of a new solid polymer electrolyte:(PEG) xLiClO4.* Bulletin of Materials Science, 2003. **26**(7): p. 707-714.
222. Weber, J., P.C. Beard, and S.E. Bohndiek, *Contrast agents for molecular photoacoustic imaging.* Nat Meth, 2016. **13**(8): p. 639-650.

223. Stevens, C.A., L. Safazadeh, and B.J. Berron, *Thiol-yne adsorbates for stable, low-density, self-assembled monolayers on gold.* Langmuir, 2014. **30**(8): p. 1949-1956.
224. Dietrich, P., et al., *An anchoring strategy for photoswitchable biosensor technology: azobenzene-modified SAMs on Si (111).* Applied Physics A: Materials Science & Processing, 2008. **93**(2): p. 285-292.
225. Papra, A., N. Gadegaard, and N.B. Larsen, *Characterization of ultrathin poly (ethylene glycol) monolayers on silicon substrates.* Langmuir, 2001. **17**(5): p. 1457-1460.
226. White, J. and A. Turnbull, *Weathering of polymers: mechanisms of degradation and stabilization, testing strategies and modelling.* Journal of materials science, 1994. **29**(3): p. 584-613.
227. Drelich, J., et al., *Contact Angles for Liquid Drops at a Model Heterogeneous Surface Consisting of Alternating and Parallel Hydrophobic/Hydrophilic Strips.* Langmuir, 1996. **12**(7): p. 1913-1922.
228. Drelich, J., J.D. Miller, and R.J. Good, *The Effect of Drop (Bubble) Size on Advancing and Receding Contact Angles for Heterogeneous and Rough Solid Surfaces as Observed with Sessile-Drop and Captive-Bubble Techniques.* Journal of Colloid and Interface Science, 1996. **179**(1): p. 37-50.
229. Nguyen, S.T., et al., *Ring-Opening Metathesis Polymerization (Romp) of Norbornene by a Group-Viii Carbene Complex in Protic Media.* Journal of the American Chemical Society, 1992. **114**(10): p. 3974-3975.
230. Matyjaszewski, K., et al., *Polymers at interfaces: Using atom transfer radical polymerization in the controlled growth of homopolymers and block copolymers from silicon surfaces in the absence of untethered sacrificial initiator.* Macromolecules, 1999. **32**(26): p. 8716-8724.
231. Brantley, E.L., T.C. Holmes, and G.K. Jennings, *Modification of ATRP surface-initiated poly(hydroxyethyl methacrylate) films with hydrocarbon side chains.* Journal of Physical Chemistry B, 2004. **108**(41): p. 16077-16084.
232. Huang, Q., et al., *Surface functionalized SiO 2 nanoparticles with cationic polymers via the combination of mussel inspired chemistry and surface initiated atom transfer radical polymerization: Characterization and enhanced removal of organic dye.* Journal of Colloid and Interface Science, 2017. **499**: p. 170-179.
233. Charpentier, T.V., et al., *Development of anti-icing materials by chemical tailoring of hydrophobic textured metallic surfaces.* Journal of colloid and interface science, 2013. **394**: p. 539-544.
234. Schmaljohann, D., *Thermo-and pH-responsive polymers in drug delivery.* Advanced drug delivery reviews, 2006. **58**(15): p. 1655-1670.
235. Bertrand, O. and J.-F. Gohy, *Photo-responsive polymers: synthesis and applications.* Polymer Chemistry, 2017. **8**(1): p. 52-73.
236. Wang, D., et al., *Designing a Photoresponsive Molecularly Imprinted System on a Silicon Wafer Substrate Surface.* Langmuir, 2013. **29**(26): p. 8311-8319.
237. Dai, S., P. Ravi, and K.C. Tam, *pH-Responsive polymers: synthesis, properties and applications.* Soft Matter, 2008. **4**(3): p. 435-449.
238. Heskins, M. and J.E. Guillet, *Solution properties of poly (N-isopropylacrylamide).* Journal of Macromolecular Science—Chemistry, 1968. **2**(8): p. 1441-1455.

239. Rittersma, Z., *Recent achievements in miniaturised humidity sensors—a review of transduction techniques.* Sensors and Actuators A: Physical, 2002. **96**(2): p. 196-210.
240. Sakai, Y., Y. Sadaoka, and M. Matsuguchi, *Humidity sensors based on polymer thin films.* Sensors and Actuators B: Chemical, 1996. **35**(1-3): p. 85-90.
241. Tanaka, T., et al., *Collapse of gels in an electric field.* Science, 1982. **218**(4571): p. 467-469.
242. Thévenot, J., et al., *Magnetic responsive polymer composite materials.* Chemical Society Reviews, 2013. **42**(17): p. 7099-7116.
243. Irie, M., *Properties and applications of photoresponsive polymers.* Pure and Applied Chemistry, 1990. **62**(8): p. 1495-1502.
244. De La Rica, R., D. Aili, and M.M. Stevens, *Enzyme-responsive nanoparticles for drug release and diagnostics.* Advanced drug delivery reviews, 2012. **64**(11): p. 967-978.
245. Ulijn, R.V., *Enzyme-responsive materials: a new class of smart biomaterials.* Journal of Materials Chemistry, 2006. **16**(23): p. 2217-2225.
246. Davis, D., et al., *TJ Martı nez, SR White, JS Moore and NR Sottos.* Nature, 2009. **459**: p. 68.
247. Caruso, M.M., et al., *Mechanically-induced chemical changes in polymeric materials.* Chemical Reviews, 2009. **109**(11): p. 5755-5798.
248. Chatani, S., C.J. Kloxin, and C.N. Bowman, *The power of light in polymer science: photochemical processes to manipulate polymer formation, structure, and properties.* Polymer Chemistry, 2014. **5**(7): p. 2187-2201.
249. Yan, Q., D. Han, and Y. Zhao, *Main-chain photoresponsive polymers with controlled location of light-cleavable units: from synthetic strategies to structural engineering.* Polymer Chemistry, 2013. **4**(19): p. 5026-5037.
250. Gohy, J.-F. and Y. Zhao, *Photo-responsive block copolymer micelles: design and behavior.* Chemical Society Reviews, 2013. **42**(17): p. 7117-7129.
251. Zhao, Y., *Light-responsive block copolymer micelles.* Macromolecules, 2012. **45**(9): p. 3647-3657.
252. Rochon, P., et al., *Azo polymers for reversible optical storage. III. Effect of film thickness on net phase retardation and writing speed.* Applied optics, 1993. **32**(35): p. 7277-7280.
253. García-Amorós, J. and D. Velasco, *Recent advances towards azobenzene-based light-driven real-time information-transmitting materials.* Beilstein journal of organic chemistry, 2012. **8**: p. 1003.
254. Weis, P., D. Wang, and S. Wu, *Visible-Light-Responsive Azopolymers with Inhibited π–π Stacking Enable Fully Reversible Photopatterning.* Macromolecules, 2016. **49**(17): p. 6368-6373.
255. Harris, B.P., et al., *Photopatterned polymer brushes promoting cell adhesion gradients.* Langmuir, 2006. **22**(10): p. 4467-4471.
256. Rodebaugh, R., B. Fraser-Reid, and H.M. Geysen, *A new o-nitrobenzyl photocleavable linker for solid phase synthesis.* Tetrahedron letters, 1997. **38**(44): p. 7653-7656.
257. Kumar, G.S. and D.C. Neckers, *Photochemistry of azobenzene-containing polymers.* Chemical Reviews, 1989.

258. Georgi, U., et al., *Synthesis of azobenzene-containing polymers and investigation of their substituent-dependent isomerisation behaviour*. Reactive and Functional Polymers, 2012. **72**(4): p. 242-251.
259. Priimagi, A., et al., *Location of the Azobenzene Moieties within the Cross-Linked Liquid-Crystalline Polymers Can Dictate the Direction of Photoinduced Bending.* ACS Macro Letters, 2012. **1**(1): p. 96-99.
260. Keum, C.-D., et al., *Photodeformation Behavior of Photodynamic Polymers Bearing Azobenzene Moieties in Their Main and/or Side Chain.* Macromolecules, 2003. **36**(13): p. 4916-4923.
261. Birnie, D.P., *Rational solvent selection strategies to combat striation formation during spin coating of thin films.* Journal of Materials Research, 2001. **16**(4): p. 1145-1154.
262. Birnie III, D.P., et al., *Film/substrate/vacuum-chuck interactions during spin-coating.* Optical Engineering, 1992. **31**(9): p. 2012-2020.
263. Vogel, N., et al., *Transparency and damage tolerance of patternable omniphobic lubricated surfaces based on inverse colloidal monolayers.* Nature communications, 2013. **4**: p. 2167.
264. Lynn, D.M., B. Mohr, and R.H. Grubbs, *Living ring-opening metathesis polymerization in water.* Journal of the American Chemical Society, 1998. **120**(7): p. 1627-1628.
265. Hoveyda, A.H. and A.R. Zhugralin, *The remarkable metal-catalysed olefin metathesis reaction.* Nature, 2007. **450**(7167): p. 243.
266. Zhou, Q., et al., *Toward Spatiotemporally Controlled Synthesis of Photoresponsive Polymers: Computational Design of Azobenzene-Containing Monomers for Light-Mediated ROMP.* The Journal of Physical Chemistry A, 2016. **120**(36): p. 7101-7111.
267. *Ring-Closing Metathesis and Related Processes in Organic Synthesis.* Accounts of Chemical Research, 1995. **28**(11): p. 446452.
268. *Ring-Closing Metathesis: Novel Routes to Aromatic Heterocycles.* Chemistry - A European Journal, 2008. **14**(19): p. 5716-5726.
269. Majumdar, K., H. Rahaman, and B. Roy, *Synthesis of macrocyclic compounds by ring closing metathesis.* Current Organic Chemistry, 2007. **11**(15): p. 1339-1365.
270. Martin, E.M., *Synthesis of Medium-Sized Rings by the Ring-Closing Metathesis Reaction.* Angewandte Chemie International Edition, 2000.
271. Pasco Santurri, F.R., and Robert Stubbings. *4,4'-DIAAMINOAZOBENZENE*. 1960 [cited 1960; Available from: http://www.orgsyn.org/demo.aspx?prep=CV5P0341.
272. Formentín, P., et al., *Reactivity of Grubbs' Catalysts with Urea- and Amide-Substituted Olefins. Metathesis and Isomerization.* The Journal of Organic Chemistry, 2005. **70**(20): p. 8235-8238.
273. Choi, T.L., A.K. Chatterjee, and R.H. Grubbs, *Synthesis of α, β-Unsaturated Amides by Olefin Cross-Metathesis.* Angewandte Chemie International Edition, 2001. **40**(7): p. 1277-1279.
274. Armstrong, S.K., *Ring closing diene metathesis in organic synthesis.* Journal of the Chemical Society, Perkin Transactions 1, 1998(2): p. 371-388.

275. Rutjes, F.P. and H.E. Schoemaker, *Ruthenium-catalyzed ring closing olefin metathesis of non-natural α-amino acids.* Tetrahedron letters, 1997. **38**(4): p. 677-680.
276. Ziółkowski, B., M. Czugala, and D. Diamond, *Integrating stimulus responsive materials and microfluidics: The key to next-generation chemical sensors.* Journal of Intelligent Material Systems and Structures, 2013. **24**(18): p. 2221-2238.
277. Sadovski, O., et al., *Spectral Tuning of Azobenzene Photoswitches for Biological Applications.* Angewandte Chemie International Edition, 2009. **48**(8): p. 1484-1486.
278. Kravchenko, A., et al., *Optical Interference Lithography Using Azobenzene-Functionalized Polymers for Micro-and Nanopatterning of Silicon.* Advanced materials, 2011. **23**(36): p. 4174-4177.
279. Probst, C., et al., *Athermal Azobenzene-Based Nanoimprint Lithography.* Advanced Materials, 2016. **28**(13): p. 2624-2628.
280. Jeon, N.L., et al., *Patterned polymer growth on silicon surfaces using microcontact printing and surface-initiated polymerization.* Applied Physics Letters, 1999. **75**(26): p. 4201-4203.
281. Ooi, H.W., et al., *Photo-initiated thiol–ene "click" hydrogels from RAFT-synthesized poly (N-isopropylacrylamide).* Journal of Polymer Science Part A: Polymer Chemistry, 2013. **51**(21): p. 4626-4636.
282. Merino, E. and M. Ribagorda, *Control over molecular motion using the cis–trans photoisomerization of the azo group.* Beilstein journal of organic chemistry, 2012. **8**: p. 1071.
283. Han, D., et al., *Cyclic azobenzene-containing side-chain liquid crystalline polymers: synthesis and topological effect on mesophase transition, order, and photoinduced birefringence.* Macromolecules, 2010. **43**(8): p. 3664-3671.
284. Chang, C.-W., et al., *Photoisomerization Dynamics of Azobenzene in Solution with S1 Excitation: A Femtosecond Fluorescence Anisotropy Study.* Journal of the American Chemical Society, 2004. **126**(32): p. 10109-10118.
285. *Azobenzene photoswitches for biomolecules.* Chemical Society Reviews, 2011. **40**(8): p. 4422-4437.
286. N'Guyen, D.A., et al., *Synthesis and characterization of high grafting density bottle-brush poly (oxa) norbornene-g-poly (ε-caprolactone).* Polymer Chemistry, 2016. **7**(9): p. 1730-1738.
287. Kumar, J., et al., *Gradient force: The mechanism for surface relief grating formation in azobenzene functionalized polymers.* Applied Physics Letters, 1998. **72**(17): p. 2096-2098.
288. Galinski, H., et al., *Instability-induced pattern formation of photoactivated functional polymers.* Proceedings of the National Academy of Sciences, 2014. **111**(48): p. 17017-17022.
289. Wu, X., et al., *Optically accelerated formation of one-and two-dimensional holographic surface relief gratings on dr1/pmma,* in *Holography-Basic Principles and Contemporary Applications*. 2013, InTech.
290. Ma, H., et al., *"Non-Fouling" Oligo (ethylene glycol)-Functionalized Polymer Brushes Synthesized by Surface-Initiated Atom Transfer Radical Polymerization.* Advanced Materials, 2004. **16**(4): p. 338-341.

291. Choi, J., et al., *Direct Fabrication of Micro/Nano-Patterned Surfaces by Vertical-Directional Photofluidization of Azobenzene Materials.* ACS nano, 2017. **11**(2): p. 1320-1327.
292. Bortolus, P. and S. Monti, *cis. dblharw. trans Photoisomerization of azobenzene-cyclodextrin inclusion complexes.* Journal of Physical Chemistry, 1987. **91**(19): p. 5046-5050.
293. Wang, D., et al., *Supramolecular hydrogels constructed by red-light-responsive host-guest interactions for photo-controlled protein release in deep tissue.* Soft Matter, 2015. **11**(38): p. 7656-7662.
294. Takashima, Y., et al., *Complex formation and gelation between copolymers containing pendant azobenzene groups and cyclodextrin polymers.* Chemistry letters, 2004. **33**(7): p. 890-891.
295. Fairbanks, B.D., et al., *A versatile synthetic extracellular matrix mimic via thiol-norbornene photopolymerization.* Advanced Materials, 2009. **21**(48): p. 5005-5010.
296. Lin, C.C., C.S. Ki, and H. Shih, *Thiol–norbornene photoclick hydrogels for tissue engineering applications.* Journal of applied polymer science, 2015. **132**(8).

Vita

Ishan A. Fursule

EDUCATION:

Institute of Chemical Technology (formerly UDCT), Mumbai, India 7/2008 – 5/2012
Bachelor of Chemical Engineering
Project: Design of industrial manufacturing plant to produce 100 TPA of pyridoxine

WORK EXPERIENCE:

Research Assistant, University of Kentucky 8/2012 – 12/2017

- Designed and Synthesized UV responsive ROMP monomers, and invented a novel approach of 'light-mediated reversible ROMP' for smart polymers and coatings
- Designed, synthesized and incorporated cross-linker in polymer coatings and increased stability against oxidative degradation in organic solvents by 45% without changing the coating conductivity
- Modified the SI ROMP coating of polynorbornene by free radical thiol-ene (click chemistry) grafting using photo-initiator to change the surface functionality
- Discovered photoresponsive aggregates of azobenzene derivatives having property of spatial control using UV-visible light radiations

Teaching Assistant, University of Kentucky 8/2012 – 5/2013

Assisted undergraduate students to understand chemical engineering courses like separation processes (CME415), fluid mechanics (CME330) and chemical engineering process design (CME 456)

Chemical Engineering Internships, Aarti Industries Ltd, India 5/2011 – 7/2011

- Studied amination plants, shut down and start-up procedure, and assisted at process control panel
- Designed the reactors for the manufacturing of amine based products and wastewater scrubber for downstream unit of plant
- Assisted chemists in quality control laboratory (QC) for sample analysis

SELECTED PUBLICATIONS:

- Fursule, I., Abtahi, A.,Watkins, C., Graham, K., Berron, B., "In-situ crosslinking of Surface-Initiated Ring Opening Metathesis Polymerization of Polynorbornene for improved stability," Journal of Colloid and Interface Science, 2017, 510, 86-94.
- Zhou, Q., Fursule, I., Berron, B., Beck, M., "Towards spatiotemporal Controlled synthesis of photoresponsive polymers: computational design of azobenzene containing monomers for light-mediated ROMP," The Journal of Physical Chemistry A, 2016, 120, 7101-7111.

- Yu,Y., Fursule, I., Payne, C., "CHARMM additive all-atom force field for 2-(2'-hydroxyphenyl) benzene sulfinate, 2-hydroxybiphenyl, and related analogs", Journal of Molecular Graphics and Modelling, 2016, 72, 32-42.

SELECTED PRESENTATIONS:

- "Photo-active monomer for light-mediated ring opening metathesis polymerization," Photo-polymerization Fundamentals 2015, Boulder, Colorado
- "Photo-responsive monomer for light-mediated ring opening metathesis polymerization," ACS Central regional meeting 2016, Cincinnati, Ohio
- "Photo-active ring monomer for light-mediated ring opening metathesis polymerization," 12th National Graduate Polymer Research Conference 2016, Akron, Ohio.
- "A novel crosslinker for polyolefinic surface coatings by surface initiated ring opening metathesis polymerization," 2016 AIChE Annual Meeting, San Francisco, California
- "Photo-responsive monomer for light-mediated ROMP," 2016 AIChE Annual Meeting, San Francisco, California